Functional roles for postsynaptic α2δ-2 proteins in Purkinje cells

Kathleen A. Beeson

A DISSERTATION
presented to the Neuroscience Graduate Program
at the Vollum Institute & the
Oregon Health & Science University
School of Medicine
in partial fulfillment of
the requirements for the degree of
DOCTOR IN PHILOSOPHY

March 2021

Advisor, Eric Schnell, MD/PhD

Member & Chair, Kevin Wright, PhD

Member, Gary Westbrook, MD

Member, Mary Logan, PhD

Member, Henrique von Gersdorff, PhD

Member, Swetha Murthy, PhD

TABLE OF CONTENTS

List of Figures & Tables

AAV	Adeno-associated virus
AHP	Afterhyperpolarization
AMPA	α-amino-3-hydroxy-5-methyl-4-isoxazolepropionic acid
BAPTA	1,2-bis(o-aminophenoxy) ethane-N,N,N′,N′-tetraacetic acid
BK	Maxi-K, KCa1.1, slo-1
CB_1R	Cannabinoid receptor 1
CF	Climbing fiber
CNS	Central nervous system
CpS	Complex spike
CSD	Chemosensor-like domain
DAGα	Diacylglycerol lipase-α
DCN	Deep cerebellar nuclei
DSE	Depolarization-induced suppression of excitation
eCB	Endocannabinoid
EGTA	Ethylene glycol-bis(β-aminoethyl ether)-N,N,N′,N′-tetraacetic acid
EM	Electron microscopy
EPSC	Excitatory postsynaptic current
GABA	γ-aminobutyric acid
GBP	Gabapentin
GC	Granule cell
GCL	Granule cell layer
GFP	Green fluorescent protein
GPI	Glycosylphosphatidylinositol
IHC	Immunohistochemistry
IO	Inferior olive
IPSC	Inhibitory postsynaptic current
IRES	Internal ribosome entry site
K_{Ca}	Calcium-dependent potassium channels
KO	Knockout
ML	Molecular layer
NLG	Neuroligin
NMDA	N-methyl-D-aspartate
NRX	Neurexin
OE	Overexpression
PBS	Phosphate buffered saline
PC	Purkinje cell
PCL	Purkinje cell layer
PLCß	Phospholipase C-ß
PF	Parallel fiber
PFA	Paraformaldehyde
P_R	Probability of release
PSD	Postsynaptic density
PV	Parvalbumin
tdT	td-Tomato
TEM	Transmission electron microscopy
TSP	Thrombospondin
VGCC	Voltage-gated calcium channel
VGLUT2	Vesicular glutamate transporter
V_m	Membrane voltage
VWF	von Willebrand Factor
WT	Wildtype

Acknowledgements

Throughout my graduate career, I have been astounded by the generosity and encouragement I have received from mentors, members of the Vollum and my peers. I simply could not have gotten this far without my community and I thank everyone for making these years at Oregon Health & Science University some of the best of my life.

I would like to especially acknowledge the enthusiasm, curiosity, and mentorship of my advisor, Dr. Eric Schnell. He has not only been an excellent teacher and motivator, but always has emboldened me to keep digging and "follow my nose." I am so grateful for the independence he has granted me; it has provided me outstanding academic training and personal growth. I also would like to thank Dr. Gary Westbrook, who has been an incredible co-mentor throughout my graduate career. Gary has undoubtedly influenced my critical thinking, approach to problem solving, civil rights work and manuscript writing. Both have supported my efforts in teaching and mentoring undergraduate interns, helped me develop as a public speaker and independent scientist; and have encouraged me to pursue every opportunity, whether it be career development, social justice work or visiting my family.

Beyond science, I am grateful to all who supported my growth as an activist and leader with the Alliance for Visible Diversity in Science. During my third year, I was approached by Dr. Antoinette Foster to help found a student-led group with the mission to support racial minoritized scientists at OHSU. I must also acknowledge Dr. Letisha Wyatt for her patience and guidance, as well as Dr. Lucille Moore. It has been fulfilling, educational and inspiring to see our group gain traction. Over the last 4 years, numerous peers have collaborated, and worked passionately on nights/weekends to steer this volunteer, grassroots group. I look forward to the continued growth towards racial equity at OHSU and in my own life.

I'm thankful for my peers in academia, who have cheered me on, given advice & made my graduate experience fun and supportive; namely Heather McConnell, Christina Chatzi,

and Chris Vaaga. Too many friends to list have enriched my life by sharing their expertise, talents and passions, but I am thankful for each influential one of them. My "Oregon Family" at Adaptive Seeds, Andrew Still and Sarah Kleeger, have taught me so much about the adventuring and growing food in the Pacific Northwest over the last ten years. I am forever grateful to my extended family, Mary Helgren, and Claudia and Mike Masterson, who have consistently and lovingly supported my family and I every step of the way.

My parents, Thom and Donna, have encouraged me from day-one to pursue my interests, to explore, and to value precious time. Their perseverance through monumental challenges and hardship, while somehow maintaining positivity and creativity to strategize, has given me strength. My ten siblings: Colleen, Ryne, Myles, Drew, Callan, Haley, Clair, Nolan, Charly and Wesley, as well as their partners and children, bring light to all my days - each one has helped me grow in so many ways. I am thankful for the perspective I have learned from my family and the family nursery business – to work and support the team, have individual responsibility & integrity, be resourceful and keep a sense of humor.

Finally, my incredible husband, Spencer Masterson, has made this entire journey infinitely more joyful, memorable, and rewarding. Spencer has patiently supported my long days in the lab, work on weekends, helped me cope when I've become overwhelmed with stress and exhaustion, and showered my small "wins" with celebration. He has astounded me with dedication, and has fed me *incredible* meals nearly every night. While solidly supporting my science, he also encourages me to escape on outdoor adventures, have fun and grow creatively. Especially during the hardships of 2020-2021, Spencer has ensured every day is the best it could be, and shown unwavering support and selflessness. Along with our cats, Reuben and Murl, my little home and garden in St. John's has proven to be a vital oasis that I am so grateful for, and has filled these years with excellent memories.

Abstract

α2δ proteins (*CACNA2D1-4*) are auxiliary subunits to voltage-gated calcium channels (VGCCs), and they contribute to VGCC trafficking to the plasma membrane. However, there is now evidence that their roles extend beyond VGCC-dependent function in neurons[1]. In fact, α2δ-1 promotes excitatory synapse formation in a calcium-independent manner (Eroglu et al., 2009; Kurshan et al., 2009; Risher et al., 2018). However, little is known about the potential functional redundancies of α2δ isoforms, or whether they operate pre- or postsynaptically.

Thus, we investigated postsynaptic functions of the α2δ-2 proteins (*CACNA2D2*) in two studies. While most neurons in the brain concurrently express multiple α2δ isoforms, Purkinje cells (PCs) of the cerebellum exclusively express α2δ-2 (Cole et al., 2005; Lein et al., 2007; Beeson et al., 2020). We harnessed this isoform specific expression pattern, to elucidate the role of α2δ-2 at excitatory climbing fiber (CF) synapses, and in calcium signaling domains, by examining the functional effects of *CACNA2D2* deletion.

In Chapter 3, we use CF-PC synapses as a model to study postsynaptic deletion of α2δ-2 in excitatory synaptogenesis. Using whole-cell electrophysiology, immunofluorescence microscopy, qPCR, computational modeling and electron microscopy, we demonstrated profound and surprising alterations to CF innervation in α2δ-2 KO mice. α2δ-2 KO resulted in higher glutamate release due to increased number of CF release sites, as well as altered innervation of PCs by CF axons. Altogether, this led to defunct PC spike output. Because CF axons arise from inferior olivary cells that highly express α2δ-1 (Lein et al., 2007; Beeson et al., 2020), our findings suggest that α2δ-2 either 1) has specific, non-redundant roles in CF

[1] A related story has been revealed for the γ2 auxiliary subunit (*CACNG2*) a.k.a. stargazin, which is involved in trafficking and modulation of glutamatergic AMPA receptors rather than VGCCs (although the original nomenclature remains).

terminals that α2δ-1 cannot compensate for, and/or 2) α2δ-2 functions as a postsynaptic organizer of presynaptic innervation.

In Chapter 4, we focus on roles of α2δ-2 in postsynaptic VGCC nanodomain signaling in PCs. Precise spatial relationships between calcium influx and calcium-dependent effector molecules is critical for normal neuronal function. PCs exhibit calcium-dependent release of endocannabinoids, which act to acutely reduce presynaptic vesicle release – a phenomenon called depolarization-induced suppression of excitation (DSE). Because VGCCs are coupled to endocannabinoid release machinery in nanodomains (<100 nm), high concentrations of exogenous calcium buffers are required to disrupt DSE. In PC recordings, we show that DSE is blocked by moderate concentrations of EGTA in the α2δ-2 KO, while WT PCs are unaffected. Reducing EGTA application reveals DSE in the KO, indicating the mechanisms of DSE expression are still functional. We next looked at VGCC-K_{Ca} coupling, as K_{Ca} effluxes potassium resulting in the afterhyperpolarization (AHP) following action potentials, controlling spike rate. We found that, not only are spontaneous spike frequencies lower in KO PCs, their AHP amplitudes are reduced compared to WT. Moreover, application of EGTA in WT mimicked the KO AHP, but has no further impact on α2δ-2 KO. Finally, we show by immunohistochemistry that K_{Ca} channels are still intact at KO PC membranes. Thus, loss of α2δ-2 disrupts the functional coupling of VGCC nanodomains, highlighting an important and undescribed role for α2δ proteins in neuronal regulation.

CHAPTER 1: INTRODUCTION

The complexity of the brain is boundless, with billions of intertwining neurons, each making hundreds-of-thousands of connections. Information processing, even at the level of even a single neuron, is multidimensional and dynamic. Neuronal output is a culmination of electrical and chemical signals shaped by the neuron's unique connectivity, architecture, and molecular properties: the localization of synaptic inputs, the subcellular composition of receptors, and the organization of various signaling molecules that can further diversify output. For example, calcium influx via voltage-dependent calcium channels (VGCCs) on the membrane can activate intracellular calcium-dependent effector molecules, which can then alter dynamics of subsequent responses (a.k.a. plasticity) – an extraordinary molecular solution that further expands the dimensionality of neuronal computation!

At the final stage of neuronal processing, synaptic transmission, activation of presynaptic VGCCs elicits calcium-dependent exocytosis of neurotransmitter-filled vesicles in a probabilistic manner, determined by the specific identity and arrangement of presynaptic molecules in relation to the source of calcium influx (Nakamura et al., 2018). Thus, identification of the molecules involved in strategic arrangement of subcellular organizations, such as synaptic inputs or VGCC signaling domains, will advance our fundamental understanding of neuronal computations. This dissertation will highlight the multifaceted contributions of one such molecule, α2δ-2 (*CACNA2D2*), to neuronal function.

A felicitous model: the CACNA2D2 knockout mouse

In 1946, mice "with a peculiar, waddling gait" were discovered at Jackson Laboratories, inspiring the name "the *ducky* mouse." Because of its striking behavioral and neurological phenotypes, which also include spike-wave seizures, low muscle mass[2] and premature death (p35), the underlying genetic mutations became of interest to researchers. The original colony of *ducky* mice was tragically lost in a fire, only to be revived by one surviving male who had been gifted to another lab (Snell, 1955). Later, it was determined that the *ducky* had a 2-base pair mutation in *CACNA2D2*, resulting in loss of α2δ-2 - a protein that is abundant in brain, lung, and muscle tissues (Barclay et al., 2001b).

Because our investigations use a *CACNA2D2* knockout (KO) mouse[3], which exhibits the same phenotypes as the *ducky* (Ivanov et al., 2004), I will draw parallels between these two mouse models throughout the dissertation. The chosen cell type for our studies is the Purkinje cell (PC) of the cerebellum, which expresses a single α2δ isoform, α2δ-2 (Cole et al., 2005; Lein et al., 2007; Beeson et al., 2020). In our functional comparisons of wildtype (WT) and *CACNA2D2* mutants, we investigated the roles of α2δ-2 proteins in organizing two critical neuronal compartments: stereotyped excitatory climbing fiber synapses onto PCs and postsynaptic VGCC signaling domains controlling calcium-dependent endocannabinoid (eCB) release and potassium channel activation (K_{Ca}).

[2] α2δ proteins are expressed in muscle, where they are known to be important for excitation-contraction coupling and adhesion Garcia K, Nabhani T, Garcia J (2008) The calcium channel alpha2/delta1 subunit is involved in extracellular signalling. J Physiol 586:727-738, Wu J, Yan Z, Li Z, Qian X, Lu S, Dong M, Zhou Q, Yan N (2016) Structure of the voltage-gated calcium channel Ca(v)1.1 at 3.6 A resolution. Nature 537:191-196..

[3] The *CACNA2D2* knockout mouse was made to study cancers, as the authors note that many tumors lack the α2δ-2 isoform, hypothesizing that α2δ-2 acts as a tumor suppressant.

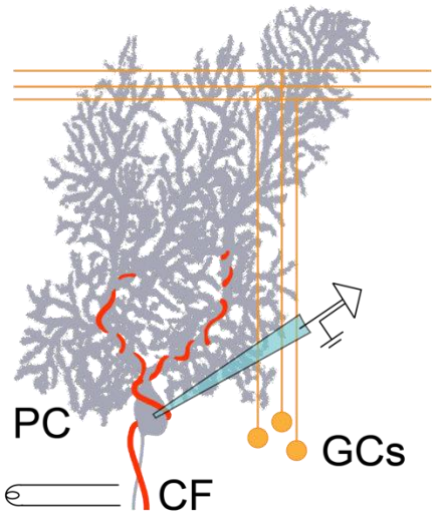

Figure 1.1 Illustration of the excitatory inputs onto Purkinje cells (PCs)

PCs are innervated by a single climbing fiber (CF; red), which arise from the inferior olive and synapses onto primary dendrites. Distal PC dendrites receive input from 100s-of-thousands of parallel fibers (PFs; yellow), which arise from granule cells (GC).

Experiments in this dissertation record from PCs in whole-cell patch clamp, and in some cases, stimulate CFs to evoke glutamate release.

Chapter 3 explores whether α2δ-2 organizes excitatory synapses, as few studies have investigated this potential function for the α2δ-2 isoform. An advantage of our model was that the α2δ-2 KO PCs selectively lacked postsynaptic α2δ proteins, whereas the excitatory presynaptic terminals synapsing onto PCs (emanating from inferior olivary and cerebellar granule cells; see **Figure 1.1** above) highly expressed another isoform, α2δ-1, and therefore was not affected (Cole et al., 2005; Lein et al., 2007; Beeson et al., 2020). In addition to this cell-type-specific expression pattern of α2δ isoforms, cerebellar circuitry is an ideal model for synaptic characterizations because of its stereotyped organization.

When mature (p21), PCs are innervated by a single climbing fiber (CF) axon, making this excitatory input particularly tractable to observe synaptic phenotypes. Furthermore, CF terminals can be visualized by immunostaining for vesicular glutamate transporter 2 (VGLUT2)[4], enabling morphological and quantitative characterization of this synapse by light microscopy. Using whole-cell recordings from PCs, immunofluorescence and electron microscopy of CF morphology, computational modeling, and qPCR of microdissected

[4] Parallel fibers (PFs) express vesicular glutamate transporter type 1, however these terminals are abundant in the molecular layer, making quantitation challenging.

tissues, we demonstrate a role for α2δ-2 in postsynaptic control of excitatory synapse formation in our first study.

The studies in Chapter 4 investigated the contribution of α2δ-2 proteins to the organization of functional VGCC nanodomains in PCs between two distinct calcium-dependent effectors, endocannabinoid (eCB) release machinery and K_{Ca} channels. Few good tools exist for visualizing endogenous expression of α2δ proteins or VGCCs, especially in tissues. However, whole-cell electrophysiology, calcium chelators (e.g., EGTA), and a strong calcium-dependent readout can be very informative in understanding calcium signaling and approximating the spatial relationships of calcium source to effector molecules (Nakamura et al., 2018). Using intracellular application of EGTA in α2δ-2 KO or WT PCs, we found that loss of α2δ-2 affects the functional coupling of VGCC to effector mechanisms, which normally require nanodomain (< 100 nm) proximity.

Our findings add to the wide variety of known functions that α2δ proteins have in neurons, reviewed below. For clarity, these prominent roles are discussed separately, as they may represent independent functions of α2δ proteins; though many mechanistic questions addressing how α2δ proteins function remain.

The α2δ proteins

α2δ proteins have been conserved > 100 million years – from expression of one isoform in *C. elegans* (UNC-36 or α2δ-3) and *Drosophila* neurons to the evolution of four α2δ isoforms (*CACNA2D1-4*) in mammals – evidence of their neurological importance. Further demonstrating the significance of α2δ proteins in brain function, mutations in *CACNA2D* genes lead to severe neurological disorders, such as epilepsy, schizophrenia, ataxia, and lethality in mice and humans (Dolphin and Lee, 2020). Interestingly, α2δ-1 and α2δ-2 are

Figure 1.2 Schematic of CACNA2D gene transcripts and the alpha2delta protein

Top left, linear sequence of the α2 protein, consisting of arginine repeats (RRR) where GBP is known to bind the Von Willebrand Factor domain (VWF), at least two Cache domains (CSDs), followed by the δ sequence (magenta). Open circles identify predicted glycosylation sites; *Bottom left*, α2δ proteins differ slightly (only α2δ-1 and -2 contain the RRR sequence that GBP binds); *Right*, cartoon of the α2δ molecule. α2 is entirely extracellular and heavily glycosylated (feather protrusions) and is connected to the δ subunit via a disulfide bridge ("S-S"). The δ protein tethers the molecule to the membrane via a GPI anchor.

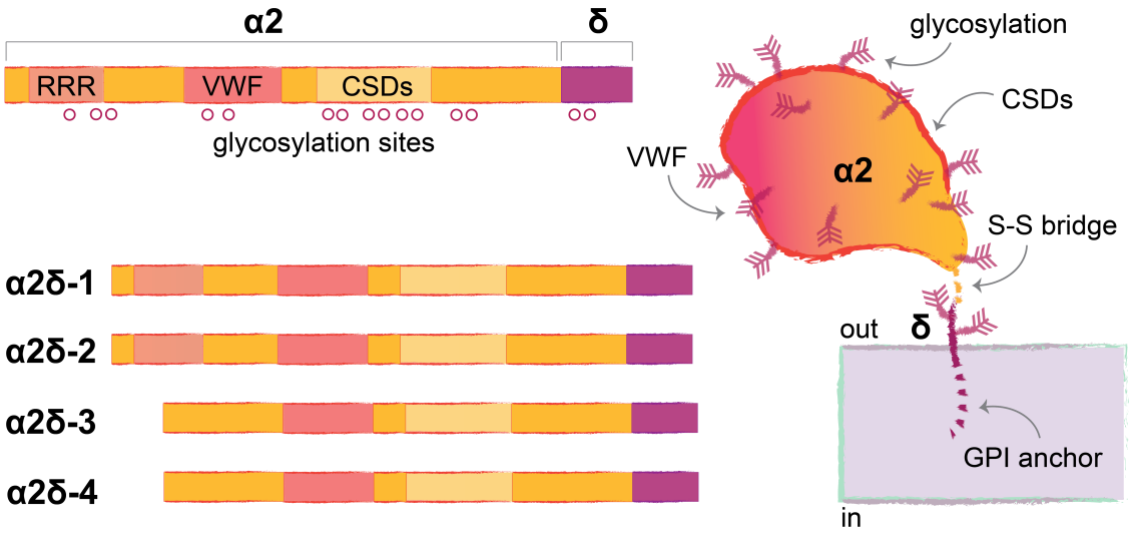

also the potent receptors for a highly prescribed antiepileptic and analgesic, gabapentin (GBP)[5]. Thus, while the influence of α2δ proteins on neurological function is evident, their specific functions within neurons remain obscure.

α2δ-1-3 are highly expressed by neurons in the mammalian brain[6], often concomitantly within most neuronal subtypes. While tools to visualize α2δ isoforms are lacking, mRNA expression profiles show that excitatory neurons of the adult mouse brain

[5] GBP was designed as a GABA-mimetic to target $GABA_A$ receptors, as the name implies, to treat seizures. While it is clinically used for this purpose, as well as to manage chronic pain, it was later discovered that the drug potently bound to α2δ-1 (K_d = 59 nM/L) and α2δ-2 (K_d = 153 nM/L) at the arginine repeats near the N-terminus, and mutation in these amino acids results in loss of efficacy (Gee *et al.*, 1996).

[6] α2δ-4 (*CACNA2D4*) is expressed in peripheral neurons such as in retina, and α2δ-1/2 are expressed in other tissues such as lung, muscle, and osteocytes.

generally express a combination of α2δ-1, α2δ-3, and possibly α2δ-2, while inhibitory parvalbumin^{+} (PV^{+}) neurons seem to express α2δ-2 (Cole et al., 2005; Lein et al., 2007; Dolphin, 2013). As such, α2δ isoforms may differ in function or subcellular localization. However, the commonalities of their protein structure provide intriguing clues as to potential functions.

α2δ molecules each are transcribed as a single gene transcript from their respective genes, *CACNA2D1-4* (see **Figure 1.2** above), post-translationally cleaved into 2 peptides [the α2 (~150 kDa) and δ (17-25 kDa) subunits] and then re-bonded via a disulfide bridge (Dolphin, 2013). After heavy glycosylation, a feature permitting protein-protein interactions, α2δ proteins are transported to the plasma membrane where they are entirely extracellular. Features from the α2 subunit include a Von Willebrand Factor (VWF) domain, a region ~200 residues long important for cell-adhesion to extracellular matrix proteins as well as protein-protein interactions[7]. Within this domain, α2δ proteins contain a motif (known as a metal ion adhesion or MIDAS) that interacts with calcium and magnesium ions and may be important for protein interactions. Upstream of the VWF domain is a sequence of arginine repeats, where GBP is known to bind with high affinity (< 40 nM) (Gee et al., 1996). This sequence may inhibit VWF function (Eroglu et al., 2009). α2δ proteins also have two Cache domains (i.e., chemosensing domains or CSDs). While the function of CSDs in α2δ proteins is entirely unknown, they do play a role in the detection of chemicals, such as glutamate, and in chemotaxis in other molecules of bacteria (Dolphin, 2013). Finally, the δ subunit, which tethers the molecule to the plasma membrane, is predicted to contain only two hydrophilic residues and a glycosyl-phosphatidylinositol (GPI) anchor (Davies et al., 2010). While it is

[7] Other cell adhesion molecules that contain a VWF domain include some integrins, laminins, and collagens.

unclear how α2δ proteins signal across the lipid bilayer without intracellular domains, they may coordinate molecular interactions extracellularly.

α2δ proteins as auxiliary subunits of voltage-gated calcium channels

VGCCs consist of an α1 pore subunit (*CACNA1*) from the Cav1, Cav2, or Cav3 families, classified by their pharmacology and threshold for activation relative to a typical neuronal resting membrane potential (-60 mV): low voltage-activating channels open at hyperpolarized membrane potentials, while high voltage-activating VGCCs open at more depolarized potentials, producing maximal currents at ~ 0 mV (Dolphin and Lee, 2020). Immunoprecipitation of the α1 subunit of the Cav1.1 channel from rabbit skeletal muscle identified several associated molecules, or auxiliary VGCC subunits (Ellis et al., 1988). Intracellular ß auxiliary subunits (*CACNB1-4*), are required to traffic α1 subunits to the plasma membrane (see **Figure 1.3** below), and their interaction with the intracellular α1 C-terminus can modulate channel function (Dolphin and Lee, 2020). In some cases, VGCCs are also accompanied by transmembrane γ subunits[8] (*CACNG1-8*), and it is now appreciated that this family is functionally diverse. Finally, the extracellular α2 and δ subunits contribute to trafficking of high-voltage-activating calcium channels, though they do not influence VGCC gating or kinetics (Barclay et al., 2001b; Dolphin, 2012; Patel et al., 2013; Fell et al., 2016).

It is unclear whether α2δ isoforms interact with specific populations or subtypes of VGCCs endogenously, as work in heterologous systems suggests α2δ proteins traffic VGCC subtypes indiscriminately. As for α2δ proteins, visualization of native VGCCs is unreliable.

[8] Though eight γ proteins were initially categorized as belonging to VGCC auxiliary subunits, several are now known to function in calcium-dependent roles. For example, the molecule called stargazin (*CACNG2*) interacts with AMPA receptors.

Thus, investigations of α2δ-Cav relationships have relied on heterologous expression systems, calcium-dependent physiology, and biochemical studies. As functionally distinct VGCCs have different distributions throughout neuronal compartments, and expression patterns of VGCCs and α2δ isoforms differ across neuronal populations, the potential for diverse α2δ-dependent VGCC functions in neurons is remarkable. With this in mind, I will indicate specific α2δ-Cav interactions from biochemical and functional studies (see **Table 1.1** below).

Figure 1.3 Schematic of the voltage-gated calcium channel complex.

α1 pore subunits (blue) of VGCCs are trafficked to the plasma membrane by ß subunits (purple), which interact with the intracellular C-terminus of the α1 subunits. α2δ proteins (orange gradient) may interact with some VGCCs on the α1 subunit's extracellular face.

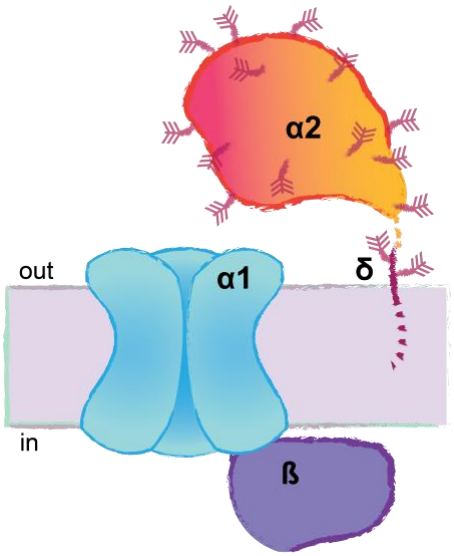

Direct interactions between α2δ proteins with VGCCs have been found by cryogenic electron microscopy of Cav1 or Cav3 channels. Though there is little functional evidence of α2δ protein interactions with low-voltage activated (T-type) VGCCs, single particle analysis of one of these channels (Cav3.1) revealed a density associating with the extracellular region, which was presumed to be the α2δ-1 subunit (Walsh et al., 2009). In another study at higher resolution, analysis of the Cav1.1 channel identified the VWF of α2δ-1 interacting with an extracellular loop of the α1 pore (Wu et al., 2016). Interestingly, this structure also revealed 2 unknown cache domains in α2δ-1, bringing the total to 4, as well as 15/16 predicted glycosylation sites.

Less robust evidence exists for direct interaction between α2δ proteins and Cav2 proteins. Coexpression of α2δ-1 and Cav2.2 in heterologous cells occludes antibody staining of α2δ-1 (Cassidy et al., 2014), implying an extracellular interaction. However, to identify molecules in the vicinity of Cav2.1-3 nanodomains, whole-brain lysate was solubilized (the authors estimated micelles ~ 70 nm in diameter), affinity-purified for the α1 pore subunits, and associated molecules were analyzed by mass spectroscopy (Muller et al., 2010). Unlike the ß auxiliary subunit, which was detected in equimolar abundance with α1 protein (regardless of detergent), α2δ proteins were present at ~10% of the levels of α1 in these preparations (Muller et al., 2010). One interpretation of these results is that, although α2δ proteins exert a profound influence on VGCCs, only few are needed for auxiliary function. Alternatively, α2δ-Cav2 interactions may be transient and/or weak. Notwithstanding, this approach yielded few extracellular matrix proteins in general; as α2δ protein is extracellular, it may be poorly represented in this dataset.

Table 1: Voltage-gated calcium channels (VGCCs)

Gene	***Subtype***	***Classification***	
CACNA1S	Cav1.1	L-type	High-voltage activated channels that associate with α2δ and ß auxiliary subunits
CACNA1C	Cav1.2		
CACNA1D	Cav1.3		
CACNA1F	Cav1.4		
CACNA1A	Cav2.1	P/Q-type	
CACNA1B	Cav2.2	N-type	
CACNA1E	Cav2.3	R-type	
CACNA1G	Cav3.1	T-type	Low-voltage activated channels
CACNA1H	Cav3.2		
CACNA1I	Cav3.3		

Functional studies of α2δ proteins can show modest to severe VGCC phenotypes, depending on cell-type. In heterologous expression systems, such as HEK293 or COS-7 cells, VGCC surface expression is reliant on α2δ proteins (Brodbeck et al., 2002; Held et al., 2020). Neurons, however, show a more moderate trafficking phenotype. In whole-cell recordings from inner hair cells, which predominantly express α2δ-2 and Cav1.3 (Fell et al., 2016), as well as dissociated Purkinje cells (PCs), which express α2δ-2 and predominantly Cav2.1[9], both displayed a ~30% reduction in VGCC current density in the *ducky* mutant (Donato et al., 2006). Likewise, recordings from dorsal root ganglion neurons, which highly express α2δ-1, revealed a 30% reduction in VGCC current density (Patel et al., 2013). Furthermore, these studies found no difference in the activation/inactivation voltage of calcium currents, or alteration of VGCC α1 isoform expression (based on the ratio of current inhibition by subtype-specific toxins), suggesting α2δ proteins impact trafficking of VGCC subtypes indiscriminately.

Does the 30% of VGCCs trafficked by α2δ proteins represent a distinct, functional population? In cholesterol-rich membranes (lipid rafts) prepared from cerebellar homogenates, α2δ-2 concentrates with Cav2.1, while Cav2.1 alone isolates in non-lipid raft fractions (Davies et al., 2006). Thus, α2δ proteins may traffic a subset of VGCCs to lipid raft membranes. As lipid rafts may localize to synaptic specializations (Gil et al., 2006; Suzuki et al., 2011), α2δ proteins may contribute to VGCC localization at synapses and thereby enhance their functional coupling to other synaptically localized effectors.

[9] The "P-type" nomenclature for Cav2.1 stands for "Purkinje."

Voltage-gated calcium channel nanodomains

Many intracellular signaling cascades begin with a common messenger, calcium, which enters via VGCCs on the plasma membrane. Activation of VGCCs by membrane depolarization leads to rapid, local increases of calcium, which last for the duration of channel opening (Nakamura et al., 2015). Because calcium signaling can drive numerous molecular cascades, endogenous calcium buffers and intracellular calcium uptake are required to maintain minimal free intracellular calcium and signaling specificity. In the face of these constraints, fidelity for divergent signaling cascades is partly achieved by close coupling between VGCCs and downstream effector molecules in compartments termed nanodomains (< 100 nm). For example, presynaptic vesicle release is sharply calcium-dependent, and the proximity of VGCCs to calcium-sensitive SNARE molecules can alter the probability of vesicle exocytosis (Nakamura et al., 2015). As prior studies established a role for α2δ proteins in trafficking VGCCs in neurons, investigations to understand α2δ-dependent control of VGCC-effector coupling naturally begun at presynaptic terminals.

In mouse hippocampal cultures, overexpression (OE) of α2δ-1 proteins increases presynaptic VGCC abundance (Hoppa et al., 2012; Schneider et al., 2015). However, beyond this primary conclusion, divergent conclusions have been reached. Hoppa *et al*. reported enhanced vesicle release from α2δ-1 OE neurons, despite reduced calcium influx within these terminals, as measured by calcium imaging. This paradox was explained by tighter coupling between VGCCs and vesicle release machinery, as α2δ-1 OE neurons also had decreased sensitivity to intracellular EGTA buffering (Hoppa et al., 2012). However, a different study expressed fluorescently-tagged Cav2.1 or Cav2.2 in hippocampal cultures and tracked their mobility at presynaptic terminals. When Cav2 constructs were co-expressed

with α2δ-1, VGCC abundance and presynaptic terminal size increased[10]. Furthermore, because the mobility of presynaptic Cav2s was unchanged by α2δ-1, they concluded that VGCCs density was not affected (Schneider et al., 2015). One caveat to both of these studies is the use of overexpression in a neuron population that expresses multiple α2δ isoforms to begin with, which could obscure α2δ-dependent VGCC coupling.

Finally, a recent study has investigated the presynaptic expression patterns of α2δ-1 and Cav2s using antibody labeling of endogenous proteins in hippocampal cultures and superresolution microscopy. Surprisingly, they found that the distribution of α2δ-1 protein does not overlap well with Cav2.1 or Cav2.2. Instead, α2δ-1 has a broader distribution at boutons, with signal peaking between 100-200 nm from the postsynaptic density (PSD)[11], whereas Cav2s are most concentrated closer to the active zone where vesicles are released, between 70-90 nm from the PSD (Held et al., 2020)[12]. Unfortunately, because the available antibodies were incompatible, the authors could not test colocalization of Cav2 and α2δ-1 simultaneously. Thus, although α2δ proteins may influence functional coupling of VGCCs with vesicle release machinery at presynaptic terminals, the mechanism remains unresolved.

Like presynaptic terminals, postsynaptic VGCC nanodomains (see **Figure 1.3** below) are also critical for neuronal signaling functions. For example, PCs of the cerebellum exhibit retrograde endocannabinoid (eCB) signaling, which drives a form of short-term depression known as depolarization-induced suppression of excitation (DSE) (Kreitzer and Regehr, 2001; Brenowitz, 2003; Brown et al., 2003; Brown et al., 2004). The eCB arachidonoylglycerol (2-

[10] While Hoppa *et al.* did not measure terminal morphology after α2δ-1 overexpression, their fluorescent microscopy findings also suggest larger boutons.

[11] It is important to note that, despite the very high signal-to-noise capability of STED microscopy of cultured neurons, the authors show that antibodies against α2δ-1 still label nonspecific background in an α2δ-1 conditional knockout.

[12] In fact, Cav2 localization to presynaptic terminals requires its intracellular C-terminus binding to scaffold molecules such as RIM (Held *et al.,* 2020).

AG) is produced and released from PCs and binds to presynaptic cannabinoid receptors (CB_1Rs), which mediate a short-term decrease in release probability of vesicle from CF terminals (Kreitzer and Regehr, 2001; Liu et al., 2016). Though 2-AG can be produced in several ways, the following is the primary cascade in PCs during DSE, and will be referred to as "eCB machinery" hereafter: depolarization of PCs activates VGCCs, generating calcium influx in the micromolar range (Brenowitz, 2003). In turn, calcium-dependent activation of phospholipase-Cß (PLCß)[13] produces diacylglycerol (DAG), which is then processed by DAGα lipase, generating 2-AG (Uchigashima et al., 2007; Liu et al., 2016).

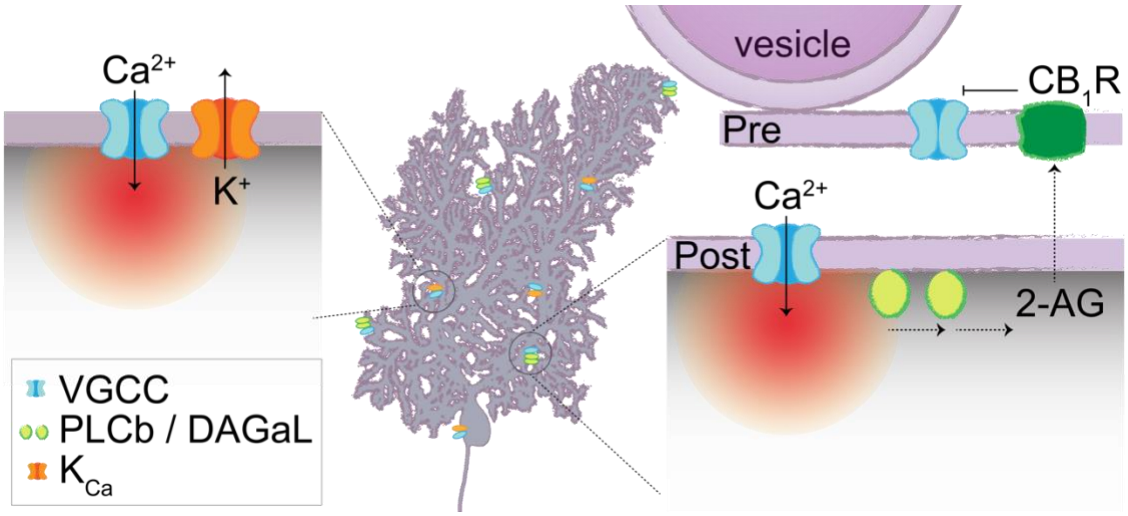

Figure 1.3 Two examples of postsynaptic VGCC nanodomains in PCs.

Left, calcium influx (red) via VGCCs on the membrane activate K_{Ca} channels, which efflux potassium. *Right,* postsynaptic calcium influx (red) via VGCCs activate a molecular cascade involving phospholipase-Cß (PLCß) and DAGα lipase (DAGαL), resulting in retrograde release of arachidonoylglycerol (2-AG) endocannabinoids. 2-AG is an agonist for the cannabinoid receptor type 1 (CB_1R) on presynaptic terminals, which reduces presynaptic probability of release upon activation.

[13] Co-activation of PLCß by mGluR signaling and calcium results in a supralinear production of DAG, which is thought to be physiologically relevant given the reduced requirement for calcium activation Baggelaar MP, Maccarrone M, van der Stelt M (2018) 2-Arachidonoylglycerol: A signaling lipid with manifold actions in the brain. Prog Lipid Res 71:1-17.

As all inputs onto PCs express CB_1Rs, eCB signaling exerts powerful, calcium-dependent control over PC computation. VGCCs and the eCB machinery require nanodomain-type coupling, as eCB signaling can only be disrupted through postsynaptic intracellular application of fast calcium buffering at high concentrations (40 mM BAPTA) (Kreitzer and Regehr, 2001; Brenowitz et al., 2006). Although little is known about whether α2δ proteins influence postsynaptic VGCC nanodomains, eCB signaling is deficient in *ducky* PCs (Wang et al., 2013).

Another well-defined and critical postsynaptic VGCC nanodomain in PCs is calcium-dependent potassium channels (K_{Ca}). Cav2.1 and K_{Ca} channels form clusters (< 40 nm between Cav2.1 and K_{Ca} on average) throughout PC somata and dendrites (Indriati et al., 2013). Together, they function to generate the afterhyperpolarization (AHP) following sodium spikes, ultimately setting spontaneous spike rates (Raman and Bean, 1999; Womack et al., 2004). Current-clamp recordings from *ducky* PCs show a reduction in spontaneous spike frequency (Donato et al., 2006; Walter et al., 2006), though the underlying mechanisms controlling this decrease are unknown. Furthermore, the K_{Ca} channel implicated in driving the AHP, the BK channel (Edgerton and Reinhart, 2003; Niday and Bean, 2021), may directly bind α2δ-1 subunits (Zhang et al., 2018). Thus, α2δ proteins may contribute to VGCC-K_{Ca} coupling, perhaps by direct interaction, to generate the AHP.

Summary of α2δ protein auxiliary functions

As auxiliary subunits to VGCCs in neurons, α2δ proteins modestly contribute to VGCC trafficking based on measurements of total channel abundance on the membrane. As discussed, VGCCs are indispensable for numerous calcium-dependent processes in neurons, many of which require VGCC-effector coupling. There is some evidence in presynaptic terminals that α2δ proteins may participate in this nanodomain organization (Hoppa et al., 2012), though many questions remain. In Chapter 4, we investigated whether α2δ-2 proteins contribute to two distinct postsynaptic VGCC nanodomains, eCB and K_{Ca}, both of which critically influence neurophysiology.

However, recent studies have shed light on new, VGCC-independent roles for α2δ proteins. As discussed in Chapter 3, loss of α2δ proteins can phenotypically differ from VGCC mutants, and distribution of α2δ proteins may not overlap with VGCCs entirely (Held et al., 2020). Since 2009, α2δ proteins have gained recognition for their VGCC-independent roles in excitatory synapse formation. Here, I review some foundational research to provide insight about possible molecular mechanisms relating to this role, though our understanding of α2δ protein function(s), interactions, and signaling is still preliminary.

"In biology, nothing is clear, everything is too complicated, everything is a mess, and just when you think you understand something, you peel off a layer and find deeper complications beneath. Nature is anything but simple." – Richard Preston, *The Hot Zone: The terrifying true story of the origins of the Ebola virus*

Synaptogenesis & synaptogenic molecules

Nearly 100 years ago, some of the earliest efforts to study alignment of pre- and postsynaptic terminals were performed by Ramon y Cajal's student, Fernando Tello y Muñoz, at the neuromuscular junction. He noted that severed peripheral motorneurons could regrow to the original synaptic location and restore functional transmission to the muscle (de Castro, 2016). This suggested that synaptic innervation could be controlled by microscopic landmarks. Indeed, future investigation would show that an extracellular matrix protein, ß2 laminin (a component of the basal lamina), is produced by the target muscle and organizes presynaptic specializations through interactions with VGCCs (Kandel, 2013). It is now appreciated that presynaptic neurons also produce molecular signals to organize postsynaptic structures, for example, agrin from motorneurons. Thus, the accuracy of synaptic alignment requires cooperative molecular signaling from both pre- and postsynaptic terminals.

While much has been learned from the neuromuscular junction, excitatory synapses[14] of the central nervous system (CNS) lack a basal lamina and make tighter, more direct connections (~20 vs. ~50 nm synaptic clefts, respectively) (Yamagata et al., 2003). Furthermore, the high density and variety of synapses in the mammalian brain require a diverse molecular code to orchestrate proper connectivity across brain regions, given the plethora of neuronal types.

In recent decades, dozens of extracellular synaptic proteins categorized as "adhesion molecules" have been identified as critical components of CNS synapses. Adhesion molecules fulfill roles in synaptogenesis to stabilize the synaptic association across the cleft, regulate synaptic strength and efficacy, provide target landmarks for synaptogenesis, or allow

[14] Many of the same principles regarding molecular coding for synapse specificity may apply to inhibitory synapses. However, this dissertation will focus on asymmetric, Gray's type I excitatory synapses for brevity.

for synaptic differentiation of unspecialized membrane between neuronal contacts (Yamagata et al., 2003). At mammalian excitatory synapses, each family of adhesion molecules, consisting of multiple isoforms and splice variants, may also participate in encoding synapse-specificity. Given the extracellular nature of α2δ proteins, their structural features indicating adhesive properties, and their apparent function at synapses (see Table 1.2 for summary), α2δ proteins may become the newest member of the synaptic adhesion molecules (see **Table 2** below).

Table 2: α2δ Protein Synaptogenic Phenotypes

Isoform	***Cell type & manipulation***	***Synaptic phenotype***	***Model organism***	***Author***
α2δ-1	Retinal ganglion cells, OE	i. Increased density of pre- and postsynaptic markers ii. Increased mEPSCs	Mouse	(Eroglu et al., 2009)
	Cortical neurons, OE			(Risher et al., 2018)
	Dorsal root ganglion, OE	Increased mEPSCs		(Park et al., 2016)
	Hippocampal neurons, KO	Unchanged PSD		(Held et al., 2020)
α2δ-2	Inner hair cell, presynaptic KO	i. Reduced synaptic transmission from inner hair cell ii. Mislocalization of postsynaptic AMPARs	Mouse	(Fell et al., 2016)
	Purkinje cell, postsynaptic KO	i. Increased synaptic transmission ii. Aberrant presynaptic innervation		(Beeson et al., 2020)
α2δ-3	Neuromuscular junction, KO	Reduced synaptic transmission	*C. elegans*	(Tong et al., 2017)
	Neuromuscular junction, KO	Altered presynaptic bouton morphology	*Drosophila*	(Kurshan et al., 2009)
α2δ-4	Retinal rods & cones, KO	Dysfunctional synaptic transmission	Mouse	(Wycisk et al., 2006)
Abbreviations:	*OE, overexpression; mEPSC, miniature excitatory postsynaptic currents; PSD, postsynaptic density; KO, knockout; AMPARs, AMPA receptors*			

α2δ receptors in synapse formation

Astrocytes are glia-derived cells that outnumber neurons in the CNS, where they support neuronal health, signal transmission, and connectivity through the promotion of synapse formation. The first investigation clearly demonstrating the role of glia in synaptogenesis used retinal ganglion cell cultures from rats, co-cultured with or without glia (Pfrieger and Barres, 1997). Surprisingly, recordings from neurons cultured in the presence of glia revealed a 70-fold increase in the frequency of spontaneous excitatory postsynaptic currents (sEPSCs) and 5-fold increase in the amplitude of these events, illustrating enhanced synaptic connectivity. Subsequent work identified the molecule responsible for inducing excitatory synapse formation as the astrocyte-secreted glycoprotein, thrombospondin (TSP) (Christopherson et al., 2005). In addition to evidence from *in vitro* systems, TSPs are highly expressed early in brain development and upregulated after ischemia or brain injury, when synaptic reorganization is crucial for restoration of neurological function. However, because TSPs are extracellular matrix proteins, it was suggested that they might be ligands for neuronal receptors that drive synaptogenesis.

Based on the sequence of a minimal fragment of TSP that could induce synaptogenesis in retinal ganglion cultures, it was inferred that TSPs likely bound to a VWF domain. Integrins, a family of cell-adhesion molecules containing VWF domains, were shown not to impact TSP-induced synaptogenesis. Therefore, researchers turned to another VWF-containing molecule expressed in neurons: the α2δ proteins. Using immunoprecipitation binding assays as well as a combination of immunohistochemistry and sEPSC recordings in retinal ganglion cultures after knockdown or overexpression of α2δ-1 proteins, Eroglu *et al.,* identified a novel role for this protein family in driving TSP-induced

excitatory synapse formation as the neuronal TSP receptors (Eroglu et al., 2009)[15]. Importantly, although α2δ proteins are classified as auxiliary subunits to VGCCs, TSP-induced synaptogenesis persisted in the presence of VGCC blockers, indicating that α2δ-mediated synaptogenesis occurred independent of its role in VGCC signaling. Consistent with this, studies in *Drosophila* neuromuscular junction showed that although loss of VGCC pore-forming proteins did not impact presynaptic terminal bouton formation, α2δ-3 deletion (the only α2δ isoform expressed in this organism) produced aberrant boutons by electron microscopy (Kurshan et al., 2009).

Like TSP, neurons highly express α2δ-1 and α2δ-2 throughout early brain development and upregulate α2δ expression after injury or chronic pain, suggesting a role in circuit remodeling (Li et al., 2004). In fact, transgenic mice that overexpress α2δ-1 have enhanced miniature EPSC frequency (Eroglu et al., 2009; Park et al., 2016). Although it is still unclear how α2δ proteins transmit synaptogenic signals, recent work from mouse cortical neurons suggests that the α2δ-1 extracellular domain is critical in fully rescuing excitatory synapse formation in single cells in an α2δ-1 KO animal[16] (Risher et al., 2018). Thus, in addition to an implied adhesion role of α2δ proteins, this single-cell rescue demonstrates that α2δ-1-mediated synaptogenesis is driven via postsynaptic mechanisms at these synapses.

Recent superresolution microscopy studies from hippocampal neuronal cultures contradict findings that suggest a synaptogenic role for α2δ-1, and question this isoform's postsynaptic locus of action. In these studies, deletion of α2δ-1 failed to change PSD95 (a

[15] Eroglu *et al* also showed that GBP inhibits excitatory synapse formation by blocking TSP interaction with the α2δ-1 VWF domain, preventing the formation of new synapses but not 'dissolving' stabilized, mature synapses.

[16] In these experiments, authors tested the possibility that α2δ-1 transforms synaptogenic signals by activating intracellular Rac1. Thus, for full rescue of excitatory spine formation in α2δ-1 KO mice, individual cells were transfected with the α2 extracellular subunit and a fast-cycling Rac1 mutant to promote Rac1 activation.

major postsynaptic scaffolding protein) expression or alter synapse morphology (Held et al., 2020). As there was no investigation of synaptic density after loss of α2δ-1 in these experiments, it is possible that remaining synapses were not dependent on α2δ-1. Furthermore, the authors note that in control neurons, postsynaptic expression of α2δ-1 was markedly less than presynaptic terminal expression. Given the lack of α2δ antibody specificity[17] used in these studies, high off-target labeling of presynaptic proteins was possible. Hence, more detailed investigations of the roles of α2δ isoforms in synaptogenesis are warranted.

Potential α2δ protein binding partners

Much is yet to be learned about how α2δ proteins mechanistically promote excitatory synaptogenesis. Many different interacting molecules have been proposed, though few of these studies have been replicated. One theory suggests that α2δ-1 promotes the synaptic localization or sensitivity of glutamatergic NMDA receptors, thus facilitating the growth of excitatory postsynaptic spines (however, see (Adesnik et al., 2008). This hypothesis is supported by evidence that NMDA receptor-mediated currents are enhanced when neurons are grown in TSP-containing media, and decreased when α2δ-1 is deleted (Christopherson et al., 2005; Risher et al., 2018). However, not all excitatory synapses express NMDA receptors, even in early development; for example, the climbing fiber (CF) to PC synapse.

Neurexins (NRXs) have also been implicated in α2δ protein function. In mammals, presynaptic NRXs interact with postsynaptic neuroligins (NLGs; which also have a VWF domain), as important transsynaptic adhesion molecules (Tsetsenis et al., 2014). Deletion of

[17] Commercial α2δ antibodies are knockout verified and specific for western blot but show high background in knockout tissue immunohistochemistry.

NRX affects presynaptic vesicle release, and loss of NLGs impacts synaptic alignment and function (Missler et al., 2003; Chanda et al., 2017).

Nevertheless, two studies have suggested a relationship between NRX and α2δ proteins. In *C. elegans*, Tong *et al.* found that NRXs immunoprecipitated with α2δ-3, and their coexpression reduced calcium currents from Cav2.2 (Tong et al., 2017). Notably, NRXs are expressed postsynaptically in *C. elegans*; thus, the authors propose a soluble form of NRX is necessary for α2δ-3-mediated presynaptic calcium regulation. In a separate study, fluorescent calcium indicators in hippocampal neuronal cultures indicated facilitation of presynaptic Cav2 currents by expression of NRX and α2δ proteins (Brockhaus et al., 2018). Furthermore, co-expression of NRX and α2δ-1, but not α2δ-3, in tSA201 cells confirmed enhanced calcium influx by Cav2.1 via whole-cell recordings. However, follow-up immunoprecipitation assays by Brockhaus *et al.* failed to show specific binding by α2δ proteins, leading the authors to conclude that any interactions between α2δ and NRXs are not stable[18], and perhaps only transient during adjustments of synaptic strength.

α2δ proteins (~170 kDa) are even larger than NRX's known binding partner, NLGs (~120 kDa), and they also contain a VWF domain located near the N-terminus. Thus, a transsynaptic adhesion role for α2δ proteins, either with NRX or an unidentified binding partner, is feasible. However, pan-deletion of NRX isoforms from synapses in culture or *in vivo* does not alter synapse morphology (Missler et al., 2003) indicating that α2δ proteins function independent from NRX to mediate synaptogenesis. If immunoprecipitation assays for α2δ proteins are unreliable, as Brockhaus *et al*. report, functional comparison of single and double mutants for α2δ and NRX proteins may provide insight into this potential

[18] Brockhaus *et al*., also demonstrated that α2δ proteins bound to the Fc-coupled beads rather than NRX, resulting in unspecific labeling. They mention that this may also pose as a caveat to Tong *et al*.'s findings and immunoprecipitation binding of α2δ proteins in general.

relationship (e.g., whether α2δ-induced synaptogenesis by TSP is reliant on expression of NRX).

Are voltage-gated calcium channels required for synapse formation?

In both *Drosophila* and mice, complete elimination of Cav2 channels did not alter synaptic morphology or synaptic protein abundance (such as PSD95), by electron or superresolution microscopy (Kurshan et al., 2009; Biederer et al., 2017; Held et al., 2020). Presynaptic terminals of most excitatory neurons predominantly express Cav2; therefore, these findings indicate that α2δ proteins function independently of Cav2 channels to promote excitatory synapse formation. Additionally, complete block of calcium influx by culturing neurons in a cocktail of VGCC subtype-specific blockers did not affect synapse formation (Eroglu et al., 2009; Held et al., 2020), and calcium imaging of neurons grown in TSP while overexpressing α2δ-1 did not show increased dendritic calcium influx (Eroglu et al., 2009). Thus, calcium signaling is not required for excitatory synapse formation either. In fact, the observation that α2δ membrane expression is independent of Cav2s in heterologous systems and presynaptic terminals (Kurshan et al., 2009; Held et al., 2020) implies a VGCC-independent role. Still, the possibility remains that other Cav channels (low-voltage activating, for example), alone or in association with α2δ proteins, may provide molecular landmarks that could nucleate sites for synapse formation (Biederer et al., 2017).

Summary of α2δ proteins as synaptogenic molecules

α2δ proteins are now recognized as synaptogenic molecules, independent from their VGCC auxiliary functions. But our understanding of many important mechanistic and functional details remains unanswered. For example, little is known about whether α2δ isoforms are functionally redundant, as most studies have focused on the synaptogenic function of α2δ-1. Another unresolved question is whether α2δ isoform distributions differ in neurons (pre- vs. postsynaptic).

While one study discussed above demonstrated a postsynaptic locus for α2δ-1 protein's function in synapse formation, this work was unpublished at the time we began our investigations of the synaptogenic role of α2δ-2 in 2017. Many studies of α2δ proteins have utilized excitatory neurons, such as hippocampal or cortical pyramidal neurons, which express multiple α2δ isoforms. However, we used inhibitory Purkinje cells (PCs) of the cerebellum, as they solely rely on the α2δ-2 isoform, to investigate the effect of *CACNA2D2* deletion on excitatory innervation of PCs. Thus, in Chapter 3, we provide evidence for postsynaptic α2δ-2 in regulating excitatory synapse formation, and true to the unpredictable and enigmatic tale of these molecules, our findings are surprising.

CHAPTER 2: MATERIALS AND METHODS

Animals

Cacna2d2 knockout mice (*Cacna2d2*^{tm1Svi}, MGI = 3055290; generously supplied by Drs. Sergey Ivanov and Lino Tessarollo) were obtained as cryopreserved sperm and re-derived via *in vitro* fertilization on a C57B/6J background. Breeding mice were kept heterozygous, and genotyping was performed using the following primers: forward 5'-ACTGGTGGGCATCTTACAGC-3', reverse mutant 5' -AAAGAACGGAGCCGGTTG-3', reverse wildtype 5'-TGTTAGCGGGGAGGTCACTA- 3'. This produced a ~700 bp product from the wildtype allele and a ~550 bp product from the mutant allele. Mice were born in the Mendelian ratio of 1:2:1; with WT mice having two copies of the intact *Cacna2d2* gene, and KO mice as homozygous mutants. Because ~50% of KO mice die prematurely (Ivanov et al., 2004), all experiments used male and female mice between p21-p30, when CF-PC synapses have reached maturity, but before significant loss of KO mice.

Cacna2d2 deletion was validated, and *Cacna2d* isoform abundance were measured, using quantitative PCR from fresh-frozen tissues. Regions of the inferior olive (IO) and the Purkinje cell layer (PCL), including the proximal molecular layer, were microdissected by laser capture for pre- vs. postsynaptic comparative analysis. Briefly, mice were deeply anesthetized by inhalation of 4% isoflurane followed by injection of 0.8 ml of 2% avertin i.p. (Sigma-Aldrich) and rapidly decapitated. Brains were rapidly dissected, mounted in OCT medium (Tissue-Tek) on dry ice, and placed at -20°C for cryosectioning. 25 µm coronal sections from cerebellum and brainstem were collected on RNase-treated PEN membrane slides (Zeiss). Slides were then dehydrated through a succession of EtOH rinses (70% EtOH 30 seconds, 100% EtOH 30 seconds), and nuclei stained using 1 mg/mL Cresyl Violet in 100% EtOH (1 minute). IO and PCL regions were identified based on anatomic criteria, and isolated using laser microdissection (Zeiss). Samples were resuspended in 20 µl QIAzol Lysis

Reagent (Qiagen) for 20 minutes at RT and stored at -80°C. RNA isolation and qPCR were performed by the Oregon Health & Science University Gene Profiling/RNA and DNA Services Shared Resource. In brief, RNA was isolated using the Trizol/RNeasy hybrid protocol with QIAcube automation. SuperScript™ IV VILO™ Master Mix (Invitrogen) was used for reverse transcription with 636 pg of input RNA per 20 µl reaction. Following reverse transcription, cDNA was quantified and normalized for 7500ng of cDNA input for pre-amplification in 14 PCR cycles. A 1:4 dilution of the pre-amp reaction was used as input for qPCR. The TaqMan Universal master mix (Life Technologies) was used for the PCR reaction, using a single master mix per TaqMan probe set for *Cacna2d1* (Mm00486607_m1), *Cacna2d2* (Mm01230564_g1), *Cacna2d3* (Mm00486641_m1), *Cacna2d4* (Mm01190080_m1), and *ACTB* (Mm04394036_g1) as the endogenous control. Data were acquired using Applied Biosystems QuantStudio 12K Flex Software v1.2.2 (Life Technologies) with settings set to default. Measurements are reported as either ΔCt values (difference in cycle time for gene of interest relative to ACTB, in which a higher ΔCt indicates lower relative expression) or mean fold difference, as determined by $2^{\wedge\text{-(Ct target – Ct ACTB target) – (Ct reference – Ct ACTB reference)}} \pm$ SEM.

Mice were maintained in facilities fully accredited by the Association for Assessment and Accreditation of Laboratory Animal Care and veterinary care was provided by Oregon Health & Science University's Department of Comparative Medicine. All animal care and experiments were performed in accordance with state and federal guidelines, and all protocols were approved by the OHSU Institutional Animal Care and Use Committee.

Immunohistochemistry

Following deep anesthesia as described above, p21 *Cacna2d2* KO and WT littermates were transcardially perfused with 5 ml phosphate-buffered saline (PBS) followed by 4% paraformaldehyde-PBS (PFA-PBS). Mice were decapitated, and brains were removed and post-fixed for 24 hrs. in 4% PFA-PBS. Cerebella were cut in sagittal sections at 50 μm on a vibratome and stored in PBS at 4°C. Sections containing vermis lobe VI were permeabilized with 0.4% Triton-PBS containing 10% normal goat serum for 1hr at room temperature. For VGLUT2 puncta, slices were stained with mouse anti-Calbindin 1:20 (Neuromab #73-452) and guinea pig anti-VGLUT2 1:200 (Synaptic Systems #135404) at 4°C overnight. For BK localization, slices were stained with goat anti-Parvalbumin (Swant #PVG-213; 1:1000) and mouse anti-BK (Neuromab #73-022; 1:500) overnight at 4°C. After rinsing, corresponding fluorescently-labeled secondaries (Invitrogen) were applied at 1:400 and glass coverslips were mounted on glass slides with Fluoromount G (Sigma-Aldrich).

To image VGLUT2$^+$ synapses, 6 μm z-stack images from the vermis lobe VI were acquired at 0.2 μm intervals with a Zeiss LSM780 laser scanning confocal microscope at 40x magnification and 1024 x 1024 pixel density using ZEN software. This produced images of the entire thickness of the molecular layer, including the PC somata. Images were then analyzed in FIJI/ImageJ. VGLUT2$^+$ puncta distribution/density were quantified from maximum projection images as distinct VGLUT2$^+$ puncta of at least 0.2 μm^2, after subtracting the background for increased contrast. For each punctum, the y-distance from the top of the PC layer to the terminal was measured. Per image, a minimum of 100 μm of linear PC layer was quantified. VGLUT2$^+$ puncta distributions were then binned into 10 μm distances. VGLUT2$^+$ puncta size and a second measure of density (from whole volume of tissue) were calculated using a masking feature in FIJI/ImageJ that captures puncta between 0.1-5μm^2, and this was normalized to the length of PCL imaged to produce a measure of

density per μm of PCL. Punctum distribution, density and size data were averaged from 2-3 sections/animal, using 5-6 animals of each genotype. Slides were coded prior to imaging, and image acquisition and analysis were performed by investigators blinded to genotype. Sections were stained side-by-side with the same antibody mixtures, and imaging parameters were kept constant between samples.

BK membrane expression was imaged using 63x oil immersion lens on a LSM980 microscope with ZEN software. ~7 μm z-stack images of primary PC dendrites were acquired at 0.15 μm intervals using the PV channel at 4.5 x zoom with 680 x 680 pixel resolution. Airyscan images were processed using default settings in ZEN. Quantification of membrane localized BK puncta was done by a separate researcher, blinded to genotype, using the most transverse section of dendrite from each z-stack. For presentation, images were processed in Fiji/ImageJ, illustrating 0.45 μm maximum projections, and the panel was assembled using Adobe Photoshop.

Slice Preparation for Electrophysiology

KO or WT littermates were deeply anesthetized as described above, and transcardially perfused with ice-cold sucrose-based solution containing (mM): 87 NaCl, 2.5 KCl, 1.25NaH_2PO_4, 0.4 ascorbate, 2 Na pyruvate, 25 D-glucose, 25 $NaHCO_3$, 75 Sucrose, 7 $MgCl_2$, 0.5 $CaCl_2$ (osmolarity adjusted to 300-305 mOsm) and equilibrated with 95% O_2 and 5% CO_2 gas mixture. Acute 300 μm sagittal slices were cut from cerebellum using a vibratome (VT1200, Leica Microsystems), and incubated for 30 minutes in standard artificial cerebral spinal fluid (aCSF) at 34°C. External solution contained (in mM): 125 NaCl, 25 $NaHCO_3$, 1.25 NaH_2PO_4, 3 KCl, 25 Dextrose, 2 $CaCl_2$, 1 $MgCl_2$ (osmolarity adjusted to 300 mOsm) and was continuously perfused via roller pump.

PCs from the vermis, lobe VI, were identified by soma size and location in the PC layer using live infrared differential contrast microscopy on an upright Olympus microscope. All cells were first recorded in voltage clamp mode, where a hyperpolarizing step of -10 mV was applied to monitor cell capacitance, series resistance and input resistance. Series resistance was not compensated; cells with series resistance >10 MΩ, or a >2 MΩ change in series resistance over the course of the experiment, were excluded. Signals were amplified with a MultiClamp 700B (Molecular Devices) amplifier and pipette capacitance was compensated for using MultiClamp software. Signals were low-pass filtered at 6 kHz and sampled at 10 kHz, and digitized with a National Instruments analog-to-digital board. Some spontaneous spike recordings were sampled at 50 kHz. All recordings were acquired and analyzed using IgorPro-based (Wavemetrics) software. All recordings were performed at room temperature except for spontaneous spike experiments, in which an in-line heater was used to maintain 36°C bath temperature.

Voltage clamp experiments

Whole-cell recordings were obtained using 1-3 MΩ borosilicate glass pipettes filled $CsCl_2$-based internal solution. For CF EPSC recordings, the internal solution contained (in mM): 100 $CsMeSO_4$, 35 CsCl, 15 TEA-Cl, 1 $MgCl_2$, 15 HEPES, 0.2 EGTA, 2 ATP-Mg, 0.3 TrisGTP, 10 phosphocreatine, and 2 QX-314, pH 7.3 adjusted with CsOH (osmolarity adjusted to 295 mOsm). For DSE experiments, internal recipe was made in triplicate, equally divided and 10, 2 or 0.2 mM EGTA was added to each third before adjusting pH and osmolarity. In addition to blocking inhibition, 0.2-0.5 μM NBQX (Tocris) was included in external aCSF to maintain voltage clamp of CF-mediated excitatory postsynaptic currents (EPSCs).

PCs were held at -70 mV and brief hyperpolarizing steps (-10 mV) were delivered to monitor PC access and input resistance preceding each CF-evoked EPSC. EPSCs were evoked using theta or monopolar glass electrode stimulation in the granule cell layer (0.1 ms, 0-100 V square pulses; 0.1 or 0.05 Hz stimulation frequency), placed ~50 μm from the PC, and the stimulation electrode position was adjusted as needed to obtain a CF response. CF responses were identified as large all-or-none EPSCs that appeared during incremental increases in stimulation intensity, with paired-pulse depression when stimulated with 2 pulses 50 ms apart. Ten CF EPSC trials were averaged, and these averages were used to determine peak amplitude, 20-80% rise time and tau of decay (from single-exponential fits of the EPSC decay). Then, ten paired-pulse responses with an inter-stimulus interval of 50 ms were collected, followed by 10 Hz trains of CF stimulation or drug wash-in experiments. For DL-TBOA experiments, baseline EPSCs were acquired at 0.05 Hz before 50 μM DL-TBOA (Tocris) was added to the bath. For kynurenic acid (KYN) experiments, aCSF excluded NBQX and PCs were held at -20 mV to maintain voltage-clamp during 0.1 Hz CF stimulation. After acquiring baseline EPSCs, 1 mM KYN (Sigma-Aldrich) was added to the

perfusate. Quantification of EPSC peak amplitude and tau of decay from drug wash-in experiments used averages from 10 sweeps prior to wash-on compared to 10 sweeps after 10 minutes of exposure to drug (For KYN effect: $(EPSC_{Control} - EPSC_{KYN}) * 100$; For TBOA effect: $(\tau_{TBOA} - \tau_{Control}) * 100$). For asynchronous EPSC (aEPSC) experiments, aCSF was composed of 1.3 mM Sr^{2+} in replacement of Ca^{2+}, 3.3 mM Mg^{2+}, and NBQX was omitted. PCs were held at -70 mV and CFs were stimulated at 0.05 Hz. ~10 trials were used for quantification of aEPSCs, which were sampled from a 500 ms window starting at 150 ms from CF stimulation, and selected manually. For data presentation, aEPSC traces were off-line box-filtered at 1 kHz. To estimate the readily releasable pool, cumulative CF response amplitudes were plotted, and the last third of the train was fit with a linear regression that was extrapolated to time 0 Schneggenburger et al. (1999).

For DSE experiments, PCs were held at -70 mV while climbing fiber-mediated EPSCs were evoked using a monopolar glass electrode in the granule cell layer. After obtaining 2 minutes of baseline responses at 0.2 Hz, a depolarizing voltage step to 0 mV of 1 s, 500 ms or 250 ms duration was delivered to induce DSE, after which PCs were returned to -70 mV and 0.2 Hz stimulation was continued. DSE plasticity is acute, and most synapses recover back to baseline EPSC amplitudes within < 60 seconds (Brenowitz, 2003). As a small amount of "run down" was routinely observed in the evoked CF-mediated EPSC amplitude, DSE inclusion criteria required EPSC amplitudes to return to 80% baseline within 2 minutes post-stimulation (opposed to "stepping" to decreased amplitude without recovery). A minimum of 5 minutes were waited between DSE inductions, and step length was randomized throughout experiment. Series resistance was not compensated; cells with series resistance >10 MΩ, or a >2 MΩ change in series resistance over the course of the experiment were excluded.

For analysis, EPSC amplitudes were binned every 10 seconds (2 traces) and normalized to the 1 minute of baseline immediately proceeding the depolarizing step. The 'magnitude of DSE' (e.g. Figure 2E) is based on the average of EPSC amplitude 5 and 10 s after the depolarizing step. Example traces shown are from 5 s after the depolarizing step. A minimum of 3 mice per genotype were used for each manipulation, with no more than 2 cells/treatment coming from one mouse. For data presentation, EPSC traces were off-line box-filtered at 1 kHz in Igor64 software.

Current clamp experiments

For CF evoked complex spikes, internal solution contained (in mM): 135 K-gluconate, 10 HEPES, 10 NaCl, 1 $MgCl_2$, 0.1 BAPTA, 0.1 $CaCl_2$, 2 ATP-Mg, and 10 phosphocreatine, pH 7.28 adjusted with KOH (osmolarity adjusted to 289 mOsm). PC resting membrane potential was measured by holding the cell in zero current mode, then a small amount of bias current (approximately -130 pA) was injected to keep the cell near -60 mV for complex spike and current step experiments. Bridge balance was applied to compensate for pipette and series resistance throughout the recording. First, CFs were stimulated at 0.1 Hz and 10 consecutive sweeps of evoked complex spikes were recorded. Then with CF stimulation off, 500 ms steps of current injection from -200 pA– 1 nA were delivered at least 5 times per step. Cells were returned to voltage clamp mode to assess recording stability. For complex spike analysis, sweeps were averaged to measure the initial spike amplitude and rise rate. Spikelets were classified as rapid depolarizations (>1000 V/s) that reached +20 mV from baseline, from which spikelet trough-to-peak amplitudes were measured. Area under the curve was measured by integrating the trace during the first 100 ms following stimulation.

For spontaneous spike experiments, internal solution contained (in mM): 120 KCH_3SO_3, 10 HEPES, 10 NaCl, 2 $MgCl_2$, 0.5 EGTA, 4 ATP-Mg, 0.3 Tris-GTP, and 14 phosphocreatine, pH 7.35 adjusted with KOH (osmolarity adjusted to 293 mOsm). A stock of EGTA solution was added to aliquots of internal, to increase [EGTA] to 5mM as needed. Synaptic inhibition was achieved with 10 μM SR95531 (Tocris) and 10 μM NBQX (Tocris), and recordings were made at 36°C using an in-line heater. PCs in whole-cell mode from vermis lobe VI were first held in voltage clamp mode to monitor access series and input resistance before switching to current clamp. Changes in access were corrected with bridge balance using Multiclamp software. For increased action potential waveform resolution, some current clamp experiments were sampled at 50 kHz.

Spontaneous spikes from tonically firing PCs with < 400 pA holding current and < 10 MOhm series were analyzed using the Igor64 Neuromatic tools. Firing frequency data was collected from 10 seconds of recording, which yielded ~100-500 spikes. Action potential properties were assessed by averaging 50 consecutive spikes. Afterhyperpolarization (AHP) amplitude was measured as the difference between the threshold voltage (V_{thres} = depolarization rate >10 V/s) and the minimum voltage reached within 5 ms of spiking. All current clamp data was taken at least 3 minutes after break-in to allow time for internal solution to dialyze. Spike traces were box filtered for data visualization, and phase plane plots were made using Igor64.

NEURON Computational PC Model

CF simulations were performed with NEURON version 7.7.0, using source code generously supplied by Dr. Michael Häusser (Roth and Häusser, 2001). The following model parameters were kept constant across all simulations: R_m = 120.2 kΩcm^2, C_m = 0.64 μF/cm^2 and a residual uncompensated series resistance of 1 MΩ. Because the Model is based on recordings and dimensions of a p21 rat PC (Roth and Häusser, 2001), we normalized our WT measurements for CF distribution to the model cell as control, and adjusted the dendritic innervation by KO CFs based on our VGLUT2$^+$ distribution as a relative decrease in length of coverage (i.e. 0.7x CF length of control). CF EPSCs were simulated using 500 inputs of 1 nS peak conductance (simulated as the sum of two exponentials for rise and decay) with a reversal potential of 0 mV and a constant density per dendritic length distribution. Simulation time step was 10 μs for integration. Waveforms were created in IgorPro8 from simulation output to measure EPSC decay time constants by fitting with a single exponential.

Transmission Electron Microscopy (TEM)

Animals were deeply anesthetized with isoflurane and avertin, as described above, and then transcardially perfused with 10 ml ice-cold heparin (1k usp per ml; Novaplus) followed by freshly prepared 2% glutaraldehyde/2% paraformaldehyde in 0.1M PB solution filtered with #3 filter paper (VWR) and pH to 7.4. Brains were dissected, cerebella were blocked, and post-fixed for 30 minutes in 4% paraformaldehyde. Tissue was transferred to 0.1 M PB for storage at 4°C and 40 μm sagittal slices of vermis lobe VI were made using a Leica microtome. Slices were collected in separate wells to assure TEM would be from slices >100 μm apart. PFA, Glutaraldehyde and microtome blades were all from Electron Microscopy Sciences (EMS).

Tissue samples were coded before processing for TEM by a blinded investigator. Briefly, sections were incubated in 1% osmium tetroxide in PB for 30 minutes, dehydrated through a graded series of ethanols, placed into propylene oxide for 30 min, and then placed in 1:1 propylene oxide:EMBed resin (EMS) rotating at room temperature overnight. Sections were then incubated in 100% resin for 2 hrs, embedded between sheets of Aclar plastic, and incubated at 60°C for 48 hrs. Cerebellum sections were then glued to resin blocks and ultrathin sections (50 nm) were collected onto 400 mesh copper grids (EMS). The ultrathin sections were then counterstained with uranyl acetate and Reynolds lead citrate and examined using a FEI Tecnai 12 electron microscope (Hillsboro, OR) and images were captured using an Advanced Microscopy Techniques digital camera.

CF terminals were imaged from the most highly innervated region of the molecular layer (20-60 μm from PC somata) and identified at 6800x magnification by the following criteria: proximity (<3 μm) to PC primary dendrites, dense-packing of round vesicles, and when synaptic contacts were present, asymmetric Gray's type-1 excitatory synaptic markers. Images were taken at 18500x magnification and CF terminals with clearly delineated

membranes that met the criteria described above were analyzed using Fiji/ImageJ software by a separate blinded investigator. Terminal area, total SV density, the length and number of synaptic contacts made by each terminal (as determined by the opposing postsynaptic density), as well as the number of SVs within 100 nm of each synaptic contact as a proxy for the readily releasable pool were measured. Quantifications from ~10-15 CF images/animal were averaged (n = animal).

Statistics

Data was tested for Gaussian distribution using the Kolmogorov-Smirnov normality test with Dallal-Wilkinson-Lillie for P value; normality was tested using Shapiro-Wilk test for smaller data sets (e.g., BK membrane density). In all experiments, use of male and female mice were noted. As no differences were apparent in our measurements, both sexes were grouped.

Differences between genotypes in VGLUT2+ puncta distribution and TEM total synaptic contacts/terminal were tested for significance using Kolmogorov-Smirnov test. For other nonparametric data, the Mann-Whitney test was used (i.e. CpS spikelet number). Immunofluorescence, TEM, and electrophysiology data with normal distributions were analyzed using Student's t-tests. Normalized and cumulative amplitude responses during repetitive CF stimulation were compared between genotypes using Multiple t-tests with Holm-Sidak correction. The difference in magnitude of DSE between the WT 250 ms depolarization step condition and other groups were compared using a one-way ANOVA with Dunnett's correction for multiple comparisons. For spontaneous spike data, student's unpaired t-tests were used for spike frequency comparison between WT and KO. In experiments using 5 mM EGTA, only AHP amplitude was significantly different (measurements, such as coefficient of variation of inter-spike interval, were not different). For this data, a one-way ANOVA with Fisher's LSD was used to compare all groups to WT 0.5 mM EGTA condition.

For morphology data, multiple images per animal were averaged where n = # mice, and compared using Student's t-test. For electrophysiology, all experiments utilized > 3 animals per genotype, where n = # cells. Data were graphed in Prism GraphPad version 8 and are reported as the mean ± SEM. *$p<0.05$, **$p<0.01$, ***$p<0.001$, ****$p<0.0001$.

CHAPTER 3: ALPHA2DELTA-2 PROTEIN CONTROLS STRUCTURE AND FUNCTION AT THE CLIMBING FIBER TO PURKINJE CELL SYNAPSE

Kathleen A. Beeson[1,2], Ryne Beeson[3], Gary L. Westbrook[4], Eric Schnell[2,5,*]

1 Neuroscience Graduate Program, Oregon Health & Science University, Portland, OR, 97239; 2 Department of Anesthesiology and Perioperative Medicine, Oregon Health & Science University, Portland, OR, 97239; 3 Department of Aerospace Engineering, University of Illinois at Urbana-Champaign, Urbana, IL, 61801; 4 The Vollum Institute, Oregon Health & Science University, Portland, OR, 97239; 5 Operative Care Division, Portland VA Health Care System, Portland, OR, 97239

Beeson, K., Beeson, R., Westbrook, G., & Schnell, E. (2020). "alpha2delta-2 protein controls structure and function at the climbing fiber to Purkinje cell synapse." *Journal of Neuroscience* 40(12): 2403-2415

Acknowledgments

This material was supported in part by the Department of Veterans Affairs, Veterans Health Administration, Office of Research and Development, Biomedical Laboratory Research and Development Merit Review Award I01-BX002949 (ES), a Department of Defense CDMRP Award W81XWH-18-1-0598 (ES), NIH T32NS007466 (KAB), NIH R01-NS080979 (GLW), NINDS 1R21NS102948 (IK/ES), NIH P30NS061800 (Dr. Sue Aicher), and OHSU Innovation Fund (ES) awards. The electron microscope was purchased with funds from the Murdock Charitable Trust awarded to Dr. Aicher.

We thank Dr. Stefanie Kaech-Petrie of the OHSU Advanced Light Microscopy Core for assistance with imaging; Dr. Gail Mandel and Dr. John Sinnamon for expertise and use of laser capture equipment; the OHSU Gene Profiling/RNA and DNA Services Shared Resource for support with qPCR experiments; and Dr. Sue Aicher, James Carroll, and Jo Hill for the electron microscopy expertise. We would like to acknowledge Drs. Sergey Ivanov and Lino Tessarollo for generously providing the *Cacna2d2* knockout mice; Drs. Michael Häusser and Arnd Roth for necessary files and permission to use the NEURON model; and research associates Arielle Isakharov and Ada Zhang for outstanding technical support. We also thank Dr. Christopher Vaaga and Dr. Laurence Trussell for constructive comments on the manuscript. The contents of this manuscript do not represent the views of the U.S. Department of Veterans Affairs or the United States Government.

Abstract

α2δ proteins (*Cacna2d1-4*) are auxiliary subunits of voltage-dependent calcium channels that also drive synapse formation and maturation. Because cerebellar Purkinje cells (PCs) predominantly, if not exclusively express one isoform of this family, α2δ-2 (*Cacna2d2*), we used PCs as a model system to examine roles of α2δ in excitatory synaptic function in male and female *Cacna2d2* knockout mice. Whole-cell recordings of PCs from acute cerebellar slices revealed altered climbing fiber (CF)-evoked complex spike generation, as well as increased amplitude and faster decay of CF-evoked excitatory postsynaptic currents (EPSCs). CF terminals in the KO were localized more proximally on PC dendrites, as indicated by $VGLUT2^{+}$ immunoreactive puncta, and computational modeling demonstrated that the increased EPSC amplitude can be partly attributed to the more proximal location of CF terminals. In addition, CFs in KO mice exhibited increased multivesicular transmission, corresponding to greater sustained responses during repetitive stimulation, despite a reduction in the measured probability of release. Electron microscopy demonstrated that mutant CF terminals had twice as many vesicle release sites, providing a morphologic explanation for the enhanced glutamate release. Though KO CFs evoked larger amplitude EPSCs, the charge transfer was the same as wildtype as a result of increased glutamate re-uptake, producing faster decay kinetics. Together, the larger, faster EPSCs in the KO explain the altered complex spike responses, which degrade information transfer from PCs and likely contribute to ataxia in *Cacna2d2* KO mice. Our results also illustrate the multidimensional synaptic roles of α2δ proteins.

Introduction

Synapses are indispensable to neural circuit function, yet our understanding of synapse formation and physiology in health and neurological disease is incomplete. Recently, α2δ proteins (*Cacna2d1-4*) have been recognized as important regulators of synapse formation and plasticity (Dolphin, 2012). In addition to their roles in synaptic transmission as auxiliary subunits of voltage-dependent calcium channels (VDCCs) (Canti et al., 2005; Hoppa et al., 2012), these proteins have multiple postsynaptic roles in driving synapse formation, trans-synaptic communication, and glutamate receptor function (Eroglu et al., 2009; Kurshan et al., 2009; Fell et al., 2016; Wang et al., 2016; Brockhaus et al., 2018; Chen et al., 2018; Geisler et al., 2019). Mutations in human α2δ genes have been associated with epilepsy, movement disorders, and schizophrenia (Edvardson et al., 2013; Pippucci et al., 2013), and α2δ-1/2 proteins are the primary targets of the widely prescribed antiepileptic and analgesic, gabapentin (Gee et al., 1996; Brown and Gee, 1998; Boning Gao, 2000). However, the roles of α2δ proteins in controlling synaptic and network function at any given synapse are still elusive, due in part to expression of multiple isoforms in many neurons.

Purkinje cells (PCs), the primary output pathway from the cerebellar cortex, appear to exclusively and abundantly express the α2δ-2 isoform (*Cacna2d2*) (Barclay et al., 2001a; Cole et al., 2005; Lein et al., 2007; Dolphin, 2012), thus providing an opportunity to determine how this protein contributes to synaptic transmission. Like the spontaneous 'ducky' mouse mutants (du^{2J}/du^{2J} or du/du), targeted deletion of α2δ-2 causes cerebellar ataxia, epilepsy and premature death (Barclay et al., 2001b; Brodbeck et al., 2002; Ivanov et al., 2004; Donato et al., 2006), indicative of its importance in neurological function.

The global loss of α2δ-2 likely impacts synapses throughout the brain. However, the climbing fiber (CF) to PC synapse has multiple distinctive features, including the mono-innervation of mature PCs by a single CF (Hashimoto et al., 2009) and presynaptic expression

of vesicular glutamate transporter 2 (VGLUT2), allowing for the visualization of CF terminals and making this an ideal site to determine how α2δ-2 contributes to synaptic function. In contrast to Purkinje cells, the inferior olivary cells (from which CFs arise) predominantly express the α2δ-1 isoform, with low expression of α2δ-2/3 isoforms (Cole et al., 2005; Lein et al., 2007). Finally, CF activity drives complex spike (CpS) generation in PCs, which produces a high-fidelity error prediction signal important to the processing of motor coordination and learning (Yang and Lisberger, 2014; Heffley et al., 2018).

We combined structural and electrophysiological analysis of the CF to PC synapse in *Cacna2d2* knockout mice (Ivanov et al., 2004) to elucidate the contribution of α2δ-2 to excitatory synapse formation and transmission. Contrary to positive regulation of excitatory synaptogenesis by the α2δ-1 isoform (Li et al., 2004; Eroglu et al., 2009; Chen et al., 2018; Risher et al., 2018), loss of α2δ-2 increased functional synaptic innervation by CFs. α2δ-2 KO CFs had elevated glutamate release and clearance compared to WT, resulting in profound deficiencies in the generation of CpS spikelets. Together, our studies demonstrate the critical role of α2δ-2 in proper CF-PC synapse organization and network function, and allude to the wide versatility of α2δ proteins in synaptic transmission.

Results

α2δ-2 controls Purkinje cell spiking patterns in response to climbing fiber activation

To examine how the loss of α2δ-2 affects cerebellar output, we performed whole-cell recordings from PCs in acutely prepared cerebellar slices from α2δ-2 knockout (KO) mice and their wildtype (WT) littermates at p21-p30, after CF innervation has reached maturity (Hashimoto et al., 2009). We focally stimulated CFs in the granule cell layer and unitary CF-mediated EPSCs were identified by their large amplitude, all-or-nothing nature and paired-pulse depression (Dittman and Regehr, 1998; Hashimoto and Kano, 1998; Liu and Friel, 2008; Rudolph et al., 2011). CF-evoked CpSs were then recorded in current clamp mode.

The voltage envelope of CpS waveforms was comparable between WT and KO (**Figure 3.1A**; Integral of CpS between time 0 - 100 ms: WT = 0.96 ± 0.06 V • s, n = 10; KO = 0.81 ± 0.06 V • s, n = 11; p = 0.1; unpaired Student's t-test), but the number of CpS spikelets was substantially reduced in KO PCs (**Figure 3.1B**; WT = 3.2 ± 0.5, n = 10; KO = 1.2 ± 0.4, n = 11; p = 0.002; Mann-Whitney). In addition, the few spikelets that did occur during the KO CpS were of lower trough-to-peak amplitude. All first spikelets in the WT were >30 mV compared to 75% in the KO (**Figure 3.1C**), which is consistent with a lower probability of CpS transmission (Khaliq and Raman, 2005) in the α2δ-2 KO. Moreover, though subsequent spikelets were present in 2 of 11 KO cells, none reached 30 mV trough-to-peak amplitude (Mean KO $spikelet_2$ = 16.5 ± 5.7 mV, n = 2; $spikelet_3$ = 7.6 mV, n = 1; $spikelet_4$ = 7.2 mV, n = 1; $spikelet_5$ = 6.5 mV, n = 1). Despite the differences in CpS spikelet generation between genotypes, initial spike amplitudes (**Figure 3.1D**) and rise rates were unchanged between WT and KO (Spike slope: WT = 1790 ± 230 V/s, n = 10; KO = 1660 ± 240 V/s, n = 11; p = 0.69; unpaired Student's t-test).

The altered CpS in KO PCs were not associated with changes in the intrinsic excitability of α2δ-2 KO PCs as measured by their resting membrane potentials (**Figure 3.1E**), input resistance (WT 140 ± 20 MΩ, n = 8; KO 122 ± 7.8 MΩ, n = 11; p = 0.38, unpaired Student's t-test), or response to current injection (**Figures 3.1F** and **3.1G**). Thus, we explored whether altered CpS patterns might represent differences in CF-mediated synaptic currents.

α2δ-2 knockout mice have larger CF-evoked EPSCs with accelerated decay kinetics

The kinetics of CF-evoked excitatory postsynaptic currents (EPSCs) influence the CpS shape, such that a slower EPSC decay increases the likelihood of spikelet generation (Rudolph et al., 2011). Spikelet generation is also sensitive to the peak synaptic conductance, as an increased phasic conductance can result in depolarization block and failure to generate spikelets (Davie et al., 2008). Thus, we performed whole-cell recordings of CF EPSCs in the presence of low concentrations of the α-amino-3-hydroxy-5-methyl-4-isoxazolepropionic acid receptor (AMPAR) antagonist, NBQX (0.5 μM), to facilitate voltage clamp control (as in Dittman and Regehr, 1998; Liu and Friel, 2008; Rudolph et al., 2011).

Peak EPSC amplitudes were 37% larger in α2δ-2 KO mice (**Figures 3.2A** and **3.2B**; WT = 703 ± 63 pA, n = 17; KO = 961 ± 86 pA, n = 19, p = 0.03; unpaired Student's t-test). WT and KO EPSC decays were well-fit by a single exponential curve with KO EPSCs exhibiting faster decay kinetics (**Figures 3.2C** and **3.2D**; WT τ_{decay} = 20.6 ± 1.1 ms, n = 17; KO τ_{decay} = 13.2 ± 0.8 ms, n = 20, p < 0.0001; unpaired Student's t-test). Despite these two alterations, the EPSC in the KO had an equivalent charge transfer to that of WT EPSCs (**Figures 3.2E**), and 20-80% risetimes were similar in WT and KO PCs (**Figures 3.2F** and **3.2G**).

Proximal redistribution of CF synapses in the α2δ-2 knockout partially contributes to larger CF-evoked EPSCs

To examine the larger EPSC in KO mice, we isolated quantal events at CF synapses by desynchronizing CF evoked release. We replaced extracellular calcium with strontium (Rudolph et al., 2011; Zhang et al., 2015), and measured the amplitudes of CF-derived asynchronous quantal release events (aEPSCs). The average aEPSC was 24% larger in KO compared to WT PCs (**Figures 3.3A-C**; WT = 25.6 ± 1.0 pA, n = 8; KO = 31.8 ± 1.6 pA, n = 8, p = 0.004; unpaired Student's t-test), indicating that part, but not all, of the increased CF-evoked EPSC amplitude could be accounted for by a larger unitary response.

Therefore, we asked whether there might also be an increase in the number of CF synapses onto PCs using an immunohistochemical approach. CF terminals can be selectively identified as discrete puncta along the primary dendrites of PCs through their expression of VGLUT2 (Miyazaki et al., 2004; Zhang et al., 2015). As is apparent in **Figure 3.4A**, $VGLUT2^+$ puncta were closer to PC somata in KO mice than in WTs. CF terminals were a mean distance of 40.8 ± 0.5 μm from the PC soma in WT, whereas α2δ-2 KO mice had a mean CF terminal distance of 30.6 ± 0.3 μm (**Figures 3.4A** and **3.4C**; n = 3-5 images from 5 mice of each genotype; $p < 0.0001$; Kolmogorov-Smirnov test). Moreover, distal CF innervation (beyond 50 μm from the PC soma; **Figure 3.4B**) accounted for 23% of puncta in WT, but only 6% in KO. This shift in CF terminal distribution in KO animals was not associated with a change in $VGLUT2^+$ puncta size (**Figure 3.4D**) or overall number of puncta within the molecular layer (**Figure 3.4E**; Mean number of puncta normalized to length of PCL: WT = 1.91 ± 0.21puncta/μm_{PCL}; KO = 1.81 ± 0.14 puncta/μm_{PCL}, n = 3-5 images from 5 mice of each genotype; p = 0.7; unpaired Student's t-test). There was no change in the molecular layer width, and the density of PCs was unchanged (Mean molecular layer width; WT = 110 ± 3.8 μm; KO = 106 ± 4.8 μm, p = 0.43; Mean PC density;

WT = 0.62 ± 0.08 cells/μm_{PCL}; KO = 0.65 ± 0.06 cells/μm_{PCL}, p = 0.72; n = 8 images from 3 mice of each genotype; unpaired Student's t-test).

The more proximal location of CF inputs in the KO could contribute to both the increased EPSC amplitude and decay rate, due to decreased dendritic filtering (Roth and Häusser, 2001). To ask whether changes in CF synapse localization alone were sufficient to account for the altered EPSC amplitude and kinetics, we modified the Roth and Häusser (2001) computational model of dendritic integration of CF inputs onto PCs to match our data. This model, based on morphological reconstructions of single PCs and empirical measurements of dendritic filtering (Roth and Häusser, 2001), allowed us to simulate how redistribution of CF inputs would affect the ensemble CF EPSC. Using this model (**Figures 3.5A**; For KO, "Model $CF_{70\% Control}$" simulates the empirically observed $VGLUT2^+$ distribution from **Figure 3.4C**), a shift from the WT to the KO distribution of CF inputs produced a 16% increase in simulated EPSC amplitude and a 15% decrease in the decay time constant (**Figures 3.5B**). Thus, the proximal distribution of CF inputs in the KO augment the quantal response (**Figure 3.5C**), to account for the increase in evoked CF EPSC amplitude.

Increased multivesicular release from α2δ-2 knockout CFs

CF synapses exhibit multivesicular release, increasing the synaptic glutamate concentration (Wadiche and Jahr, 2001; Rudolph et al., 2011). To determine whether KO mice displayed altered multivesicular release, we used the low affinity, competitive AMPAR antagonist, kynurenic acid (KYN), to assay synaptic glutamate concentrations. Because KYN binds and unbinds AMPARs throughout the duration of the CF-evoked glutamate transient, KYN inhibition of the AMPAR-mediated current is inversely proportional to the concentration of glutamate present at postsynaptic receptors (Wadiche and Jahr, 2001). KYN (1μM) inhibited

WT EPSC peak amplitudes by 65% (**Figures 3.6A** and **3.6B**; $EPSC_{Peak}$ amplitude control vs. KYN; $WT_{Control}$ = 1.77 ± 0.41 nA vs. WT_{KYN} = 0.62 ± 0.16 nA, n = 6, p = 0.007; paired Student's t-test), whereas KO EPSCs were inhibited by only 40% ($EPSC_{Peak}$ amplitude control vs. KYN; $KO_{Control}$ = 2.63 ± 0.31 nA vs. KO_{KYN} = 1.57 ± 0.21 nA, n = 8, p = 0.0009; paired Student's t-test; relative change in WT vs. KO, p = 0.001; unpaired Student's t-test), demonstrating enhanced multivesicular release from KO CFs.

For these experiments, PCs were held at -20 mV to maintain voltage clamp of the CF-evoked EPSC (Harrison and Jahr, 2003; Rudolph et al., 2011) and NBQX was omitted because co-application of NBQX and KYN facilitates AMPAR-mediated responses (Prescott et al., 2006). Interestingly, at this holding potential, KO EPSCs exhibited slower decay kinetics (For τ_{decay} at baseline V_m = -20 mV; WT_{-20mV} = 11.6 ± 1.12 ms, n = 6; KO_{-20mV} = 18.5 ± 1.32 ms, n = 8, p = 0.002; unpaired Student's t-test). Although this is consistent with a larger glutamate transient due to multivesicular release (Paukert et al., 2010), it is in apparent odds with the faster decay kinetics in KO PCs at more hyperpolarized potentials. One explanation for this discrepancy in decay kinetics could be the voltage-dependence of glutamate re-uptake by PCs. PCs and surrounding Bergmann glia express high levels of glutamate transporters to manage spillover and glutamate clearance, and activity of these transporters shapes the CF-evoked EPSC waveform (Paukert et al., 2010). However, PCs play a dominant role in synaptic glutamate clearance (Auger and Attwell, 2000), and glutamate transporters have decreased efficiency at depolarized voltages (Bergles et al., 1997). In this scenario, the contributions of PC and Bergmann glia glutamate transporters together result in rapid EPSC decay in the KO at hyperpolarized potentials, but prolonged decay expected from multivesicular release dominates the EPSC waveform when KO PCs are held at depolarized potentials.

Faster EPSC decay in α2δ-2 knockout due to enhanced glutamate clearance

We further investigated the role of glutamate transporters in shaping the CF EPSC waveform in WT and KO mice while holding PCs at -70 mV in the presence of low NBQX (0.5 μM), as in our prior voltage clamp experiments (**Figure 3.2**). Block of glutamate transporters with the non-selective transport re-uptake inhibitor, DL-TBOA (50 μM), increased WT decay constants by ~30% (similar to Rudolph et al., 2011) (**Figure 3.6C**; WT τ_{decay} control vs. TBOA; $WT_{Control}$ = 13.6 ± 0.9 ms vs. WT_{TBOA} = 17.4 ± 0.9 ms, n = 7, p = 0.001; paired Student's t-test). In contrast, TBOA increased decay constants of KO EPSCs by 73% (KO τ_{decay} control vs. TBOA; $KO_{Control}$ = 11.1 ± 1.1 ms vs. KO_{TBOA} = 19.1 ± 2.2 ms, n = 7, p = 0.001; paired Student's t-test). After TBOA exposure, WT and KO had similar decay constants (τ_{decay} WT vs. KO in TBOA; p = 0.48; unpaired Student's t-test). However, the relative effect of TBOA on decay was greater in KO EPSCs (**Figure 3.6D**; % increase in τ_{decay} WT vs. KO, p = 0.003; unpaired Student's t-test) consistent with enhanced glutamate clearance by surrounding glutamate transporters.

Repetitive stimulation of CFs suggests lower release probability in the α2δ-2 knockout, though cumulative vesicle release is greater

The enhanced multivesicular release in the α2δ-2 KO (**Figure 3.6A-B**) suggests a presynaptic contribution to the CF EPSC phenotype. CF synapses have high initial probability of release (P_R), which is associated with paired-pulse depression at short interstimulus intervals (Hashimoto and Kano, 1998). However, CF-evoked EPSCs from KO mice showed a consistent increase in the paired-pulse ratio when compared with WT CFs (**Figures 3.7A** and **3.7B**; Paired-pulse ratio: WT = 0.41 ± 0.03, n = 17; KO = 0.51 ± 0.02, n = 18, p = 0.01; unpaired Student's t-test), suggesting CFs have a lower P_R when α2δ-2 is deleted. Therefore,

we hypothesized that KO CFs might have a substantially greater readily releasable pool of vesicles to exhibit increased multivesicular release while also having a lower P_R.

To estimate the relative size of the readily releasable pool in WT and KO, we stimulated CFs with a 10 Hz train. WT and KO CF synapses had strikingly different responses during repetitive stimulation. Both genotypes exhibited a delayed facilitation followed by depression, which may indicate multiple pools of vesicles with differing release probabilities (Lu and Trussell, 2016). However, KO EPSCs were larger at every stimulus throughout the train (**Figures 3.7C-E**), providing further evidence of enhanced vesicle release compared to WT. A linear fit to the last 10 responses of a cumulative amplitude plot produced a steeper slope (Linear regression using 95% Confidence Intervals; $WT_{slope} = 78.7 \pm 0.6$, n = 5; $KO_{slope} = 172.2 \pm 0.5$, n = 5; $p < 0.0001$; unpaired Student's t-test) and a larger y-intercept in KO PCs when compared to WT (**Figure 3.7F**). This analysis provided an estimate of the readily releasable pool (Schneggenburger et al., 1999), which was 29% larger in the KO compared to WT (WT y-intercept = 2.08 ± 0.02 nA, n = 5; KO y-intercept = 2.77 ± 0.01 nA, n = 5; $p < 0.0001$; unpaired Student's t-test). Thus, both a single stimulus (**Figure 3.6A-B**) and repetitive stimulation of CFs produced increased vesicle release in the α2δ-2 KO, suggesting either an enhancement of a low P_R pool of vesicles (Lu and Trussell, 2016) and/or more discrete release sites with reduced P_R compared to WT.

CF terminals in α2δ-2 knockout have more release sites

Because we did not see an increased density of VGLUT2$^+$ puncta by light microscopy, we hypothesized CF terminals in the KO had either a greater number of release sites or vesicles. CF terminals can be identified with electron microscopy (EM) by their high density of round synaptic vesicles (SVs) and contacts onto PC "thorns" along primary PC dendritic shafts (Palay and Chan-Palay, 1974; Miyazaki et al., 2004). While blinded to genotype, we imaged and quantified CF terminals from WT and KO mice (10-15 images/animal; see Materials and Methods). In agreement with VGLUT2$^+$ puncta size determined by confocal microscopy (**Figure 3.4D**), CF terminal cross-sectional area was no different between genotypes when sampled using EM (**Figures 3.8A** and **3.8B)**. WT and KO CF terminals also had an equivalent density of synaptic vesicles (SVs) (**Figure 3.8C**) and no change in number of SVs within 100 nm of the synaptic contact, a proxy for the readily releasable pool (WT = 18.5 ± 2.4 SV/$\mu m_{Contact}$, n = 5 mice; KO = 20.4 ± 2.7 SV/$\mu m_{Contact}$, n = 6 mice, p = 0.6; unpaired Student's t-test).

However, the number of synaptic contacts made by CF terminals in α2δ-2 KOs was nearly twice that of WT (**Figure 3.8A and 3.8D**; WT = 1.08 ± 0.16 contacts/terminal, n = 5 mice; KO = 2.08 ± 0.17 contacts/terminal, n = 6 mice, p = 0.009; Mann-Whitney test). Moreover, the distribution of the number of contacts made by CF terminals was right-shifted in KO (**Figure 3.8E**; $p < 0.002$; Kolmogorov-Smirnov test). Although quantifying synaptic contacts per terminal using single EM sections likely underestimates the true number of contacts per terminal, the observed doubling of discrete contacts made by KO CFs is consistent with increased multivesicular release in the α2δ-2 KO.

Differential Cacna2d isoform expression in the inferior olive and Purkinje cell layer

By *in situ* hybridization, there is robust and exclusive expression of the *Cacna2d2* isoform in PCs, and relatively low expression in the inferior olive (IO), which gives rise to climbing fibers (Cole et al., 2005; Lein et al., 2007). Given the presynaptic morphological and physiological changes we observed at *Cacna2d2* KO CF-PC synapses, we re-examined expression of α2δ isoforms in the Purkinje cell layer (PCL) and IO using quantitative PCR of fresh-frozen tissue obtained by laser capture microdissection (**Figure 3.9A**). In agreement with prior observations (Cole et al., 2005; Lein et al., 2007), PCL tissue from wildtype mice expressed the α2δ-2 isoform 3.85 ± 0.96-fold higher than presynaptic IO samples (**Figure 3.9B**; *Cacna2d2* $\Delta Ct_{PCL} = 1.62 \pm 0.17$; $\Delta Ct_{IO} = 3.37 \pm 0.38$, n = 4, p = 0.03; paired Student's t-test). As our PCL samples contained other cell types found in PCL and inner molecular layer tissues, low expression of α2δ-1 and high levels of α2δ-3 transcript were detected likely due the inclusion of Bergmann glia and molecular layer interneurons. Comparison of our PCL region of interest (**Figure 3.9A**) to α2δ expression patterns from *in situ* hybridization (Cole et al., 2005; Lein et al., 2007) demonstrates that PCs do not appear to express α2δ-1 or α2δ-3 mRNA. Consistent with previous reports, α2δ-4 was undetectable in both PCL and IO samples. Importantly, analysis of *Cacna2d* transcripts from IO samples revealed that α2δ-1 is the predominant isoform (**Figure 3.9C**), and is 7.0 ± 2.4-fold more abundant than α2δ-2 in IO samples (*Cacna2d1* $\Delta Ct_{IO} = 0.94 \pm 0.4$; *Cacna2d2* $\Delta Ct_{IO} = 3.37 \pm 0.38$, n = 4, p = 0.04; paired Student's t-test).

Discussion

In mice lacking α2δ-2, profound deficiencies in CF-induced complex spike (CpS) generation were associated with altered underlying CF-evoked EPSC amplitude and kinetics. CpSs are initiated by a AMPAR-mediated depolarization that drives an initial sodium spike followed by multiple axonally generated 'spikelets' (Davie et al., 2008). Furthermore, dynamic clamp experiments suggested that increased CF EPSC amplitudes would result in depolarization block of spikelet generation (Davie et al., 2008). Thus, we hypothesize that increased glutamatergic transmission and accelerated EPSC kinetics (Rudolph et al., 2011) shape the CpS in the α2δ-2 KO (**Figure 3.10**).

Each CF terminal in the KO contained more discrete synaptic contacts, leading to increased multivesicular release and consequently larger EPSCs, despite an apparent reduction in the probability of release. Together, these findings seem to contradict observations in which synapse formation is positively regulated by α2δ expression (Li et al., 2004; Eroglu et al., 2009; Chen et al., 2018; Risher et al., 2018), reflecting a more complex and nuanced role of α2δ proteins in the α2δ-2 KO phenotype.

α2δ-2 proteins as auxiliary Ca^{2+} channel subunits

α2δ proteins were first identified as auxiliary subunits of voltage-dependent Ca^{2+} channels (VDCCs) that facilitate surface trafficking of VDCCs in heterologous expression systems (Canti et al., 2005; Cassidy et al., 2014). α2δ-1 knockdown reduces presynaptic vesicle release in cultured hippocampal neurons (Hoppa et al., 2012), and capacitive measurements from inner hair cells of the spontaneous *Cacna2d2* mutant, *du/du*, show reduced exocytosis (Fell et al., 2016). We also observed a lowered release probability (P_R) at the CF-PC synapse, as determined by paired-pulse ratio, which is consistent with these prior observations and could

relate to altered VDCC localization or abundance in CFs. Given that α2δ-1 is the predominant isoform expressed by inferior olivary cells (Cole et al., 2005; Lein et al., 2007), if the phenotype we observed is mediated by presynaptic loss of α2δ-2, it suggests isoform-specific functions that cannot be compensated by α2δ-1. Furthermore, this raises the possibility that different α2δ isoforms in individual neurons may have distinct functional roles.

In addition to their abundant α2δ-2 expression, PCs highly express the VDCC, Cav2.1 (Barclay et al., 2001a), which localizes to PC somata and primary dendrites in scattered and clustered patterns (Indriati et al., 2013). Dissociated PCs from the spontaneous mutant, du^{2j}/du^{2j}, have ~30% reduced somatic calcium currents (Barclay et al., 2001a). Similarly, CF vesicle release is mostly (70-90%) regulated by Cav2.1 (Regehr and Mintz, 1994). Because CF-PC transmission and development has been extensively characterized in Cav2.1 mutant mice (Matsushita et al., 2002; Miyazaki et al., 2004; Hashimoto et al., 2011), we looked to this literature for clues as to whether our observed phenotypes could reflect altered pre- and/or postsynaptic VDCC function or localization.

For example, the *leaner* phenotype, in which a Cav2.1 pore mutation reduces PC calcium currents by 60%, is associated with larger, rapidly decaying CF-evoked EPSCs (Liu and Friel, 2008), like the α2δ-2 KO. However, *leaner* CFs do not exhibit changes in P_R (Liu and Friel, 2008). Other Cav2.1 pore mutants show reductions in PC calcium current analogous to α2δ-2 mutants, but display heterogeneity in EPSC phenotypes. Both *rolling Nagoya* and *tottering* mutants have 40% reductions in calcium currents, yet *rolling Nagoya* exhibits larger, slowly decaying EPSCs, whereas *tottering* EPSCs are unchanged (Matsushita et al., 2002). PC-specific Cav2.1 KO show proximal innervation by CFs (Miyazaki et al., 2012), reminiscent of the CF redistribution we observed in *Cacna2d2* KOs. This striking similarity provides evidence for postsynaptic control of CF development. Surprisingly however, global and PC-

specific Cav2.1 KOs exhibit normal CF EPSC amplitude and decay kinetics (Miyazaki et al., 2004; Hashimoto et al., 2011). Thus, although some similarities exist between the *Cacna2d2* KO and certain VDCC mutant mice, the roles of α2δ-2 at the CF-PC synapse likely involve other effector mechanisms. α2δ-2 loss may be more nuanced than altered VDCC abundance, but perhaps result from differences in VDCC localization, clustering or association with other molecules (including other VDCC subtypes).

Altered presynaptic function could result from PC-driven morphological changes in the *Cacna2d2* KO, independent of altered presynaptic VDCC trafficking. For example, alterations in presynaptic morphology alone, rather than altered presynaptic gene expression, can influence measures of apparent P_R and the readily releasable pool size by repetitive stimulation (Fekete et al., 2019). It is also possible that P_R at individual release sites is unchanged, but an increased number of release sites per terminal could allow for accumulation of $[Ca^{2+}]_i$ during repetitive stimulation via inter-site crosstalk. In this scenario, repetitive stimuli recruit vesicles from a low P_R pool, sustaining release during subsequent stimuli. Currently, there is no definitive way to distinguish between a heterogeneous population of P_R at discrete release sites, or whether the vesicle recruitment from low vs. high P_R pools differs (Kaeser and Regehr, 2017). The possibility of multiple vesicle pools in the CF, as seen by the bimodal responses in **Figure 3.7C**, complicates our ability to derive readily releasable pool size and P_R at this synapse (Neher, 2015; Lu and Trussell, 2016). Given the various possible effector mechanisms for α2δ-2 that could contribute to the phenotype in mutant mice, further experiments using cell-type selective genetic manipulations will be necessary to fully understand the locus of α2δ-2 action.

α2δ-2 proteins as synaptic organizers

Recently, roles for α2δ proteins independent of VDCCs are supported by their ability to regulate synapse formation despite pharmacological block or deletion of VDCCs (Eroglu et al., 2009; Kurshan et al., 2009). α2δ-1 induces excitatory synapse formation in response to glial-secreted thrombospondin (Eroglu et al., 2009), which is dependent on postsynaptic signaling through N-methyl-D-aspartate receptors (NMDARs) (Risher et al., 2018). Though NMDARs are transiently expressed in newborn rat PCs (Rosenmund et al., 1992), they are not detected at mouse CF-PC synapses until late adulthood (Piochon et al., 2007; Renzi et al., 2007), making this interaction unlikely to contribute to the *Cacna2d2* KO phenotype.

Studies in *C. elegans* suggest trans-synaptic roles for α2δ proteins, as presynaptic α2δ-3 and binds to postsynaptic neurexin to control neuromuscular synaptic function (Tong et al., 2017). In mammals, neurexins are presynaptically expressed (Missler et al., 2003; Zhang et al., 2015) and interact trans-synaptically with postsynaptic neuroligins. Interestingly, similar to our observations in the *Cacna2d2* KO, the neuroligin triple KO mouse (Zhang et al., 2015) also has a proximally-shifted CF distribution, without a change in $VGLUT2^{+}$ puncta size or overall density (Zhang et al., 2015). Although CF-PC synaptic function is unchanged in the neuroligin tKO (Zhang et al., 2015), this finding suggests that α2δ-2 may act in parallel with neurexin-neuroligin to coordinate features such as synaptic localization, whereas the functional components that depend on α2δ-2 involve other effector mechanisms.

The stereotyped development of the CF-PC synapse has made it an attractive model to study numerous important molecules that share mutant phenotypes, yet have quite disparate functions. For example, the CF innervation pattern is modulated by postsynaptically expressed neuroligins, TrkB, Cav2.1, GluRδ2 (exclusively expressed in PCs), cerebellins and myosin Va (reviewed in Bosman and Konnerth, 2009), revealing CF redistribution as a sensitive indicator of underlying dysfunction, and demonstrating postsynaptic control of

synaptic innervation. Although *Cacna2d2* KO mice share this phenotype, additional functional alterations at the CF-PC synapse are dissimilar from other mutant mice. Thus, our data suggest that the contributions of α2δ-2 to the CF-PC synapse may comprise both VDCC-dependent and -independent mechanisms.

Impacts of α2δ-2 loss on cerebellar function

Of the four α2δ isoforms (*Cacna2d1-4*), α2δ-2 loss has the most severe phenotype, as mice and humans with *Cacna2d2* mutations have ataxia, epilepsy and motor control deficits (Barclay et al., 2001b; Brodbeck et al., 2002; Ivanov et al., 2004; Donato et al., 2006; Pippucci et al., 2013). Because PCs provide the output from the cerebellum, some of these neurologic phenotypes likely reflect PC dysfunction. PC spike-rate and plasticity are instructed by CpSs, providing error prediction information for motor coordination, presumably graded by the number of spikelets generated (Rasmussen et al., 2013; Yang and Lisberger, 2014; Burroughs et al., 2017). As CpSs generated by *Cacna2d2* KO PCs had fewer spikelets, we predict PC information transfer is degraded, implicating direct influence of α2δ-2 loss in cerebellar dysfunction.

Particularly surprising was the variety of alterations at the Cacna2d2 KO CF-PC synapse, including enhanced glutamate re-uptake. It is likely that some phenotypes developed as compensation for a primary derangement directly related to α2δ-2 loss. Delayed conditional deletion of α2δ may help to clarify this issue. Likewise, deletion of α2δ-2 may have differential effects on other synapses and functions, either onto PCs or other cell types. As many neurons co-express multiple α2δ isoforms, it will be important to understand the role of each isoform at individual synapses, as well as address whether postsynaptic α2δ proteins instruct presynaptic development or function (or vice versa), using cell-specific

targeted rescue or deletion. Overall, our results underscore the critical roles of α2δ-2 in both proper organization and transmission at the CF-PC synapse.

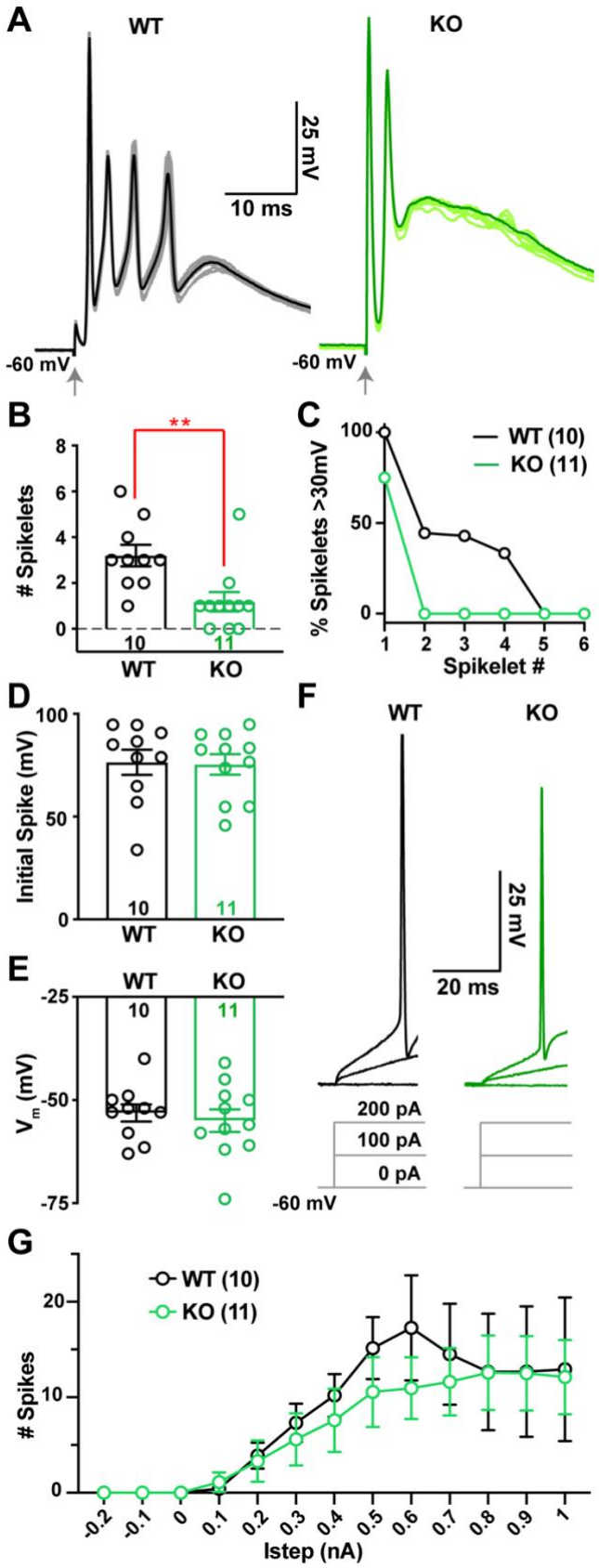
A
WT
KO
25 mV
10 ms
-60 mV
-60 mV
B
**
Spikelets
10
11
WT
KO
C
WT (10)
KO (11)
% Spikelets >30mV
Spikelet #
D
Initial Spike (mV)
10
11
WT
KO
E
WT
KO
V_m (mV)
10
11
F
WT
KO
25 mV
20 ms
200 pA
100 pA
0 pA
-60 mV
G
WT (10)
KO (11)
Spikes
Istep (nA)

Figure 3.1 Climbing fiber (CF)-evoked complex spikes (CpSs) are altered in the Cacna2d2 KO, but intrinsic PC excitability is unchanged.

(A) Representative CF-evoked complex spikes in WT (left) and KO (right) PCs, arrow indicates CF stimulation. Each trace consists of 10 overlaid traces (lighter color) and the corresponding CpS average (dark color). (*B*) Average number of spikelets per CpS in WT and KO PCs; **$p < 0.01$ (Mann-Whitney). (*C*) Percentage of spikelets exceeding 30 mV trough-to-peak amplitude, ordered by spikelet number. (*D*) Average CpS initial spike amplitude; $p = 0.89$ (NS). (*E*) Average PC membrane potential when in zero current mode; $p = 0.60$ (NS). (*F*) Representative single traces of membrane voltage responses to current injection, showing steps of 0, 100, 200 pA injections from V_m = -60 mV; *Left* WT (black); *Right* KO (green). Average I_{step} to initiate spiking WT = 200 ± 39 pA, n = 10; KO = 289 ± 82 pA, n = 9; $p = 0.33$ (NS). (*G*) Average spike count during current steps from -0.2 to 1 nA, V_m = -60 mV. WT (black) and KO (green); $p = 0.63$ (NS; Two-way ANOVA with repeated measures, $F_{(1, 19)} = 0.23$). Data shown ± SEM, n = cells; unpaired Student's t-test unless otherwise indicated.

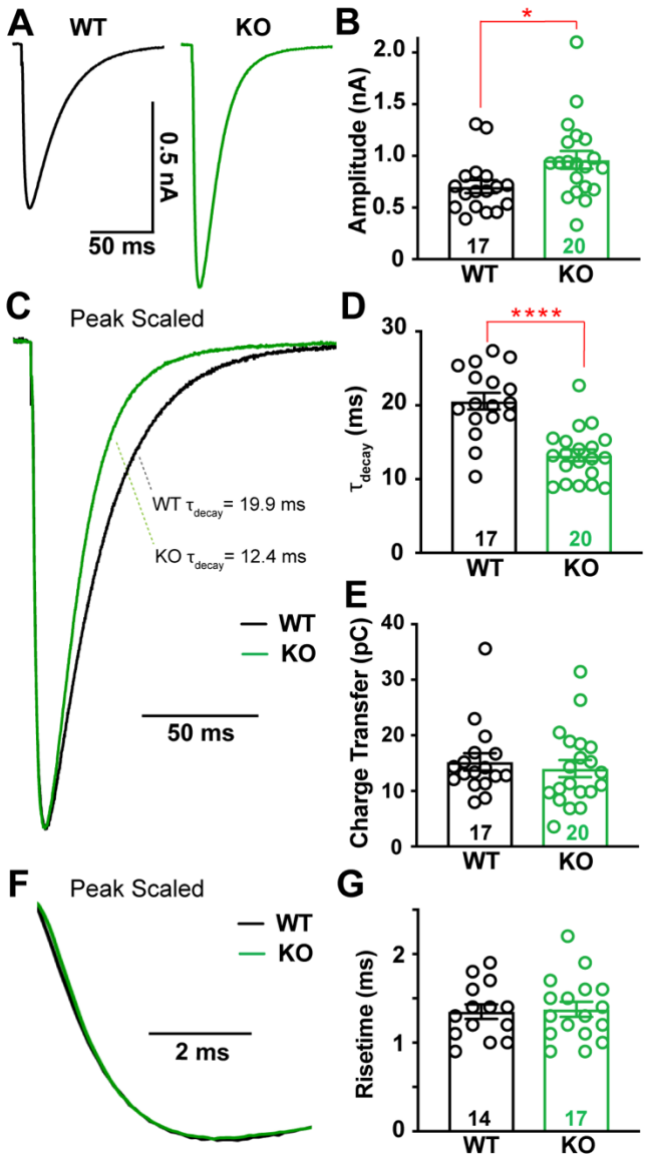

Figure 3.2 CF-evoked EPSCs are larger and faster in Cacna2d2 KO mice, but total charge transfer is conserved.

(*A*) Representative CF-evoked EPSCs. *Left* WT average (black); *Right* KO average (green). (*B*) Average peak CF EPSC amplitude; *p < 0.05. (*C*) Peak scaled EPSCs, demonstrating the relative decay time constants for these example traces (τ_{decay}) based on single exponential fits; WT (black) and KO (green). (*D*) τ_{decay} (ms) for CF EPSCs in WT vs. KO PCs; **** p< 0.0001. (*E*) Average charge transfer within the first 100 ms of EPSC; p = 0.58 (NS). (*F*) Peak

scaled EPSCs, expanded to display risetime kinetics; WT (black) and KO (green). (*G*) Average CF EPSC 20-80% risetime (ms); p = 0.83 (NS). Data shown ± SEM, n = cells; unpaired Student's t-test.

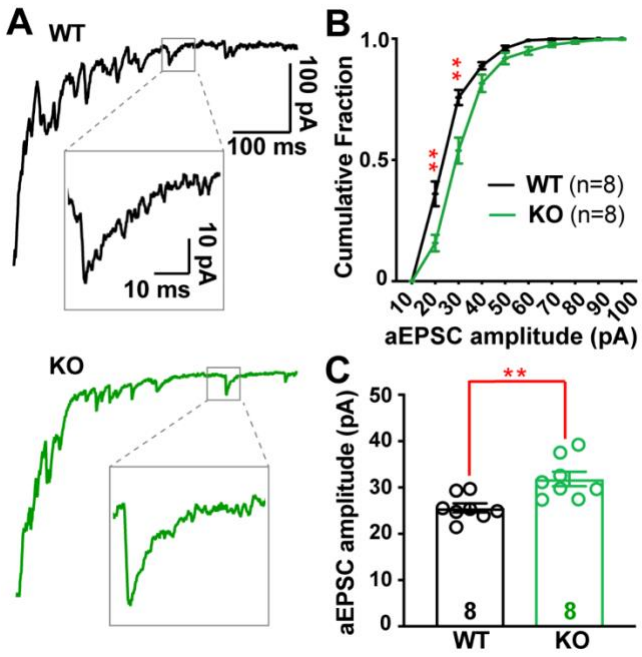

Figure 3.3 Desynchronized CF-evoked vesicle release reveals larger quantal responses in Cacna2d2 KO.

(*A*) Representative CF-evoked EPSCs in the presence of 1.3 mM Sr^{2+}; *Top* WT EPSC (black) and example asynchronous EPSC (aEPSC; inset); *Bottom* KO EPSC (green) and aEPSC (inset). (*B*) Cumulative aESPC amplitude distribution graphed in 10 pA bins; WT (black) and KO (green); **p < 0.01 for 20 and 30 pA bins, all others NS (Multiple t-tests with Holm-Sidak correction for multiple comparisons). (*C*) Average aEPSC amplitudes; **p < 0.01. Data shown ± SEM, n = cells; unpaired Student's t-test.

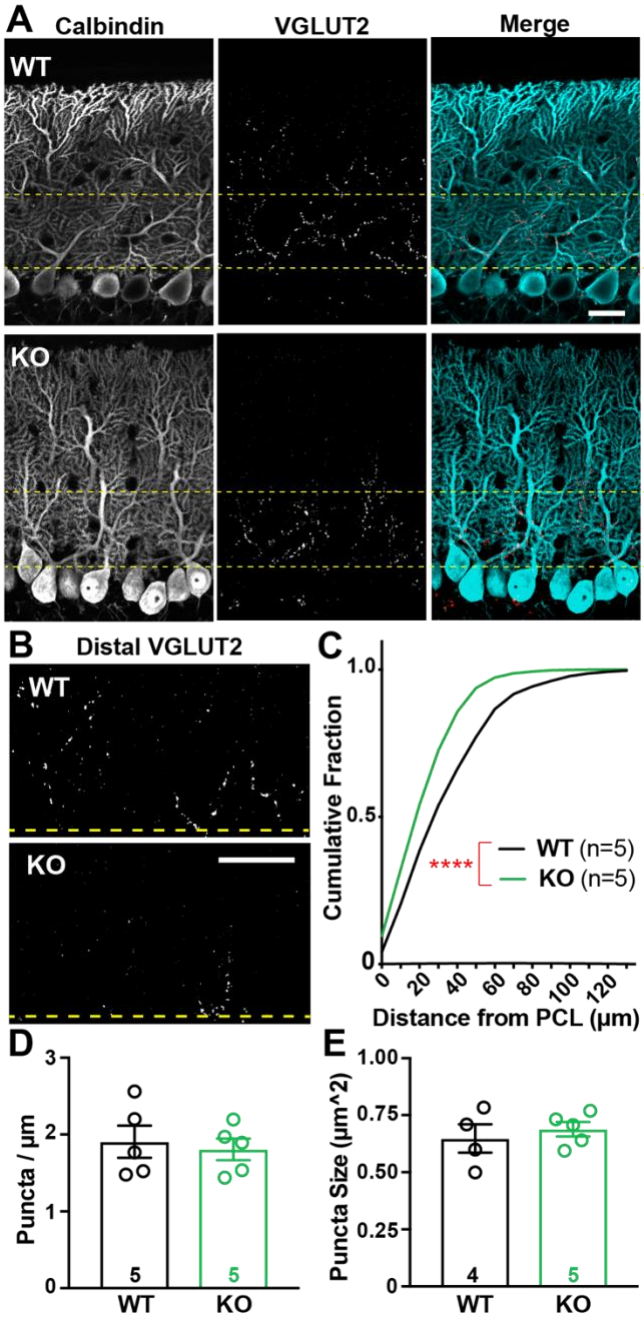

Figure 3.4 CF terminal distribution, but not number, is altered in Cacna2d2 KO cerebellum.

(*A*) Representative images from p21 WT (above) and KO (below) tissue, depicting the Purkinje cell layer (PCL). Calbindin (left/blue in merge) marks PCs, while VGLUT2 immunoreactivity (middle/red in merge) marks CF terminals. Yellow lines demarcate the 50

μm most proximal to PC somata and is the region most highly innervated by climbing fibers. Scale bar = 20 μm. (*B*) VGLUT2-immunoreactive CF terminals in the outer molecular layer, cropped at the distal yellow line (50 μm), illustrate differences in CF innervation of distal PC dendrites in WT (top) and KO (below) PCs. Scale bar = 20 μm. (*C*) Cumulative distribution of $VGLUT2^+$ puncta relative to PC somas in WT (black, n = 5 animals) and KO (green, n = 5 animals); ****$p < 0.0001$ (Kolmogorov-Smirnov test). (*D*) Average $VGLUT2^+$ punctum size was not significantly different between WT and KO terminals; $p = 0.55$ (NS). (*E*) Average $VGLUT2^+$ puncta density per length of PCL (puncta/ μm_{PCL}) was not significantly different between WT and KO; $p = 0.72$ (NS). Unless otherwise stated, data shown ± SEM, n = animal; unpaired Student's t-test.

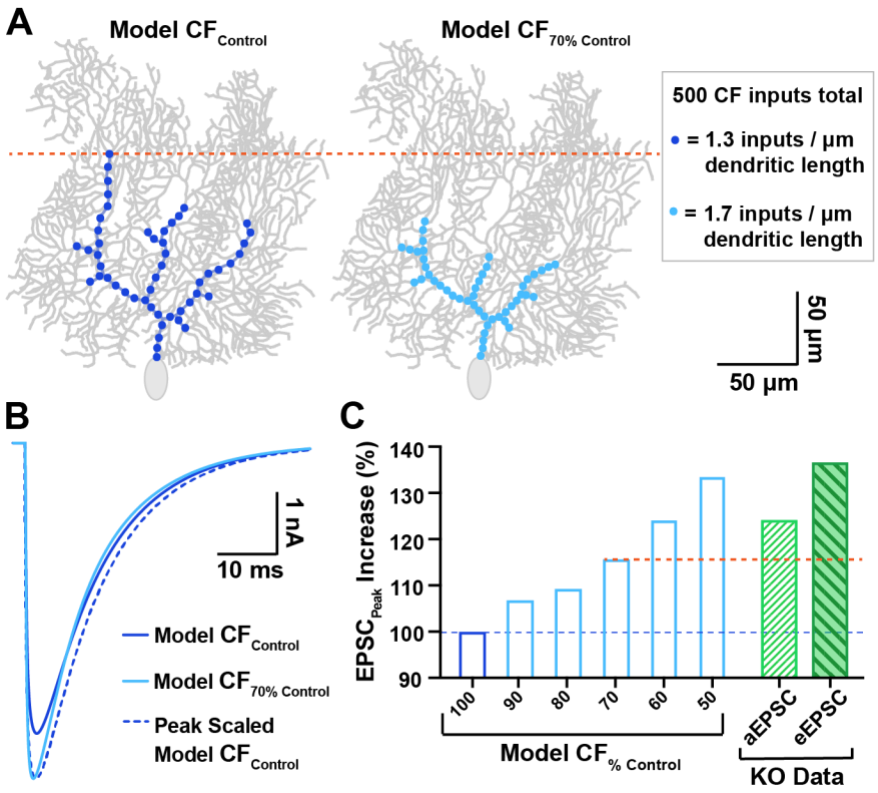

Figure 3.5 Computational PC model simulates the impact of proximally shifted CF inputs on EPSC waveform.

(*A*) *Left* Model CF input distribution similar to control PCs (dark blue; "Model $CF_{Control}$") vs. a similar PC with CF inputs shifted 30% more proximal (*right,* light blue, "Model $CF_{70\% Control}$"), which matches the degree of proximal shift in WT vs. KO innervation, respectively. All models conserved the total number of CF quantal inputs (500 inputs with 1 nS conductance), though input density was adjusted to accommodate the shortened region of CF innervation (see inset). (*B*) Overlay of EPSC output waveforms from Model $CF_{Control}$ simulations (dark blue; 4.7 nA), Model $CF_{70\% Control}$ (light blue; 5.4 nA), and peak scaled Model $CF_{Control}$ to compare decay kinetics. For tau of decay; Model $CF_{Control}$ τ_{decay} = 12.0 ms; Model $CF_{70\% Control}$ τ_{decay} = 10.2 ms). (*C*) Predicted increase in EPSC peak amplitude for various degrees of proximally shifted Model CFs (light blue bars, restricted to a zone 100-

50% the width of control CFs, all including 500 quantal inputs) compared to Model $CF_{Control}$ (dark blue bar). For comparison, the empirically determined increase in quantal EPSC (aEPSC; hatched green bar) and evoked EPSC (eEPSC; filled-hatched dark green bar) amplitudes in KO PCs are also displayed (derived from Figures 3 and 2, respectively). The orange dotted line demarcates the predicted EPSC increase from the model based on the observed shift in CF location.

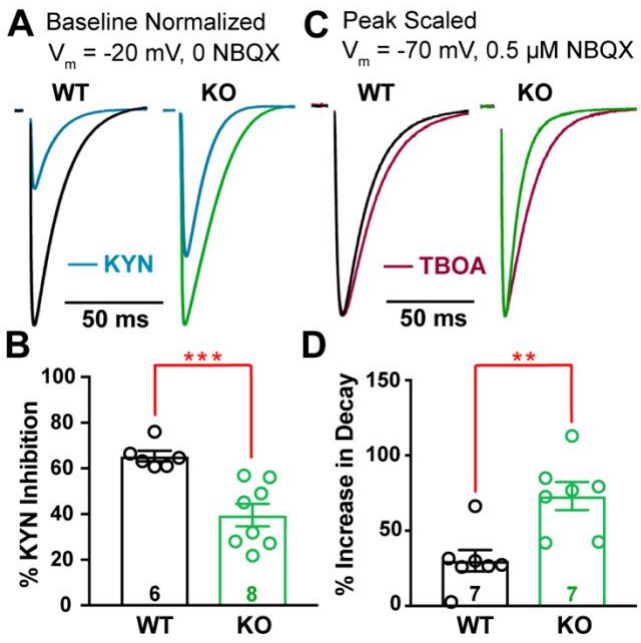

Figure 3.6 Cacna2d2 KO has increased glutamate release and clearance at CF-PC synapses.

(*A*) Representative CF EPSCs recorded at V_m = -20 mV in the absence of NBQX for WT and KO PCs (relative scales; WT = black; KO = green). For each, traces after exposure to 1 mM kynurenic acid (KYN; blue) are shown normalized to baseline EPSC amplitudes. (*B*) Percent inhibition of ESPC peak amplitude by KYN; ***p < 0.001. (*C*) Representative normalized CF-evoked EPSCs recorded at V_m = -70 mV in the presence of 0.5 µM NBQX; *Left* WT average (black); *Right* KO average (green). Overlay average peak-scaled traces after exposure to 50 µM DL-TBOA (TBOA; magenta). (*D*) Average increase in EPSC decay by TBOA; **p < 0.01. Data shown ± SEM, n = cells; unpaired Student's t-test.

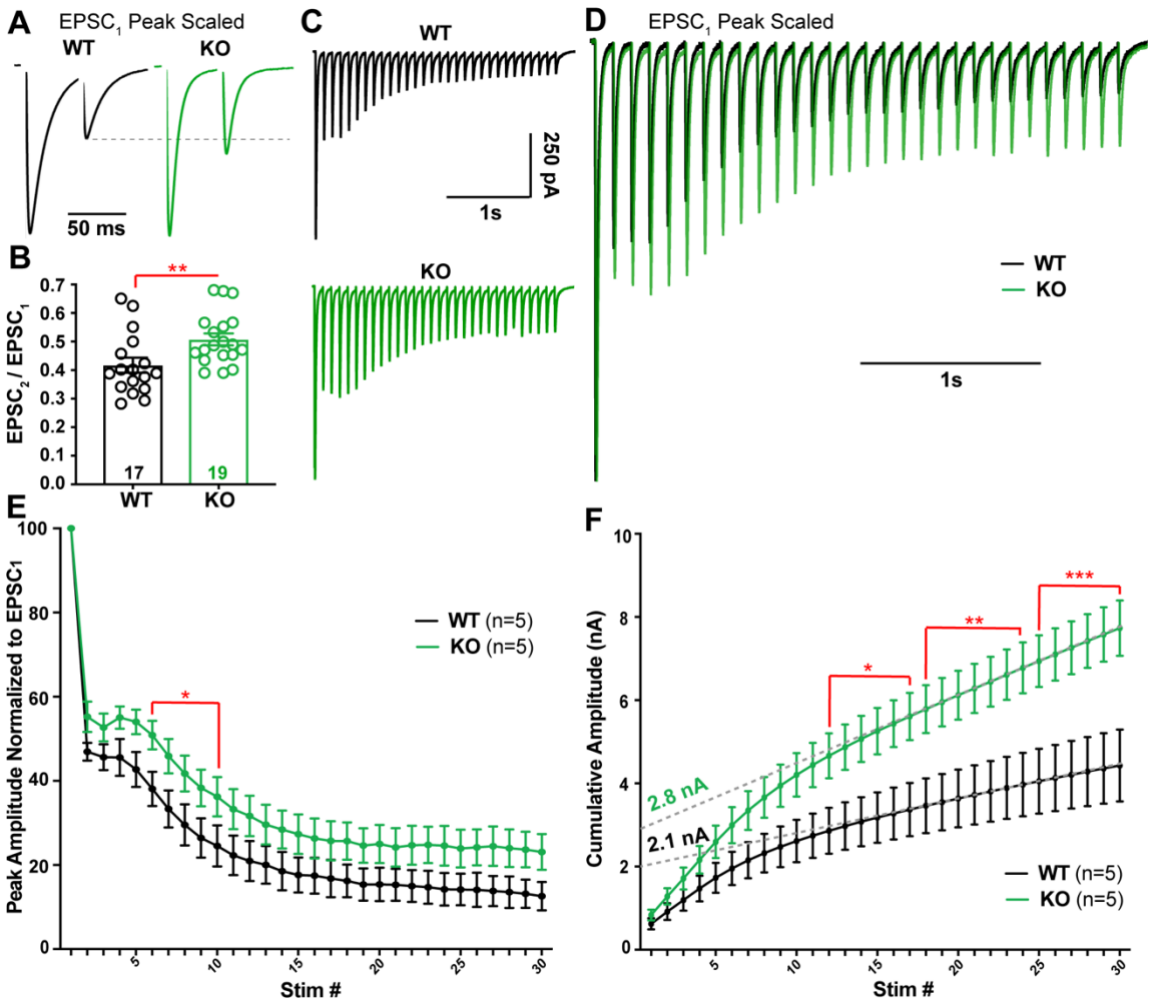

Figure 3.7 Repetitive stimulation of CF synapses reveals a lower probability of release and greater cumulative release in Cacna2d2 KO.

(A) Representative traces from WT (black) and KO (green) PCs during 50 ms paired-pulse stimulation. Traces are scaled to the first EPSC ($EPSC_1$). Dotted gray line shows paired-pulse depression of the second EPSC ($EPSC_2$) in WT compared to KO. (*B*) Average paired-pulse ratio ($EPSC_2$ /$EPSC_1$); ** $p < 0.01$. (*C*) Representative traces in response to 10 Hz stimulation; WT (black); KO (green). (*D*) Traces from (*C*) peak scaled to $EPSC_1$ and overlaid, illustrating different relative steady-state EPSC amplitudes during latter portions of the train. (*E*) Summary data of EPSC amplitudes normalized to $EPSC_1$ during 10 Hz

stimulation in WT (black) and KO (green). *p < 0.05 (Multiple t-tests with Holm-Sidak correction). (*F*) EPSC amplitudes during 10 Hz stimulation plotted as cumulative amplitude from WT (black) and KO (green). For comparison of cumulative amplitude between WT and KO at various stimulation numbers (stim #); * p < 0.05, ** p < 0.01, *** p < 0.001 (Multiple t-tests with Holm-Sidak correction). Dotted grey lines illustrate a linear fit to cumulative amplitude between stim # 20-30 from WT and KO trains. Data shown ± SEM, n = cells; unpaired Student's t-test unless otherwise indicated.

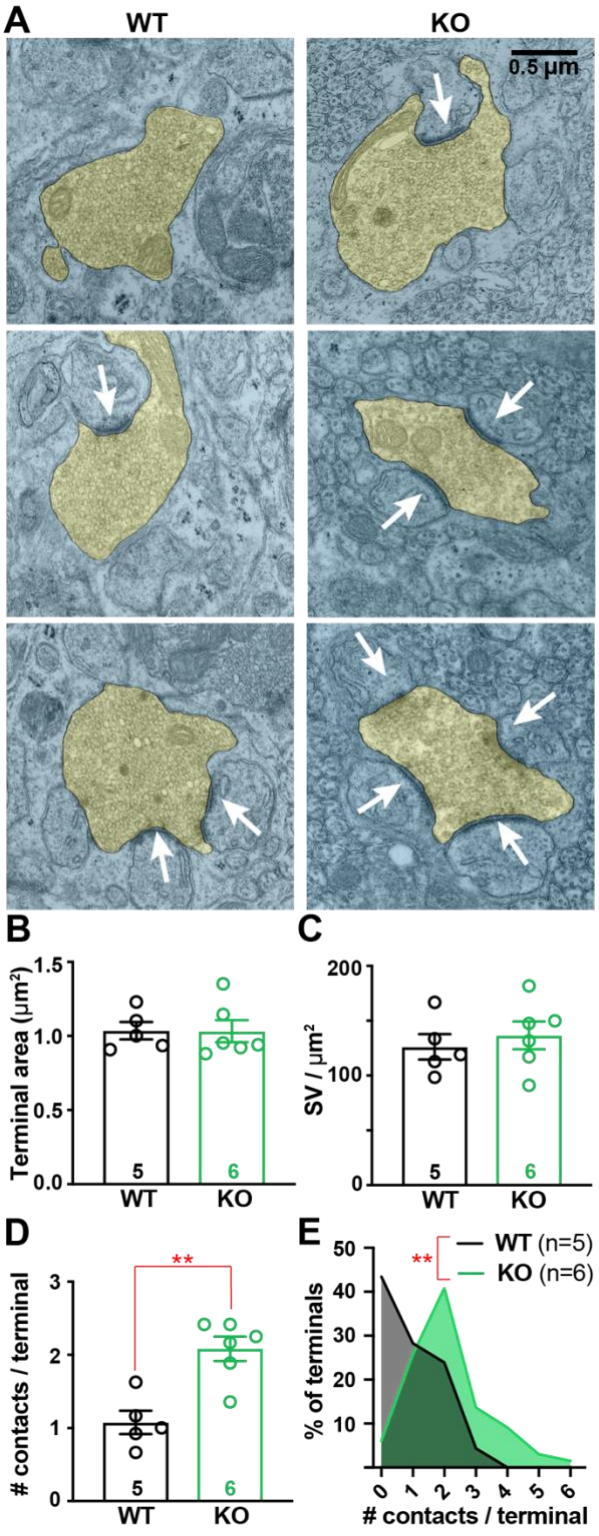

Figure 3.8 CF terminals have increased numbers of synaptic contacts in Cacna2d2 KO animals.

(A) Representative transmission electron micrographs of CF terminals (pseudocolored yellow) from p21 WT (left) and KO (right) animals. White arrows indicate postsynaptic densities used to quantify synaptic contacts/terminal. Scale bar = 0.5 μm. (*B*) Average CF terminal area (μm^2); p = 0.55 (NS). (*C*) Synaptic vesicle (SV) density (SV/ μm^2) was not different between WT and KO animals; p = 0.57 (NS). (*D*) Average number of contacts per CF terminal (# contacts/terminal) was increased in KO animals. ** p <0.01 (Mann-Whitney test). (*E*) Histogram of all CFs analyzed from WT (black) and KO (green) cerebelli, displaying the number of contacts per sampled CF terminal normalized to total number of CF terminals; p < 0.01 (Kolmogorov-Smirnov test). Data shown ± SEM, n = animals using 15-20 images/animal; unpaired Student's t-test unless otherwise stated.

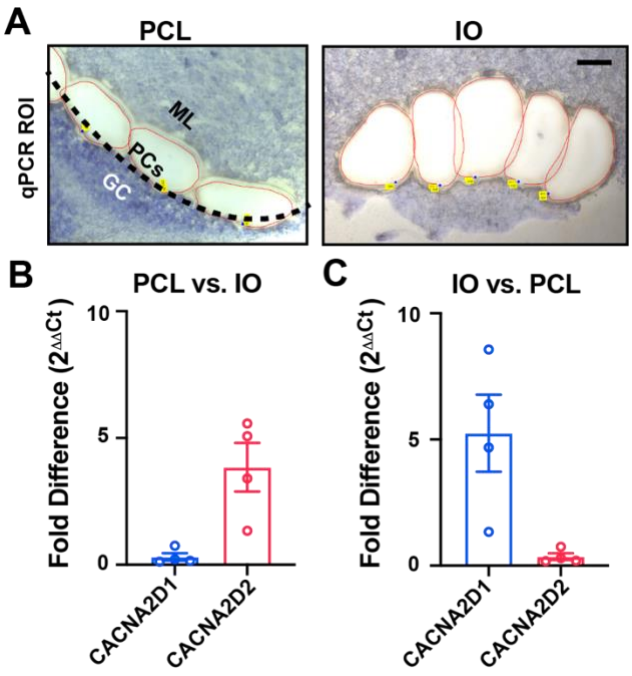

Figure 3.9 Relative expression of Cacna2d transcripts by qPCR from Purkinje cell layer and inferior olive tissues.

(*A*) Example Purkinje cell layer (PCL) and inferior olive (IO) regions of interest isolated by laser capture microdissection from fresh-frozen WT tissue. *Left, PCL region of interest;* black-dotted line indicates the monolayer of PCs that have been dissected along with regions of the inner molecular layer (ML; granule cells, GC). *Right, IO region of interest;* one hemisphere from a coronal section of ventral brainstem, scale = 100 µm. (*B, C*) Fold difference ($2^{-\Delta\Delta Ct}$) expression of *Cacna2d* isoforms by quantitative PCR comparing (*B*) PCL vs. IO, and (*C*) IO vs. PCL samples. Data shown ± SEM, n = 4 animals.

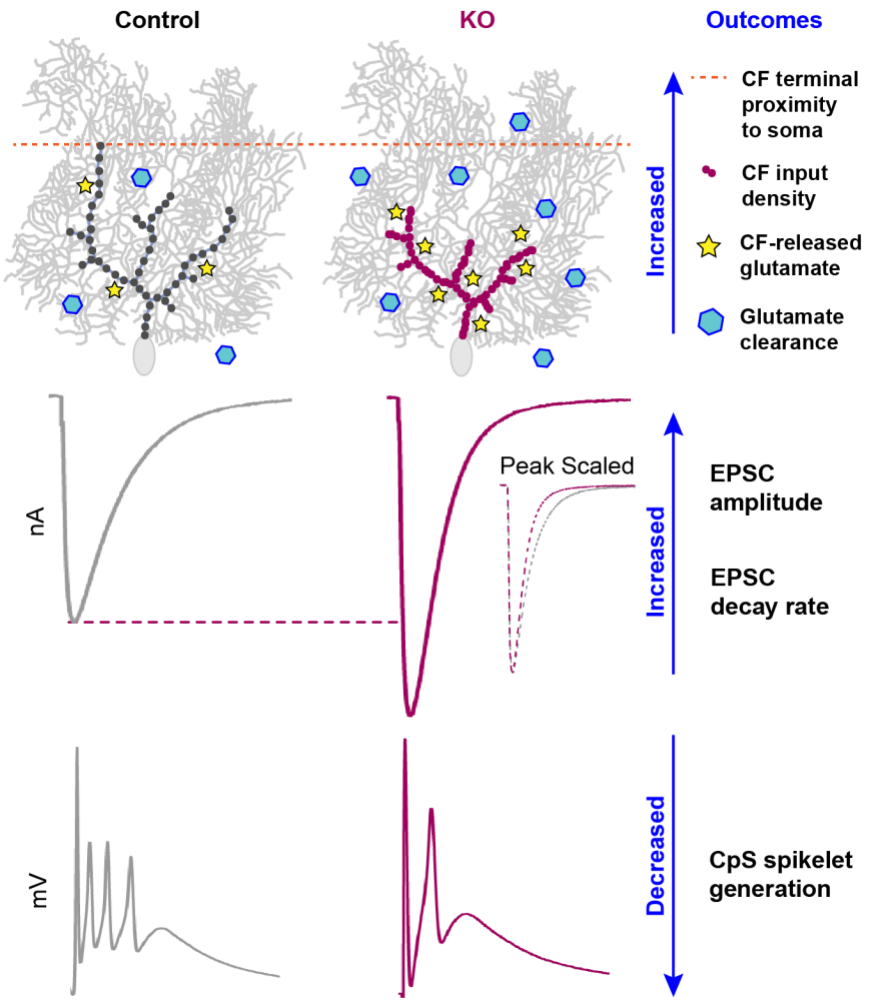

Figure 3.10 Summary of CF-PC phenotypes in Cacna2d2 KO mice.

Proximal distribution of CF inputs onto KO Purkinje cells enhanced postsynaptic quantal responses to CF glutamate release, and the increased number of synaptic release sites increased total glutamate concentration. Together, this resulted in a 140% EPSC amplitude in the KO compared to control. Counteracting effects included a lower CF P_R and enhanced glutamate clearance, which doubled the EPSC decay rate. Ultimately, larger synaptic

conductances in the KO likely contribute to depolarization block of CF-evoked spikelet generation.

CHAPTER 4: ALPHA2DELTA-2 IS REQUIRED FOR FUNCTIONAL POSTSYNAPTIC CALCIUM CHANNEL NANODOMAIN SIGNALING

Kathleen A. Beeson[1,2], Gary L. Westbrook[3], Eric Schnell[2,4*]

1 Neuroscience Graduate Program, Oregon Health & Science University, Portland, OR, 97239; 2 Department of Anesthesiology and Perioperative Medicine, Oregon Health & Science University, Portland, OR, 97239; 3 The Vollum Institute, Oregon Health & Science University, Portland, OR, 97239; 4 Operative Care Division, Portland VA Health Care System, Portland, OR, 97239

In preparation for submission to eLife Short Reports, March 2021.

Acknowledgements

This research was supported in part by the Department of Veterans Affairs, Veterans Health Administration, Office of Research and Development, Biomedical Laboratory Research and Development Merit Review Award I01-BX004938 (ES), a Department of Defense CDMRP Award W81XWH-18-1-0598 (ES), NIH T32NS007466 (KAB), NIH R01-NS080979 (GLW), and NINDS 1R21NS102948 (Ines Koerner/ES). We would like to acknowledge the OHSU Advanced Light Microscopy Center and imaging support from the NIH P30NS061800 (OHSU). The contents of this manuscript do not represent the views of the U.S. Department of Veterans Affairs or the United States Government.

Abstract

α2δ proteins (*CACNA2D1-4*) are required for normal neurological function, although the mechanisms whereby α2δ proteins control neuronal output remain unclear. Using whole-cell recordings of mouse cerebellar Purkinje cells, we show that α2δ-2 is required for coupling postsynaptic voltage-dependent calcium entry to effector mechanisms controlling depolarization-induced suppression of excitation as well as action potential afterhyperpolarization. Our findings indicate that α2δ-2 is necessary for the organization of postsynaptic calcium channel nanodomains.

Introduction

Many intracellular signaling cascades are triggered by a common messenger: calcium entering via voltage-gated Ca^{2+} channels (VGCCs) on the plasma membrane. Specificity of Ca^{2+}-dependent signaling at the membrane depends on proximity of VGCCs to effectors in functional "nanodomains", in which [Ca^{2+}] declines steeply with distance from a VGCC (Nakamura et al., 2018). These nanodomains are critical for neuronal function. For example, in Purkinje cells (PCs), depolarization-induced suppression of excitation (DSE) is initiated via Ca^{2+}-dependent endocannabinoid release that mediates short-term presynaptic depression (Kreitzer and Regehr, 2001; Brenowitz, 2003; Brown et al., 2004). Likewise, VGCC-K_{Ca} clusters, expressed throughout PC somata and dendrites (Indriati et al., 2013), generate the afterhyperpolarization (AHP) following action potentials, ultimately setting spontaneous spike rate (Raman and Bean, 1999; Womack et al., 2004). Thus, molecules coupling VGCCs to effector-specific signaling critically contribute to transduction of neuronal outputs.

Auxiliary VGCC α2δ proteins (*CACNA2D1-4*) contribute to VGCC membrane trafficking in heterologous cells and neurons (Dolphin and Lee, 2020), and may play a role in presynaptic VGCC coupling to vesicle release machinery (Hoppa et al., 2012). However, little is known about VGCC auxiliary functions of α2δ outside of these contexts, and previous examination of their postsynaptic roles suggest Ca^{2+}-independent functions (Eroglu et al., 2009). Here we report that in PCs, which abundantly and exclusively express α2δ-2 (Cole et al., 2005; Lein et al., 2007; Beeson et al., 2020), loss of α2δ-2 (*CACNA2D2*) disrupts two forms of postsynaptic VGCC nanodomain signaling, demonstrating previously unappreciated roles for α2δ proteins in VGCC-effector coupling.

Results

At PC climbing fiber synapses, postsynaptic VGCC-mediated Ca^{2+} entry initiates retrograde endocannabinoid signaling, acutely reducing the probability of presynaptic vesicle release - a form of plasticity known as depolarization-induced suppression of excitation, or DSE (Kreitzer and Regehr, 2001; Brown et al., 2004). Specificity of DSE signaling is achieved by tight functional coupling of postsynaptic VGCCs with Ca^{2+}-sensitive endocannabinoid release machinery (Brenowitz et al., 2006). Using whole-cell recordings of PCs in acutely prepared brain slices from *CACNA2D2* KO and WT littermate mice, we investigated whether the absence of α2δ-2 affects this postsynaptic Ca^{2+}-dependent signaling.

We held PCs at -70 mV in voltage-clamp mode during climbing fiber axon stimulation and recorded evoked excitatory postsynaptic currents (EPSCs). In WT PCs, DSE elicited with a 250 ms depolarizing step reduced the amplitude of regularly evoked EPSCs by 25% (**Fig 4.1A**). In contrast, DSE was completely absent in KO PCs (**Fig 4.1B-C**). The *ducky* mouse, which also lacks α2δ-2 protein, has a reported ~30% decrease in PC somatic VGCC density, which is thought to represent decreased surface trafficking (Donato et al., 2006). As the degree of climbing fiber DSE is related to the magnitude of Ca^{2+} influx, it is possible that the reduced VGCC density prevented DSE. However, although increasing the length of the depolarizing step enhances Ca^{2+} influx and DSE in wildtype mice (Brenowitz, 2003), a four-fold increase in depolarizing step length failed to evoke DSE in α2δ-2 KO PCs **(Fig 4.1D-F**).

As DSE was not rescued by increasing activation of VGCCs in KO PCs, we hypothesized that functional coupling of Ca^{2+} influx to effector molecules was disrupted in the absence of α2δ-2. To examine this possibility, we lowered [EGTA] in our internal solution. As expected for WT PCs, decreasing [EGTA] to either 2 mM or 0.2 mM revealed more profound DSE, which increased with longer voltage steps (**Fig 4.2A-C**), consistent

with further diffusion of Ca^{2+} from its point of entry. More notably, however, reduced Ca^{2+} buffering rescued DSE in KO PCs (**Fig 4.2D-F**), indicating that signaling mechanisms involved in DSE expression remained intact. As the reduced Ca^{2+} buffering primarily affects the distance of Ca^{2+} diffusion from its source, these data indicate that rather than affecting Ca^{2+} entry per se, α2δ-2 mediates tight functional coupling between VGCCs and endocannabinoid release.

To determine whether α2δ-2 affected coupling of other molecules to postsynaptic VGCC nanodomains, we focused on Ca^{2+}-dependent action potential AHPs. In PCs, the AHP is mediated by BK-type K_{Ca} channels (Edgerton and Reinhart, 2003; Niday and Bean, 2021), and regulates sodium channel availability and PC firing rate (Raman and Bean, 1999; M and K, 2002). To assess VGCC-K_{Ca} coupling, we recorded spontaneous spiking in PCs from WT and KO mice during whole-cell current-clamp recordings. In agreement with previous studies in the *ducky* mutant (Donato et al., 2006; Walter et al., 2006), tonic spike rate in α2δ-2 KO PCs was significantly reduced compared to WT (**Fig 4.3A-B**). More importantly, examination of individual spike waveforms revealed that the AHP amplitude was consistently smaller in α2δ-2 KO cells (**Fig 4.3C-D**), indicating reduced K_{Ca} channel activation (Edgerton and Reinhart, 2003; Womack et al., 2004). Other membrane properties were unchanged between WT and KO PCs, including the resting membrane potential, maximum and minimum membrane polarization rates, spike threshold as well as spike height (**Fig 4.3E-J**), indicating that this effect was restricted to the K_{Ca}-mediated AHP. Additionally, there was no change in BK membrane localization in PCs by immunohistochemistry (**Fig 4.3K**; Membrane BK density: WT = 0.82 ± 0.13, n = 4; KO = 0.75 ± 0.08, n = 3; p = 0.7; Student's unpaired t-test), which is also consistent with prior studies confirming normal BK expression and function in other neurons in the *ducky* mutant (Fell et al., 2016).

To determine whether K_{Ca} channels were functionally uncoupled from VGCC-mediated Ca^{2+} influx in KO mice, we dialyzed PCs with an EGTA concentration (5 mM) sufficient to uncouple VGCC-BK signaling (Fakler and Adelman, 2008). This increased Ca^{2+} buffering reduced the AHP amplitude in WT cells to the same amplitudes seen in the KO, and had no effect on the AHP in KO cells (**Fig 4.3C-D**). Thus, increased Ca^{2+} buffering uncoupled VGCC-K_{Ca} signaling in WT, but K_{Ca} channels were already functionally uncoupled in the α2δ-2 KO.

Discussion

As a primary signal in neurons, precise spatiotemporal regulation of Ca^{2+} influx is essential to maintain fidelity of Ca^{2+}-dependent processes. Consequently, the molecules controlling VGCC coupling to downstream effectors is critical to neuronal function. Since their initial discovery as VGCC-associated molecules, multiple lines of evidence suggest α2δ proteins are involved trafficking of VGCCs to the plasma membrane (Dolphin and Lee, 2020). However, these conclusions were largely based on heterologous expression systems, as most neurons express more than one α2δ isoform. Thus, information of postsynaptic auxiliary VGCC effects of α2δ in neurons is limited. Because PCs selectively express only one isoform, α2δ-2 (Cole et al., 2005; Lein et al., 2007; Beeson et al., 2020), the *CACNA2D2* KO mouse provides an ideal model to examine roles for α2δ-2 proteins in functional VGCC-signaling in postsynaptic compartments.

We found that two distinct signaling mechanisms, DSE and K_{Ca} signaling, were disrupted in α2δ-2 KO PCs, indicating a functional loss of VGCC nanodomains (Kreitzer and Regehr, 2001; Brenowitz et al., 2006; Fakler and Adelman, 2008; Indriati et al., 2013). How does α2δ-2, a largely extracellular protein, mediate functional coupling of VGCCs with intracellular effector proteins? It is possible that α2δ-2 directly associates with other extracellular proteins involved in VGCC domains (Dolphin and Lee, 2020). As endocannabinoid machinery resides at synapses (Uchigashima et al., 2007), and α2δ proteins are important for synapse formation (Cole et al., 2005; Lein et al., 2007; Eroglu et al., 2009; Beeson et al., 2020), α2δ could potentially regulate VGCC nanodomains by binding to presynaptic adhesion proteins.

Another possibility is that α2δ-2 localizes VGCCs to lipid rafts. Though VGCCs are abundant in non-lipid raft membrane fractions where they are independent of α2δ-2,

VGCCS and α2δ-2 colocalize in lipid rafts isolated from cerebellar homogenates (Davies et al., 2006). Intriguingly, DAG lipase-α, the enzyme responsible for synthesis of endocannabinoids involved in DSE, has also been isolated in lipid rafts (Rimmerman et al., 2008), and mislocalization of VGCCs away from lipid rafts might explain the reduced basal endocannabinoid tone at cerebellar synapses in the *ducky* mutant (Wang et al., 2013). Future work will be required to directly assay α2δ-2 interacting proteins, as well as subcellular localization of VGCCs, in PCs. The deficits in Ca^{2+}-dependent signaling we observed could explain some of the dramatic neurologic phenotypes in α2δ-2 KO mice, and future investigations of the potential coupling roles of other α2δ isoforms in neurons will provide valuable insights into how these proteins impact neurological functions across the brain.

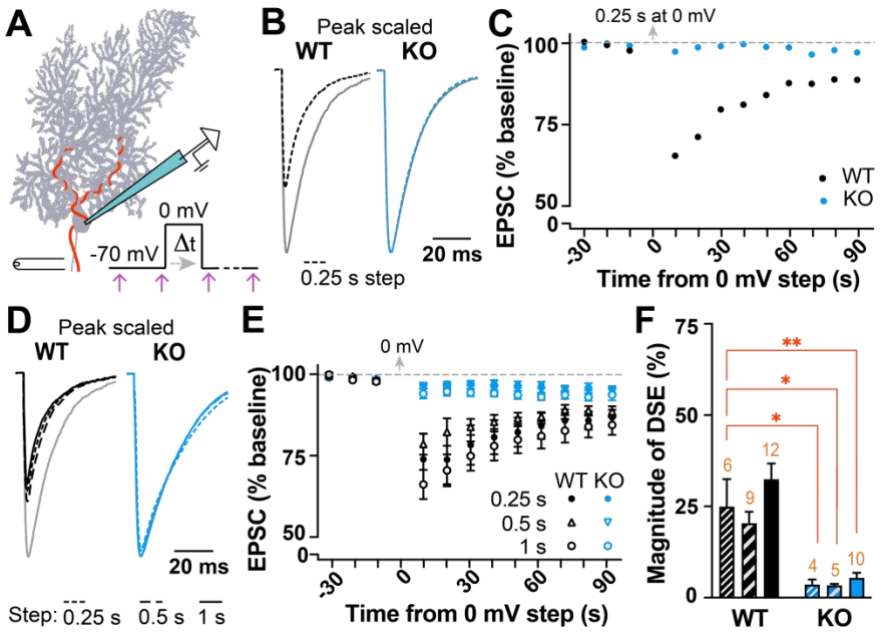

Figure 4.1 Depolarization-Induced Suppression of Excitation (DSE) reduces climbing fiber-EPSC amplitude in WT but not α2δ-2 KO Purkinje cells.

(***A***) Schematic of whole-cell electrophysiological set-up. Purkinje cell (PC) is held at -70 mV using whole-cell patch clamp while the innervating climbing fiber axon (red) is stimulated at 0.2 Hz (magenta arrows). After collection of baseline EPSCs, a depolarization step to 0 mV for a duration of 250 ms – 1s is delivered to the PC, and subsequent EPSCs are collected for >3 minutes.

(***B***) Overlay of peak-scaled EPSC traces from WT (black) and KO (blue) PCs during baseline stimulation (gray) and 5 s post-depolarization step of 250 ms duration (dotted line).

(***C***) EPSC amplitude timecourse from the representative experiment in (***B***). Each point represents the average from two consecutive EPSCs at 0.2 Hz.

(***D***) Overlay of peak-scaled EPSC traces from WT (black) and KO (blue) PCs during baseline (gray/light blue) and 5 s post-depolarization step of 250 ms (dotted line), 500 ms (dashed line), and 1 s (solid line) duration.

(***E***) Summary of DSE timecourse from WT (black) and KO (blue) experiments using three different depolarization step durations: 250 ms (filled circle), 500 ms (triangle) and 1 s (open circle). Each point represents the average of two consecutive EPSCs at 0.2 Hz.

(***F***) Magnitude of EPSC depression normalized to baseline in WT (black) and KO (blue) after 250 ms (fine stripe), 500 ms (wide stripe) and 1 s (solid) depolarization steps. One-way ANOVA comparison to average WT 250 ms response, Dunnett's correction for multiple comparisons; * $p < 0.05$, ** $p < 0.01$, *** $p < 0.001$.

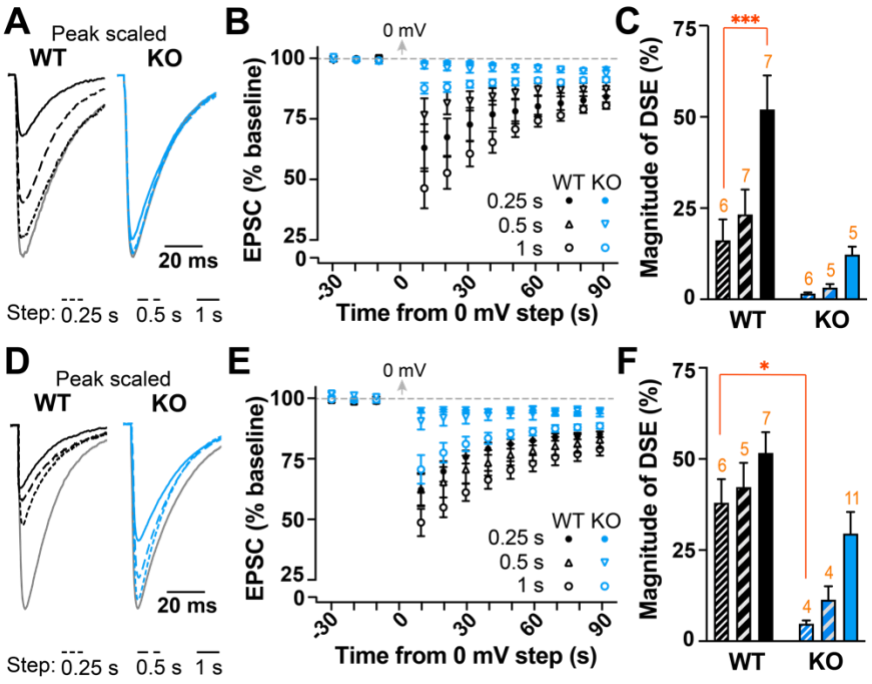

Figure 4.2 Reducing intracellular [EGTA] reveals climbing fiber DSE in the α2δ-2 KO.

(***A, D***) Overlay of peak-scaled EPSC traces from WT (black) and KO (blue) PCs during baseline stimulation (gray) and 5 s post-depolarization step of 250 ms (dotted line), 500 ms (dashed line), and 1 s (solid line) duration using a 2 mM (***A***) or 0.2 mM (***D***) EGTA intracellular solution.

(***B, E***) Summary of DSE timecourse from WT (black) and KO (blue) experiments using a 2 mM (***B***) or 0.2 mM (***E***) EGTA internal solution and three different depolarization step durations; 250 ms (filled circle), 500 ms (triangle) and 1 s (open circle). Each point represents the average from two consecutive EPSCs at 0.2 Hz.

(***C, F***) Magnitude of EPSC depression normalized to baseline in WT (black) and KO (blue) after 250 ms (fine stripe), 500 ms (wide stripe) and 1 s (solid) depolarization steps using a 2 mM (***C***) or 0.2 (***F***) EGTA intracellular solution. One-way ANOVA comparison to average WT 250 ms response, Dunnett's correction for multiple comparisons; * $p < 0.05$, ** $p < 0.01$, *** $p < 0.001$.

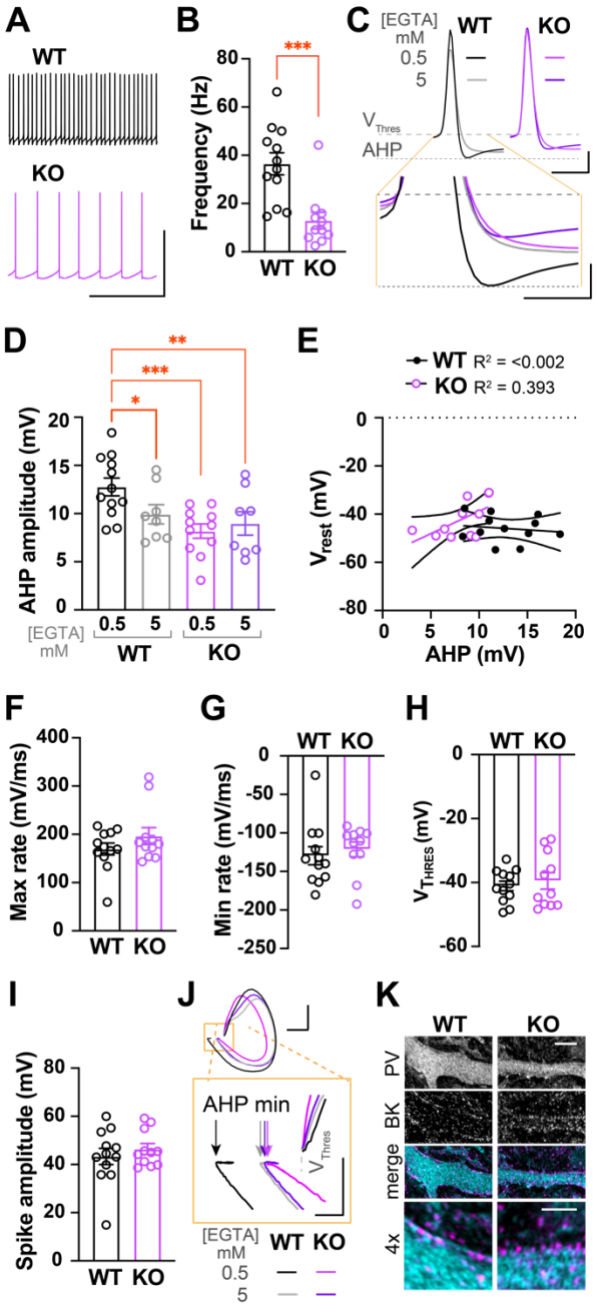

Figure 4.3 Spontaneous firing frequency, afterhyperpolarization (AHP) amplitude and Ca^{2+} uncoupling are reduced in the α2δ-2 KO.

(***A***) Example traces spontaneous action potentials in WT (0.5 mM EGTA, black; 5 mM EGTA, gray) and KO (0.5 mM EGTA, magenta; 5 mM EGTA, purple) PCs; scale = 50 mV, 0.5 s.

(***B***) Summary of average spontaneous firing frequency in PCs. Student's unpaired t-test, $p < 0.0001$.

(***C***) Average of 50 consecutive spontaneous action potentials from WT (black) and KO (magenta) during tonic firing; scale = 10 mV, 2 ms. Gray dotted lines to indicate V_{thres} as well as the minimum voltage during afterhyperpolarization (AHP). Enlarged overlay of traces below to illustrate differences in V_{thres}-AHP amplitude; scale = 5 mV, 1 ms.

(***D***) Summary of AHP amplitudes recorded after action potentials using intracellular solution containing 0.5 mM or 5 mM EGTA. One-way ANOVA comparison to average WT 0.5 mM EGTA response, uncorrected Fischer's LSD; * $p < 0.05$, ** $p < 0.01$, *** $p < 0.001$.

(***E***) Correlation of AHP amplitude vs. resting membrane potential (V_m) in WT (black) and KO (magenta) PCs using 0.5 mM EGTA intracellular solution. Linear regression and 95% confidence interval shown.

(*F-I*) Action potential waveform parameters in WT and KO PC. No significant differences found for maximum rate (***F***), minimum rate (***G***), threshold (***H***) or spike height (***I***); unpaired Student's t-tests.

(*J*) Phase plane plots of spontaneous spikes in PCs using 0.5 mM or 5 mM EGTA intracellular solution. Traces are aligned by threshold (V_{thresh}) for comparison; scale = 100 mV/ms, 20 mV. Enlarged inset to illustrate differences in AHP minimum amplitude between WT (arrows; 0.5 mM EGTA, black; 5 mM EGTA, gray) and KO (arrows; 0.5 mM EGTA, magenta; 5 mM EGTA, purple); scale = 100 mV/ms, 5 mV.

(*K*) Immunohistochemistry of WT and KO cerebellar slices stained for parvalbumin (PV; cyan) to indicate PC morphology, and the BK channel (magenta), which is involved in AHP generation; Scale 5 μm. Below merged image is a 4x zoom to illustrate membrane localization of BK channels; Scale 2 μm.

CHAPTER 5: DISCUSSION & FUTURE DIRECTIONS

Using the *CACNA2D2* KO mouse and electrophysiological analysis of PCs, we revealed new and intriguing roles for α2δ-2 proteins. In Chapter 3, we analyzed the role of α2δ-2 in postsynaptic control of CF synapse morphology and function, and in Chapter 4 we demonstrated that α2δ-2 is critical for the functional coupling of two postsynaptic VGCC nanodomains mediating eCB and K_{Ca} signaling. However, both of these studies consist of functional observations from a constitutively deleted *CACNA2D2* mouse, leaving many unanswered mechanistic questions about how α2δ-2 contributes to these specific roles. Below, I will frame some of the key findings from these studies in terms of the questions brought forth, and propose specific aims that could next be addressed.

Postsynaptic α2δ-2 controls presynaptic excitatory synapse formation

During my experiments investigating the synaptogenic effects of postsynaptic deletion of α2δ-2, Risher et al. revealed the first evidence that postsynaptic α2δ-1 drives excitatory synapse formation (Risher et al., 2018). Surprisingly, we found that loss of postsynaptic α2δ-2 in PCs enhanced CF-evoked EPSCs by a combination of effects, including a mislocalization of presynaptic terminals that positioned synapses more proximally along the PC dendritic tree, thereby conserving current amplitude. α2δ-2 KO CFs also had an enlarged pool of glutamatergic vesicles due to more synaptic contacts made onto PCs. The net result of these synaptic phenotypes was aberrant spiking in PCs, which are the sole output from cerebellar cortex. These findings may explain the behavioral phenotypes, such as ataxia, indicating cerebellar dysfunction in mutant mice.

To determine the locus of α2δ-2 protein's synaptogenic function, we used quantitative PCR for *CACNA2D* isoforms from fresh-frozen, laser-captured tissues from the

PC layer and inferior olivary nucleus, which give rise to CFs. In agreement with *in situ* hybridization data, and now single-cell mRNA sequencing data (DropViz, Broad Institute), we found that PCs exclusively express α2δ-2 while presynaptic inferior olivary cells highly express α2δ-1 (Cole et al., 2005; Lein et al., 2007; Beeson et al., 2020). Despite being expressed to a far lesser degree than α2δ-1, presynaptic α2δ-2 may simply exert stronger control over CF innervation and function. This explanation would suggest independent functions for different α2δ isoforms such that α2δ-1 could not compensate for α2δ-2 loss. However, a more likely explanation is that enhanced CF innervation and function are due to a complete loss of α2δ proteins postsynaptically. Nonetheless, our findings suggest that α2δ proteins are not redundant in function, as α2δ-1 proteins positively drive excitatory synapse formation (Eroglu et al., 2009; Kurshan et al., 2009; Hoppa et al., 2012; Risher et al., 2018).

Postsynaptic Rescue: Considerations & Logistical Challenges

Do α2δ isoforms differentially regulate excitatory synapse formation, and do α2δ proteins localize differentially to pre- or postsynaptic terminals? Ideally, we would have demonstrated α2δ-2 protein's postsynaptic role directly by replacing α2δ-2 expression in PCs, rescuing some or all of the synaptic phenotypes in KO cells. In fact, many months of my graduate training were spent on efforts to virally transduce single-PCs to test these questions. For example, α2δ-2 could be replaced with other α2δ isoforms to study functional redundancy, or tagged constructs could be delivered to visualize α2δ localization. Transducing PCs as early as possible would be advantageous, as PCs are already contacted by multiple CFs by P3 in mice, though axon competition and innervation by a dominant "winner" CF is not established until P21 (Hashimoto and Kano, 2003; Hashimoto et al., 2009).

Though PCs can be transduced with adeno-associated viruses (AAVs) in early development, the desired cargo for such experiments – ~3.5 kilobases of the *CACNA2D2*

gene plus an internal ribosome entry site type 2 (IRES2; ~500 bp) to boost translation of a fluorescent marker, such as GFP (~700 bp) – exceeds the capacity for efficient production of AAV vectors (~4 kb) (Hirai, 2008). Moreover, *CACNA2D2* KO mice are vulnerable throughout early development, and handling them while young may further reduce the chances of surviving an injection procedure. Alternatively, lentiviruses can transduce young or adult PCs with moderate efficiency, and carry ~2x the cargo (Nitta et al., 2017). Using an L7 or other PC-specific promotor is beneficial; otherwise, Bergmann glia that reside in the PC layer predominantly take up lentivirus. In our hands, high-titer lentivirus carrying a minimal L7 promotor (to increase available cargo size) and GFP still produced a low yield of dim PCs several weeks after infection. Thus, viral vector-rescue experiments in PCs pose logistical challenges for investigating the pre- or postsynaptic locus of α2δ protein's action(s) *in vivo*.

Future directions

Other brain regions or cell-types may be more amenable to viral-mediated gene manipulation (Zou et al., 2016) and, as in PCs, α2δ-2 is abundantly expressed in parvalbumin (PV^+) interneurons throughout the brain (Cole et al., 2005). The PV^+ basket interneurons of the hippocampus may be an interesting cell type in which to assess synaptic physiology and selectively rescue or replace α2δ isoforms. Like CFs, excitatory neurons of the hippocampus primarily express α2δ-1 as well as α2δ-3. Thus, synaptic phenotypes of PV^+ basket cells in *CACNA2D2* KO mice should be due to postsynaptic loss of α2δ. In fact, we have crossed $PV^{Cre\ +/+}$ mice with $Cre^{tdTomato+/+}$ marker mice to specifically label the PV^+ population. We then crossed these mice with our *CACNA2D2* $^{+/-}$ mice to yield $PV^{Cre::tdT}$::*CACNA2D2* mice. This triple-cross mouse would allow for easy identification of PV^+ basket cells for electrophysiology and the Cre-recombinase system could be used for PV^+ selective viral-mediated gene transfer. As *CACNA2D2* KO mice exhibit seizures, which may relate to

dysfunction of GABAergic signaling in the hippocampus (Drexel et al., 2017), studies of α2δ-2-dependent PV^+ function could be insightful as well.

Are similarities in CF-PC phenotypes from VGCC mutants a reflection of molecular interactions with α2δ-2 proteins?

The synaptic phenotypes observed in the α2δ-2 KO, such as the proximal distribution of CF terminals, resemble other synaptic and VGCC gene mutant phenotypes. As discussed in Chapter 3, PC-specific deletion of Cav2.1 or global mutations of Cav2 pore subunits also result in mislocalization of CF terminals. Calcium channel signaling and Cav2 expression are not required for excitatory synapse formation (Eroglu et al., 2009; Kurshan et al., 2009; Held et al., 2020), but whether VGCCs play a role in proper localization of synaptic contacts remains unknown. This question is best addressed through studies of intact circuits *in vivo*. In this hypothesis, α2δ proteins traffic VGCC to the membrane, which could nucleate or participate in postsynaptic spine formation (Biederer et al., 2017).

Cav2.1 channels are expressed in a gradient from the PC soma to distal dendrites, scattered, and in clusters, as evidenced by immunogold electron microscopy of freeze-fractured tissues (Indriati et al., 2013). PCs also express Cav1.3 and Cav3.1 (DropViz, Broad Institute; (Gruol et al., 2006; McKay et al., 2006), possibly at synapses (Doroshenko et al., 1997)[19], though this expression profile is challenging to confirm pharmacologically. Notably, expression of low-voltage activated VGCC isoforms may also influence excitatory synapse

[19] Here, Doroshenko *et al.,* show that PC inhibition by PV+ basket interneurons relies on a larger proportion of low-voltage activated VGCCs for transmission – thus, the channels in question are presynaptic. However, as PV+ neurons, basket cells are also likely impacted by *CACNA2D2* deletion. Moreover, basket cells innervate PC somata and proximal dendrites and may influence CF development Sotelo C (2008) Development of "Pinceaux" formations and dendritic translocation of climbing fibers during the acquisition of the balance between glutamatergic and gamma-aminobutyric acidergic inputs in developing Purkinje cells. J Comp Neurol 506:240-262..

formation. In this scenario, the distribution of various VGCCs via α2δ-2 regulation could facilitate CF innervation. If the primary role of α2δ-2 proteins is to properly traffic VGCCs to sites of synapse formation or orchestrate their association with other synaptically targeted molecules (as suggested by our VGCC-eCB findings in Chapter 4) this could explain both the mislocalization and high density of proximally-targeted presynaptic CFs in the α2δ -2 KO mouse. Under this hypothesis, we would expect α2δ proteins to have a distribution pattern similar to synaptogenic molecules and VGCCs. A lack of reliable commercial antibodies for α2δ proteins, especially in tissues, further complicates assessment of endogenous α2δ protein localization.

Future directions

Production of custom antibodies for α2δ proteins, or a tagged- α2δ knock-in mouse, would be the best methods to visualize α2δ isoform distribution in native tissues; though, both approaches are labor-intensive. However, expression of a tagged- α2δ protein, with careful adjustment of promotor strength, could provide useful information about where these molecules are expressed in neurons. An alternative approach to *in vivo* viral-mediated gene transfer, which can pose logistical challenges in PCs, is organotypic slice culture and biolistic transfection.

Cerebellar slices can be prepared from young (P3-P10) mice and maintained in culture for nearly 2 weeks (Uesaka et al., 2012; Rakotomamonjy, 2019). One could make slices from *CACNA2D2* KO mice and then, using a gene transfer method, rescue α2δ protein expression with tagged isoforms in single cells (ideally, several singly transfected PCs per slice, which is feasible with biolistic transfection). I have made constructs that consist of a strong promotor (CAG), HA-tagged α2δ gene, IRES-GFP or IRES-mCherry, that could be used for these experiments. Future constructs could use fluorescently labeled α2δ proteins,

under low-to-moderate promotor strengths, to visualize more natural α2δ distribution by light microscopy throughout development. Finally, Cav2.1-GFP and Cav2.2-GFP constructs (Schneider et al., 2015), as well as other fluorescently-labeled Cav or synaptic molecules, could be co-expressed with α2δ isoforms to assess colocalization. This model would allow access to gene manipulation and visualization in α2δ null neurons while maintaining some elements of the circuitry. Others have successfully co-cultured inferior olivary explants to monitor CF development *ex vivo* (Uesaka et al., 2012). Preferably, troubleshooting of constructs[20] in this system would allow for eventual cerebellar or hippocampal replacement of tagged-α2δ proteins *in vivo*.

α2δ-2 controls postsynaptic VGCC nanodomain function

In Chapter 4, we explored whether α2δ proteins contributed to the function of postsynaptic VGCC nanodomains, as they have been implicated in presynaptic vesicle release. Indeed, α2δ-2 KO cells were more sensitive to calcium buffering in an eCB short-term plasticity assay (depolarization-induced suppression of excitation or DSE), suggesting that calcium influx through VGCCs is functionally uncoupled from eCB release machinery. To understand if α2δ-2 proteins function at other postsynaptic VGCC nanodomains, we tested the effects of α2δ-2 deletion at calcium-dependent K_{Ca} signaling domains. K_{Ca} channels generate the spike AHP, which was significantly reduced in α2δ-2 KO cells, and application of EGTA in WT cells mimicked the KO AHP. However, this same treatment did not affect the KO, indicating a functional disruption of VGCC-K_{Ca} in the KO that cannot be further interrupted by EGTA. Immunostaining for the K_{Ca} channel thought to generate the AHP, the BK channel (Edgerton and Reinhart, 2003; Niday and Bean, 2021), showed that membrane

[20] For example, if α2δ-2^{GFP} traffics normally to PC membranes and the strength of the promotor is adjusted to reduce saturation, this may satisfy the AAV packaging limit.

expression between WT and KO was unchanged. Thus, two distinct postsynaptic VGCC nanodomains are disrupted after α2δ-2 deletion.

We revealed that loss of α2δ-2 uncouples VGCC-effector associations based on sensitivity to intracellular calcium buffering by EGTA. It has been suggested that sensitivity to high EGTA can occur as a result of reduced VGCC density at nanodomains, such that effector molecules are coupled with single VGCCs as opposed to VGCC clusters (Nakamura et al., 2018). Whether α2δ-2 KO sensitivity to EGTA is a result of single VGCC-containing nanodomains would require immunogold electron microscopy of freeze-fractured tissues. Alternatively, one could consider alterations in overall VGCC density by measuring changes in the total abundance of VGCCs by whole-cell electrophysiology. As PCs are large cells with complex morphology, and exhibit a leak currents (e.g. potassium channels, I_h, etc.), calcium currents are best isolated in dissociated PC preparations(Raman and Bean, 1999), in which the only the soma remains. Another advantage to this method is the application of pharmacology or ion substitution. For example, barium can pass through open VGCCs and carries more charge than calcium, thus it generates larger measurable currents.

Though the circumstances of 2020 prevented my intended experiment to directly measure whether loss of α2δ-2 results in changes to VGCC current density by whole-cell recording from dissociated PCs, this exact experiment has been performed in dissociated PCs from *ducky* mutants and showed a 30% reduction in VGCC current density (Donato et al., 2006). Similarly, recordings from inner hair cells in *ducky* mutants, as well as dorsal root ganglion neurons from α2δ-1 transgenic KOs, show the same reduction (Patel et al., 2013; Fell et al., 2016). If we predict PCs from *CACNA2D2* KOs also have a 30% reduction in VGCC membrane density, and considering the strong correlation between VGCC activation and the magnitude of DSE (Brenowitz, 2003), our findings using varying depolarization step lengths to control the amount of PC calcium influx demonstrate a more severe impairment

in VGCC-eCB signaling in KO PCs than expected. For example, in the lowest EGTA treatment (see Figure 4.2), a step length of 1 second in the KO still yielded a smaller magnitude of DSE than a 250 ms step length in WT. Therefore, despite 4x the VGCC activation, the α2δ-2 KO still exhibits eCB signaling deficiencies.

Finally, VGCCs are also expressed throughout PC dendrites (Indriati et al., 2013); thus, VGCC current density measurements from dissociated PC somata may underestimate the true reduction in the α2δ-2 KO. Several scenarios are possible: VGCC distribution to dendrites requires α2δ-2 proteins and thus, VGCC density reduction in the KO is more severe than demonstrated by dissociated PC recordings, and/or α2δ-2 is required for proper coupling between VGCCs and effector molecules. Thus, in addition to direct measurements of VGCC currents from α2δ-2 deleted cells, the experiments proposed above pertaining to the study of neuronal VGCC distribution would help determine the extent to which α2δ proteins impact overall vs. nanodomain-specific VGCC trafficking or function.

Do α2δ proteins traffic VGCC to lipid rafts to enable VGCC-effector coupling?

If α2δ-2 KO cells have a 30% reduction in VGCC abundance, and we've identified two postsynaptic nanodomains that are profoundly impacted by loss of α2δ-2, the α2δ-2-dependent population of VGCCs may belong to specialized nanodomain groupings. For example, α2δ-2 may traffic a subset of VGCCs to specialized domains, where they can functionally couple to eCB machinery, like DAGα lipase.

This hypothesis was introduced in the discussion in Chapter 4 and rests on the observations that 1) α2δ proteins are tethered to the plasma membrane via a GPI-anchor, which is required for its expression in lipid rafts on the plasma membrane (Davies et al., 2010); 2) Cav2.1 is abundant in non-lipid raft plasma membrane but is also co-expressed with α2δ-2 in lipid raft fractions from cerebellar homogenate (Davies et al., 2006); and 3)

DAGα lipase has been isolated in lipid rafts from other neurons (Rimmerman et al., 2008), as has the BK channel in non-neuronal cell-types (Noble et al., 2006).

Future directions

Membrane fractionation to detect lipid rafts requires biochemical analysis, such as western blot, after treating tissues with detergents. Specialized lipid raft molecules, including the flotillin scaffold protein, may also offer useful markers with which to identify or visualize these domains by immunofluorescence. To understand if VGCC coupling to effector molecules is dependent on α2δ-mediated trafficking to lipid raft membranes, one could analyze membrane fractions from the *CACNA2D2* KO. We would expect that in WT tissues, lipid raft fractions would contain at least the following: α2δ proteins, VGCCs, and DAGα lipase or BK channels. Furthermore, we would expect that lipid raft fractions from KO tissues would lack α2δ-2 and VGCCs. These experiments would explain why only a portion of VGCCs are affected by α2δ-2 deletion and provide insight into the mechanisms underlying α2δ protein-mediated coupling of VGCCs to effector molecules.

Are VGCC nanodomains in presynaptic terminals from CACNA2D2 KO PCs affected by deletion of α2δ-2?

Though our second study focused on postsynaptic VGCC nanodomains, presynaptic vesicle release is highly dependent on calcium, and localization of VGCCs relative to calcium-sensitive SNARE molecules affects release properties (Nakamura et al., 2015). Studies from inner hair cells show reduced vesicle exocytosis in *ducky* mutants, though these cells may also express α2δ-3, which could compensate for loss of α2δ-2 (Fell et al., 2016). Likewise, deletion or overexpression of α2δ proteins from hippocampal cultures reduces or increases vesicle exocytosis, respectively (Hoppa et al., 2012). However, excitatory neurons in the

hippocampus highly express α2δ-1 and α2δ-3, making isoform contributions to presynaptic release difficult to parse. Interestingly, Hoppa et al. found that overexpression of α2δ proteins reduced calcium influx, despite increased VGCC abundance at presynaptic terminals. Furthermore, they found that α2δ proteins promoted tighter coupling of VGCCs to exocytosis machinery, as α2δ overexpressing neurons were more resistant to intracellular EGTA application. Given the complete loss of α2δ proteins in PCs from *CACNA2D2* KO mice and the profound impacts this has on postsynaptic nanodomains, it would be interesting to investigate if presynaptic nanodomains are similarly affected.

Future directions

PCs are the sole output from the cerebellar cortex and fire action potentials at high frequencies (50-150 Hz *in vivo*), inhibiting a variety of neurons in the deep cerebellar nuclei (DCN) through the release of GABA(Najac and Raman, 2015). Thus, changes in presynaptic vesicle release could be measured using whole-cell recordings from DCN neurons while stimulating PC axons. Recording from neurons in the DCN is not trivial, as heavy myelination[21] and other heterogeneous inhibitory inputs are present. For example, approximately two-thirds of nucleo-olivary cells (of which there are at least two sub-types) receive inhibitory input from PCs, as well as from local GABAergic and glycinergic interneurons (Najac and Raman, 2015). Thus, it would be beneficial to cross the *CACNA2D2* breeder mice with a PC-specific channelrhodopsin line for selective optogenetic control of PC terminals (ex: Ai27D::Pcp2-Cre::CACNA2D2). Notably, α2δ-2 is sparsely expressed by neurons throughout the DCN, and possibly in nucleo-olivary cells (Lein et al., 2007). Thus,

[21] Specialized techniques are required to prepare slices from white matter brain regions, as myelin can obscure visibility and accessibility for patching neurons.

one would need to consider postsynaptic expression patterns of α2δ isoforms and possible synaptic effects due to α2δ-2 deletion.

Is reduced eCB function in the CACNA2D2 KO also due to presynaptic dysfunction?

While our evidence of intracellular EGTA sensitivity in KO PCs directly demonstrates a postsynaptic mechanism for reduced eCB function, CB_1R signaling may also be disrupted in the *CACNA2D2* KO[22]. For instance, even under the lowest [EGTA] conditions, the magnitude of DSE was less at KO synapses compared to WT (**Figure 4.2)**. This finding could reflect either 1) a more severe reduction in postsynaptic calcium influx and/or coupling in the KO than we should expect based on the *ducky* literature (as earlier discussed), or 2) reduced efficacy of presynaptic CB_1R signaling, or 3) a combination of pre- and postsynaptic dysfunctions. In fact, it has been reported that larger amplitude spontaneous inhibitory postsynaptic currents (sIPSCs) at *ducky* cerebellar synapses were due to deficient presynaptic CB_1R signaling[23](Wang et al., 2013). CF-evoked excitatory postsynaptic currents (EPSCs) are larger in PCs after α2δ-2 deletion (**Figure 3.2**), and postsynaptic VGCC-eCB

[22] It may be of interest to investigate whether presynaptic CB_1Rs signaling is affected by loss of α2δ-2 proteins, but mechanistic details would be challenging to acquire. Presynaptic CB_1Rs are $G_{i/o}$ GPCRs that inhibit Cav2 function when activated, however, little is known about how they specifically modulate VGCCs to reduce calcium influx, or the spatial relationships between CB_1Rs and Cav2s. Brown SP, Safo PK, Regehr WG (2004) Endocannabinoids inhibit transmission at granule cell to Purkinje cell synapses by modulating three types of presynaptic calcium channels. J Neurosci 24:5623-5631, Szabo GG, Lenkey N, Holderith N, Andrasi T, Nusser Z, Hajos N (2014) Presynaptic calcium channel inhibition underlies CB(1) cannabinoid receptor-mediated suppression of GABA release. Ibid.34:7958-7963.

[23] Wang *et al*. recorded sIPSCs in PCs from WT and *ducky* mutants and applied the CB_1R agonist, WIN55,212, followed by an antagonist, AM251, to measure the functionality of CB_1Rs and "eCB tone." Here, WIN55,212 should reduce sIPSC amplitude, demonstrating functional CB_1R signaling, and AM251 should rescue sIPSC current amplitude; the extent of rescue would indicate the ambient eCB in the tissue. The authors report that WT and *ducky* had a minor difference in the magnitude of response to WIN55,212, and also found that sIPSC amplitudes increased in both genotypes, though a decrease in amplitude was expected. Furthermore, these data are based on a low number of samples with large variability, calling the strength of their conclusions into question.

nanodomains are disrupted in KOs. Therefore, does dysfunctional eCB signaling at α2δ-2 KO synapses result in reduced eCB 'tone' that contributes to the larger CF-evoked EPSCs we observed?

Future directions

eCB activation of CB_1Rs results in a reduction of presynaptic vesicle release probability (P_R). When recording from WT and KO PCs, stimulation of the CF axon in short succession (twice for paired-pulse) can provide an estimate of P_R. This recording paradigm can be combined with pharmacology to reveal the function of CB_1Rs and estimate the ambient eCB tone contributing to persistent CB_1R activation.

For example, comparing the relative changes in P_R and EPSC amplitude, before and after application of a CB_1R agonist (such as WIN55,212), provides a measure of the maximal activation by CB_1R signaling. Subsequently, application of a CB_1R antagonist (such as AM251), in comparison to baseline responses, can indicate the presence of eCB tone or tonic eCB signaling. Here, the presence of eCB tone would be detected by EPSC amplitude increases >100% baseline (due to higher P_R). In the scenario that α2δ-2 KO synapses have deficient eCB signaling (postsynaptic in origin), and potentially reduced eCB tone, we would see a reduction in EPSC amplitude and lower P_R after agonist treatment, with a full rescue in response to CB_1R antagonist. If presynaptic CB_1R signaling is dysfunctional in α2δ-2 mutants, CB_1R activation will be less robust than in WT; whereas, if eCB tone is affected, we would predict a less robust response to CB_1R antagonism.

What is the relationship between α2δ-2 proteins and other synaptic proteins that may regulate altered eCB signaling in the CACNA2D2 KO?

Recall that in mammalian neurons, NRX is expressed on presynaptic terminals and interacts with postsynaptic NLGs. Synaptic phenotype similarities between α2δ-2 and NLG mutants,

such as mislocalization of CF terminals (see Chapter 3 discussion) and dysfunctional eCB signaling, could suggest common underlying mechanisms. For example, NLG3 mutants show a deficiency of eCB signaling at hippocampal CA1 pyramidal cell to inhibitory CCK synapses, resulting in larger amplitude IPSCs (Foldy et al., 2013). In this study, Foldy *et al.* demonstrate loss of eCB tone, and therefore a postsynaptic origin for eCB dysfunction. Remarkably, presynaptic NRX can modulate eCB signaling as well. Deletion of ß-NRX, but not α-NRX, reduces presynaptic calcium influx in response to action potentials as a consequence of increased eCB signaling by postsynaptic neurons (Anderson et al., 2015). Taken together with the NLG3 findings, it seems that NRX-NLG interactions regulate postsynaptic eCB signaling in opposing ways, such that loss of postsynaptic NLG3 reduces eCB signaling while loss of presynaptic ß-NRX results in overproduction of eCBs. As evidence from *C. elegans* suggests an interaction between α-NRX and α2δ-3 proteins (Tong et al., 2017), it is possible that α2δ-2 interacts with some or all of the NRX-NLG transsynaptic complex to produce similar mutant phenotypes.

Future directions

Because α-NRX does not impact eCB signaling (Anderson et al., 2015), it is important to investigate α2δ protein interactions with α-NRX and ß-NRX through binding assays (immunoprecipitation) and localization studies (e.g., cocultures of neurons expressing tagged-NRX or α2δ proteins to assess synaptic colocalization). Additionally, studying eCB phenotypes after deletion of α2δ and/or NLG molecules, in a ß-NRX null background, could reveal cooperativity in eCB signaling. For example, if α2δ-2 and NLG3 parallel one another to regulate eCB signaling, we might expect that deletion of either molecule would eliminate the eCB overproduction phenotype exhibited by ß-NRX mutants.

Summary & Conclusions

Together, our findings reveal previously unknown roles for α2δ-2 proteins in several critical subcellular compartments – functional coupling of two VGCC nanodomains and control of excitatory synapse innervation. Dysfunction resulting from conditional α2δ-2 deletion may exacerbate or produce secondary phenotypes; for example, reduced eCB signaling may contribute to aberrant synaptic development. Alternatively, α2δ proteins may control disparate processes depending on their specific molecular interactions. Though discovered as auxiliary subunits to VGCCs, the power of α2δ proteins does not appear to reside in modulation of VGCCs *per se*. Rather, α2δ proteins may coordinate various subcellular molecular compartments, which may or may not involve VGCCs. Careful, mechanistic investigations of α2δ protein's interactions are essential to discern how these molecules contribute to various aspects of neurological function. Likewise, uncovering how α2δ-dependent processes are affected by gabapentin pharmacology may elucidate this drug's therapeutic mechanism of action, which remains unknown.

No matter how incrementally, I hope that this body of work advances our fundamental understanding of α2δ-2 proteins and their profound contributions to neurological function; the physiological impact of their diverse roles in neurons represents an embarrassment of riches! Furthermore, I hope others find appreciation for the extraordinary molecular complexity required to achieve proper neuronal connectivity and physiology – through this work, I have.

REFERENCES

Adesnik H, Li G, During MJ, Pleasure SJ, Nicoll RA (2008) NMDA receptors inhibit synapse unsilencing during brain development. Proc Natl Acad Sci U S A 105:5597-5602.

Anderson GR, Aoto J, Tabuchi K, Foldy C, Covy J, Yee AX, Wu D, Lee SJ, Chen L, Malenka RC, Sudhof TC (2015) beta-Neurexins Control Neural Circuits by Regulating Synaptic Endocannabinoid Signaling. Cell 162:593-606.

Auger C, Attwell D (2000) Fast removal of synaptic glutamate by postsynaptic transporters. Neuron 28:547-558.

Baggelaar MP, Maccarrone M, van der Stelt M (2018) 2-Arachidonoylglycerol: A signaling lipid with manifold actions in the brain. Prog Lipid Res 71:1-17.

Barclay J, Balaguero N, Mione M, Ackerman SL, Letts VA, Brodbeck J, Canti C, Meir A, Page KM, Kusumi K, Perez-Reyes E, Lander ES, Frankel WN, Gardiner MR, Dolphin AC, Rees M (2001a) Ducky Mouse Phenotype of Epilepsy and Ataxia Is Associated with Mutations in the Cacna2d2 Gene and Decreased Calcium Channel Current in Cerebellar Purkinje Cells. The Journal of Neuroscience 21:6095-6104.

Barclay J, Balaguero N, Mione M, Ackerman SL, Letts VA, Brodbeck J, Canti C, Meir A, Page KM, Kusumi K, Perez-Reyes E, Lander ES, Frankel WN, Gardiner RM, Dolphin AC, Rees M (2001b) Ducky Mouse Phenotype of Epilepsy and Ataxia Is Associated with Mutations in the Cacna2d2 Gene and Decreased Calcium Channel Current in Cerebellar Purkinje Cells. The Journal of Neuroscience 21:6095-6104.

Beeson KA, Beeson R, Westbrook GL, Schnell E (2020) alpha2delta-2 Protein Controls Structure and Function at the Cerebellar Climbing Fiber Synapse. J Neurosci 40:2403-2415.

Bergles DE, Dzubay JA, Jahr CE (1997) Glutamate transporter currents in bergmann glial cells follow the time course of extrasynaptic glutamate. Proc Natl Acad Sci U S A 94:14821-14825.

Biederer T, Kaeser PS, Blanpied TA (2017) Transcellular Nanoalignment of Synaptic Function. Neuron 96:680-696.

Boning Gao YS, Anton Maximov, Mohamad Saad, Eva Forgacs‡, Farida Latif, Ming H. Wei (2000) Functional Properties of a New Voltage-dependent Calcium Channel The Journal of Biological Chemistry 275:12237-12242.

Bosman LW, Konnerth A (2009) Activity-dependent plasticity of developing climbing fiber-Purkinje cell synapses. Neuroscience 162:612-623.

Brenowitz SD, Best AR, Regehr WG (2006) Sustained elevation of dendritic calcium evokes widespread endocannabinoid release and suppression of synapses onto cerebellar Purkinje cells. J Neurosci 26:6841-6850.

Brenowitz SDaR, W. G. (2003) Calcium dependence of retrograde inhibition by endocannabinoids at synapses onto Purkinje cells. The Journal of Neuroscience 23:6373-6384.

Brockhaus J, Schreitmuller M, Repetto D, Klatt O, Reissner C, Elmslie K, Heine M, Missler M (2018) alpha-Neurexins Together with alpha2delta-1 Auxiliary Subunits Regulate Ca(2+) Influx through Cav2.1 Channels. J Neurosci 38:8277-8294.

Brodbeck J, Davies A, Courtney JM, Meir A, Balaguero N, Canti C, Moss FJ, Page KM, Pratt WS, Hunt SP, Barclay J, Rees M, Dolphin AC (2002) The ducky mutation in Cacna2d2 results in altered Purkinje cell morphology and is associated with the expression of a truncated alpha 2 delta-2 protein with abnormal function. J Biol Chem 277:7684-7693.

Brown JP, Gee NS (1998) Cloning and Deletion Mutagenesis of the alpha2delta Calcium Channel Subunit from Porcine Cerebral Cortex. The Journal of Biological Chemistry 273:25458-25465.

Brown SP, Brenowitz SD, Regehr WG (2003) Brief presynaptic bursts evoke synapse-specific retrograde inhibition mediated by endogenous cannabinoids. Nat Neurosci 6:1048-1057.

Brown SP, Safo PK, Regehr WG (2004) Endocannabinoids inhibit transmission at granule cell to Purkinje cell synapses by modulating three types of presynaptic calcium channels. J Neurosci 24:5623-5631.

Burroughs A, Wise AK, Xiao J, Houghton C, Tang T, Suh CY, Lang EJ, Apps R, Cerminara NL (2017) The dynamic relationship between cerebellar Purkinje cell simple spikes and the spikelet number of complex spikes. J Physiol 595:283-299.

Canti C, Nieto-Rostro M, Foucault I, Heblich F, Wratten J, Richards MW, Hendrich J, Douglas L, Page KM, Davies A, Dolphin AC (2005) The metal-ion-dependent adhesion site in the Von Willebrand factor-A domain of alpha2delta subunits is key to trafficking voltage-gated Ca2+ channels. Proc Natl Acad Sci U S A 102:11230-11235.

Cassidy JS, Ferron L, Kadurin I, Pratt WS, Dolphin AC (2014) Functional exofacially tagged N-type calcium channels elucidate the interaction with auxiliary alpha2delta-1 subunits. Proc Natl Acad Sci U S A 111:8979-8984.

Chanda S, Hale WD, Zhang B, Wernig M, Sudhof TC (2017) Unique versus Redundant Functions of Neuroligin Genes in Shaping Excitatory and Inhibitory Synapse Properties. J Neurosci 37:6816-6836.

Chen J, Li L, Chen SR, Chen H, Xie JD, Sirrieh RE, MacLean DM, Zhang Y, Zhou MH, Jayaraman V, Pan HL (2018) The alpha2delta-1-NMDA Receptor Complex Is Critically Involved in Neuropathic Pain Development and Gabapentin Therapeutic Actions. Cell Rep 22:2307-2321.

Christopherson KS, Ullian EM, Stokes CC, Mullowney CE, Hell JW, Agah A, Lawler J, Mosher DF, Bornstein P, Barres BA (2005) Thrombospondins are astrocyte-secreted proteins that promote CNS synaptogenesis. Cell 120:421-433.

Cole RL, Lechner SM, Williams ME, Prodanovich P, Bleicher L, Varney MA, Gu G (2005) Differential distribution of voltage-gated calcium channel alpha-2 delta (alpha2delta) subunit mRNA-containing cells in the rat central nervous system and the dorsal root ganglia. J Comp Neurol 491:246-269.

Davie JT, Clark BA, Hausser M (2008) The origin of the complex spike in cerebellar Purkinje cells. J Neurosci 28:7599-7609.

Davies A, Kadurin I, Alvarez-Laviada A, Douglas L, Nieto-Rostro M, Bauer CS, Pratt WS, Dolphin AC (2010) The alpha2delta subunits of voltage-gated calcium channels form GPI-anchored proteins, a posttranslational modification essential for function. Proc Natl Acad Sci U S A 107:1654-1659.

Davies A, Douglas L, Hendrich J, Wratten J, Tran Van Minh A, Foucault I, Koch D, Pratt WS, Saibil HR, Dolphin AC (2006) The calcium channel alpha2delta-2 subunit partitions with CaV2.1 into lipid rafts in cerebellum: implications for localization and function. J Neurosci 26:8748-8757.

de Castro F (2016) The Cajal School in the Peripheral Nervous System: The Transcendent Contributions of Fernando de Castro on the Microscopic Structure of Sensory and Autonomic Motor Ganglia. Front Neuroanat 10:43.

Dittman JS, Regehr WG (1998) Calcium Dependence and Recovery Kinetics of Presynaptic Depression at the Climbing Fiber to Purkinje Cell Synapse. The Journal of Neuroscience 18:6147-6162.

Dolphin AC (2012) Calcium channel auxiliary alpha2delta and beta subunits: trafficking and one step beyond. Nat Rev Neurosci 13:542-555.

Dolphin AC (2013) The alpha2delta subunits of voltage-gated calcium channels. Biochim Biophys Acta 1828:1541-1549.

Dolphin AC, Lee A (2020) Presynaptic calcium channels: specialized control of synaptic neurotransmitter release. Nat Rev Neurosci 21:213-229.

Donato R, Page KM, Koch D, Nieto-Rostro M, Foucault I, Davies A, Wilkinson T, Rees M, Edwards FA, Dolphin AC (2006) The ducky(2J) mutation in Cacna2d2 results in reduced spontaneous Purkinje cell activity and altered gene expression. J Neurosci 26:12576-12586.

Doroshenko PA, Woppmann A, Miljanich G, Augustine GJ (1997) Pharmacologically distinct presynaptic calcium channels in cerebellar excitatory and inhibitory synapses. Neuropharmacology 36:865-872.

Drexel M, Romanov RA, Wood J, Weger S, Heilbronn R, Wulff P, Tasan RO, Harkany T, Sperk G (2017) Selective Silencing of Hippocampal Parvalbumin Interneurons Induces Development of Recurrent Spontaneous Limbic Seizures in Mice. J Neurosci 37:8166-8179.

Edgerton JR, Reinhart PH (2003) Distinct contributions of small and large conductance Ca2+-activated K+ channels to rat Purkinje neuron function. J Physiol 548:53-69.

Edvardson S, Oz S, Abulhijaa FA, Taher FB, Shaag A, Zenvirt S, Dascal N, Elpeleg O (2013) Early infantile epileptic encephalopathy associated with a high voltage gated calcium channelopathy. J Med Genet 50:118-123.

Ellis SB, Williams ME, Ways NR, Brenner R, Sharp AH, Leung AT, Campbell KP, McKenna E, Koch WJ, Hui A, et al. (1988) Sequence and expression of mRNAs encoding the alpha 1 and alpha 2 subunits of a DHP-sensitive calcium channel. Science 241:1661-1664.

Eroglu C, Allen NJ, Susman MW, O'Rourke NA, Park CY, Ozkan E, Chakraborty C, Mulinyawe SB, Annis DS, Huberman AD, Green EM, Lawler J, Dolmetsch R, Garcia KC, Smith SJ, Luo ZD, Rosenthal A, Mosher DF, Barres BA (2009) Gabapentin receptor alpha2delta-1 is a neuronal thrombospondin receptor responsible for excitatory CNS synaptogenesis. Cell 139:380-392.

Fakler B, Adelman JP (2008) Control of K(Ca) channels by calcium nano/microdomains. Neuron 59:873-881.

Fekete A, Nakamura Y, Yang YM, Herlitze S, Mark MD, DiGregorio DA, Wang LY (2019) Underpinning heterogeneity in synaptic transmission by presynaptic ensembles of distinct morphological modules. Nat Commun 10:826.

Fell B, Eckrich S, Blum K, Eckrich T, Hecker D, Obermair GJ, Munkner S, Flockerzi V, Schick B, Engel J (2016) alpha2delta2 Controls the Function and Trans-Synaptic Coupling of Cav1.3 Channels in Mouse Inner Hair Cells and Is Essential for Normal Hearing. J Neurosci 36:11024-11036.

Foldy C, Malenka RC, Sudhof TC (2013) Autism-associated neuroligin-3 mutations commonly disrupt tonic endocannabinoid signaling. Neuron 78:498-509.

Garcia K, Nabhani T, Garcia J (2008) The calcium channel alpha2/delta1 subunit is involved in extracellular signalling. J Physiol 586:727-738.

Gee NS, Brown JP, Dissanayake VUK, Offord J, Thurlow R, Woodruff GN (1996) The Novel Anticonvulsant Drug, Gabapentin (Neurontin), Binds to the alpha2delta Subunit of a Calcium Channel. The Journal of Biological Chemistry 271:5768-5776.

Geisler S, Schopf CL, Stanika R, Kalb M, Campiglio M, Repetto D, Traxler L, Missler M, Obermair GJ (2019) Presynaptic alpha2delta-2 Calcium Channel Subunits Regulate Postsynaptic GABAA Receptor Abundance and Axonal Wiring. J Neurosci 39:2581-2605.

Gil C, Cubi R, Blasi J, Aguilera J (2006) Synaptic proteins associate with a sub-set of lipid rafts when isolated from nerve endings at physiological temperature. Biochem Biophys Res Commun 348:1334-1342.

Gruol DL, Netzeband JG, Schneeloch J, Gullette CE (2006) L-type Ca2+ channels contribute to current-evoked spike firing and associated Ca2+ signals in cerebellar Purkinje neurons. Cerebellum 5:146-154.

Harrison J, Jahr CE (2003) Receptor Occupancy Limits Synaptic Depression at Climbing Fiber Synapses. The Journal of Neuroscience 23:377-383.

Hashimoto K, Kano M (1998) Presynaptic origin of paired-pulse depression at climbing fibre-Purkinje cell synapses in the rat cerebellum. J Physiol 506 (Pt 2):391-405.

Hashimoto K, Kano M (2003) Functional differentiation of multiple climbing fiber inputs during synapse elimination in the developing cerebellum. Neuron 38:785-796.

Hashimoto K, Ichikawa R, Kitamura K, Watanabe M, Kano M (2009) Translocation of a "winner" climbing fiber to the Purkinje cell dendrite and subsequent elimination of "losers" from the soma in developing cerebellum. Neuron 63:106-118.

Hashimoto K, Tsujita M, Miyazaki T, Kitamura K, Yamazaki M, Shin HS, Watanabe M, Sakimura K, Kano M (2011) Postsynaptic P/Q-type Ca2+ channel in Purkinje cell mediates synaptic competition and elimination in developing cerebellum. Proc Natl Acad Sci U S A 108:9987-9992.

Heffley W, Song EY, Xu Z, Taylor BN, Hughes MA, McKinney A, Joshua M, Hull C (2018) Coordinated cerebellar climbing fiber activity signals learned sensorimotor predictions. Nat Neurosci 21:1431-1441.

Held RG, Liu C, Ma K, Ramsey AM, Tarr TB, De Nola G, Wang SSH, Wang J, van den Maagdenberg A, Schneider T, Sun J, Blanpied TA, Kaeser PS (2020) Synapse and Active Zone Assembly in the Absence of Presynaptic Ca(2+) Channels and Ca(2+) Entry. Neuron 107:667-683 e669.

Hirai H (2008) Progress in transduction of cerebellar Purkinje cells in vivo using viral vectors. Cerebellum 7:273-278.

Hoppa MB, Lana B, Margas W, Dolphin AC, Ryan TA (2012) alpha2delta expression sets presynaptic calcium channel abundance and release probability. Nature 486:122-125.

Indriati DW, Kamasawa N, Matsui K, Meredith AL, Watanabe M, Shigemoto R (2013) Quantitative localization of Cav2.1 (P/Q-type) voltage-dependent calcium channels in Purkinje cells: somatodendritic gradient and distinct somatic coclustering with calcium-activated potassium channels. J Neurosci 33:3668-3678.

Ivanov SV, Ward JM, Tessarollo L, McAreavey D, Sachdev V (2004) Cerebellar Ataxia, Seizures, Premature Death, and Cardiac Abnormalities in Mice with Targeted Disruption of the Cacna2d2 Gene. American Journal of Pathology 165:1007-1018.

Kaeser PS, Regehr WG (2017) The readily releasable pool of synaptic vesicles. Curr Opin Neurobiol 43:63-70.

Kandel ER (2013) Principles of neural science, 5th Edition. New York: McGraw-Hill.

Khaliq ZM, Raman IM (2005) Axonal propagation of simple and complex spikes in cerebellar Purkinje neurons. J Neurosci 25:454-463.

Kreitzer AC, Regehr WG (2001) Retrograde Inhibition of Presynaptic Calcium Influx by Endogenous Cannabinoids at Excitatory Synapses onto Purkinje Cells. Neuron 29:10.

Kurshan PT, Oztan A, Schwarz TL (2009) Presynaptic alpha2delta-3 is required for synaptic morphogenesis independent of its Ca2+-channel functions. Nat Neurosci 12:1415-1423.

Lein ES et al. (2007) Genome-wide atlas of gene expression in the adult mouse brain. Nature 445:168-176.

Li CY, Song YH, Higuera ES, Luo ZD (2004) Spinal dorsal horn calcium channel alpha2delta-1 subunit upregulation contributes to peripheral nerve injury-induced tactile allodynia. J Neurosci 24:8494-8499.

Liu S, Friel DD (2008) Impact of the leaner P/Q-type Ca2+ channel mutation on excitatory synaptic transmission in cerebellar Purkinje cells. J Physiol 586:4501-4515.

Liu X, Chen Y, Vickstrom CR, Li Y, Viader A, Cravatt BF, Liu QS (2016) Coordinated regulation of endocannabinoid-mediated retrograde synaptic suppression in the cerebellum by neuronal and astrocytic monoacylglycerol lipase. Sci Rep 6:35829.

Lu HW, Trussell LO (2016) Spontaneous Activity Defines Effective Convergence Ratios in an Inhibitory Circuit. J Neurosci 36:3268-3280.

M W, K K (2002) Active Contribution of Dendrites to the Tonic and Trimodal Patterns of Activity in Cerebellar Purkinje Neurons. The Journal of Neuroscience 22:10603-10612.

Matsushita K, Wakamori M, Rhyu IJ, Arii T, Oda S-i, Mori Y, Imoto K (2002) Bidirectional Alterations in Cerebellar Synaptic Transmission of tottering and rolling Ca2. The Journal of Neuroscience 22:4388-4398.

McKay BE, McRory JE, Molineux ML, Hamid J, Snutch TP, Zamponi GW, Turner RW (2006) Ca(V)3 T-type calcium channel isoforms differentially distribute to somatic and dendritic compartments in rat central neurons. Eur J Neurosci 24:2581-2594.

Missler M, Zhang W, Rohlmann A, Kattenstroth G, Hammer RE, Gottmann K, Sudhof TC (2003) a-Neurexins couple Ca21 channels to synaptic vesicle exocytosis. Nature 423:939-948.

Miyazaki T, Hashimoto K, Shin HS, Kano M, Watanabe M (2004) P/Q-type Ca2+ channel alpha1A regulates synaptic competition on developing cerebellar Purkinje cells. J Neurosci 24:1734-1743.

Miyazaki T, Yamasaki M, Hashimoto K, Yamazaki M, Abe M, Usui H, Kano M, Sakimura K, Watanabe M (2012) Cav2.1 in cerebellar Purkinje cells regulates competitive excitatory synaptic wiring, cell survival, and cerebellar biochemical compartmentalization. J Neurosci 32:1311-1328.

Muller CS, Haupt A, Bildl W, Schindler J, Knaus HG, Meissner M, Rammner B, Striessnig J, Flockerzi V, Fakler B, Schulte U (2010) Quantitative proteomics of the Cav2 channel nano-environments in the mammalian brain. Proc Natl Acad Sci U S A 107:14950-14957.

Najac M, Raman IM (2015) Integration of Purkinje cell inhibition by cerebellar nucleo-olivary neurons. J Neurosci 35:544-549.

Nakamura Y, Reva M, DiGregorio DA (2018) Variations in Ca(2+) Influx Can Alter Chelator-Based Estimates of Ca(2+) Channel-Synaptic Vesicle Coupling Distance. J Neurosci 38:3971-3987.

Nakamura Y, Harada H, Kamasawa N, Matsui K, Rothman JS, Shigemoto R, Silver RA, DiGregorio DA, Takahashi T (2015) Nanoscale distribution of presynaptic Ca(2+) channels and its impact on vesicular release during development. Neuron 85:145-158.

Neher E (2015) Merits and Limitations of Vesicle Pool Models in View of Heterogeneous Populations of Synaptic Vesicles. Neuron 87:1131-1142.

Niday Z, Bean BP (2021) BK channel regulation of after-potentials and burst firing in cerebellar Purkinje neurons. J Neurosci.

Nitta K, Matsuzaki Y, Konno A, Hirai H (2017) Minimal Purkinje Cell-Specific PCP2/L7 Promoter Virally Available for Rodents and Non-human Primates. Molecular Therapy - Methods & Clinical Development 6:159-170.

Noble K, Zhang J, Wray S (2006) Lipid rafts, the sarcoplasmic reticulum and uterine calcium signalling: an integrated approach. J Physiol 570:29-35.

Palay SL, Chan-Palay V (1974) Cerebellar Cortex: Cytology and Orgnaization. Berlin, Heidelberg, New York: Springer.

Park J, Yu YP, Zhou CY, Li KW, Wang D, Chang E, Kim DS, Vo B, Zhang X, Gong N, Sharp K, Steward O, Vitko I, Perez-Reyes E, Eroglu C, Barres B, Zaucke F, Feng G, Luo ZD (2016) Central Mechanisms Mediating Thrombospondin-4-induced Pain States. J Biol Chem 291:13335-13348.

Patel R, Bauer CS, Nieto-Rostro M, Margas W, Ferron L, Chaggar K, Crews K, Ramirez JD, Bennett DL, Schwartz A, Dickenson AH, Dolphin AC (2013) alpha2delta-1 gene deletion affects somatosensory neuron function and delays mechanical hypersensitivity in response to peripheral nerve damage. J Neurosci 33:16412-16426.

Paukert M, Huang YH, Tanaka K, Rothstein JD, Bergles DE (2010) Zones of enhanced glutamate release from climbing fibers in the mammalian cerebellum. J Neurosci 30:7290-7299.

Pfrieger FW, Barres BA (1997) Synaptic efficacy enhanced by glial cells in vitro. Science 277:1684-1687.

Piochon C, Irinopoulou T, Brusciano D, Bailly Y, Mariani J, Levenes C (2007) NMDA receptor contribution to the climbing fiber response in the adult mouse Purkinje cell. J Neurosci 27:10797-10809.

Pippucci T, Parmeggiani A, Palombo F, Maresca A, Angius A, Crisponi L, Cucca F, Liguori R, Valentino ML, Seri M, Carelli V (2013) A novel null homozygous mutation confirms CACNA2D2 as a gene mutated in epileptic encephalopathy. PLoS One 8:e82154.

Prescott C, Weeks AM, Staley KJ, Partin KM (2006) Kynurenic acid has a dual action on AMPA receptor responses. Neurosci Lett 402:108-112.

Rakotomamonjy J, Guemez-Gamboa, A. (2019) Purkinje Cell Survival in Organotypic Cerebellar Slice Cultures. Journal of Visualized Experiments 154:e60353.

Raman IM, Bean BP (1999) Ionic Currents Underlying Spontaneous Action Potentials in Isolated Cerebellar Purkinje Neurons. Journal of Neuroscience 19:12.

Rasmussen A, Jirenhed DA, Zucca R, Johansson F, Svensson P, Hesslow G (2013) Number of spikes in climbing fibers determines the direction of cerebellar learning. J Neurosci 33:13436-13440.

Regehr WG, Mintz IM (1994) Participation of Multiple Calcium Channel Types in Transmission at Single Climbing Fiber to Purkinje Cell Synapses. Neuron 12:605-613.

Renzi M, Farrant M, Cull-Candy SG (2007) Climbing-fibre activation of NMDA receptors in Purkinje cells of adult mice. J Physiol 585:91-101.

Rimmerman N, Hughes HV, Bradshaw HB, Pazos MX, Mackie K, Prieto AL, Walker JM (2008) Compartmentalization of endocannabinoids into lipid rafts in a dorsal root ganglion cell line. Br J Pharmacol 153:380-389.

Risher WC, Kim N, Koh S, Choi JE, Mitev P, Spence EF, Pilaz LJ, Wang D, Feng G, Silver DL, Soderling SH, Yin HH, Eroglu C (2018) Thrombospondin receptor alpha2delta-1 promotes synaptogenesis and spinogenesis via postsynaptic Rac1. J Cell Biol 217:3747-3765.

Rosenmund C, Legendre P, Westbrook G (1992) Expression of NMDA Channels on Cerebellar Purkinje Cells Acutely Dissociated from Newborn Rats. Journal of Neurophysiology 68.

Roth A, Haüsser M (2001) Compartmental models of rat cerebellar Purkinje cells based on simultaneous somatic and dendritic patch-clamp recordings. Journal of Physiology 535:445-472.

Rudolph S, Overstreet-Wadiche L, Wadiche JI (2011) Desynchronization of multivesicular release enhances Purkinje cell output. Neuron 70:991-1004.

Schneggenburger R, Meyer AC, Neher E (1999) Released Fraction and Total Size of a Pool of Immediately Available Transmitter Quanta at a Calyx Synapse. Neuron 23:399-409.

Schneider R, Hosy E, Kohl J, Klueva J, Choquet D, Thomas U, Voigt A, Heine M (2015) Mobility of calcium channels in the presynaptic membrane. Neuron 86:672-679.

Snell GD (1955) Ducky, a new second chromosome mutation in the mouse. Journal of Heredity 46:27-29.

Sotelo C (2008) Development of "Pinceaux" formations and dendritic translocation of climbing fibers during the acquisition of the balance between glutamatergic and gamma-aminobutyric acidergic inputs in developing Purkinje cells. J Comp Neurol 506:240-262.

Suzuki T, Zhang J, Miyazawa S, Liu Q, Farzan MR, Yao WD (2011) Association of membrane rafts and postsynaptic density: proteomics, biochemical, and ultrastructural analyses. J Neurochem 119:64-77.

Szabo GG, Lenkey N, Holderith N, Andrasi T, Nusser Z, Hajos N (2014) Presynaptic calcium channel inhibition underlies CB(1) cannabinoid receptor-mediated suppression of GABA release. J Neurosci 34:7958-7963.

Tong XJ, Lopez-Soto EJ, Li L, Liu H, Nedelcu D, Lipscombe D, Hu Z, Kaplan JM (2017) Retrograde Synaptic Inhibition Is Mediated by alpha-Neurexin Binding to the alpha2delta Subunits of N-Type Calcium Channels. Neuron 95:326-340 e325.

Tsetsenis T, Boucard AA, Arac D, Brunger AT, Sudhof TC (2014) Direct visualization of trans-synaptic neurexin-neuroligin interactions during synapse formation. J Neurosci 34:15083-15096.

Uchigashima M, Narushima M, Fukaya M, Katona I, Kano M, Watanabe M (2007) Subcellular arrangement of molecules for 2-arachidonoyl-glycerol-mediated retrograde signaling and its physiological contribution to synaptic modulation in the striatum. J Neurosci 27:3663-3676.

Uesaka N, Mikuni T, Hashimoto K, Hirai H, Sakimura K, Kano M (2012) Organotypic coculture preparation for the study of developmental synapse elimination in mammalian brain. J Neurosci 32:11657-11670.

Wadiche JI, Jahr CE (2001) Multivesicular release at climbing fiber-Purkinje cell synapses. Neuron 32:301-313.

Walsh CP, Davies A, Nieto-Rostro M, Dolphin AC, Kitmitto A (2009) Labelling of the 3D structure of the cardiac L-type voltage-gated calcium channel. Channels (Austin) 3:387-392.

Walter JT, Alvina K, Womack MD, Chevez C, Khodakhah K (2006) Decreases in the precision of Purkinje cell pacemaking cause cerebellar dysfunction and ataxia. Nat Neurosci 9:389-397.

Wang T, Jones RT, Whippen JM, Davis GW (2016) alpha2delta-3 Is Required for Rapid Transsynaptic Homeostatic Signaling. Cell Rep 16:2875-2888.

Wang X, Whalley BJ, Stephens GJ (2013) The du(2J) mouse model of ataxia and absence epilepsy has deficient cannabinoid CB(1) receptor-mediated signalling. J Physiol 591:3919-3933.

Womack MD, Chevez C, Khodakhah K (2004) Calcium-activated potassium channels are selectively coupled to P/Q-type calcium channels in cerebellar Purkinje neurons. J Neurosci 24:8818-8822.

Wu J, Yan Z, Li Z, Qian X, Lu S, Dong M, Zhou Q, Yan N (2016) Structure of the voltage-gated calcium channel Ca(v)1.1 at 3.6 A resolution. Nature 537:191-196.

Wycisk KA, Budde B, Feil S, Skosyrski S, Buzzi F, Neidhardt J, Glaus E, Nurnberg P, Ruether K, Berger W (2006) Structural and functional abnormalities of retinal ribbon synapses due to Cacna2d4 mutation. Invest Ophthalmol Vis Sci 47:3523-3530.

Yamagata M, Sanes JR, Weiner JA (2003) Synaptic adhesion molecules. Curr Opin Cell Biol 15:621-632.

Yang Y, Lisberger SG (2014) Purkinje-cell plasticity and cerebellar motor learning are graded by complex-spike duration. Nature 510:529-532.

Zhang B, Chen LY, Liu X, Maxeiner S, Lee SJ, Gokce O, Sudhof TC (2015) Neuroligins Sculpt Cerebellar Purkinje-Cell Circuits by Differential Control of Distinct Classes of Synapses. Neuron 87:781-796.

Zhang FX, Gadotti VM, Souza IA, Chen L, Zamponi GW (2018) BK Potassium Channels Suppress Cavalpha2delta Subunit Function to Reduce Inflammatory and Neuropathic Pain. Cell Rep 22:1956-1964.

Zou D, Chen L, Deng D, Jiang D, Dong F, McSweeney C, Zhou Y, Liu L, Chen G, Wu Y, Mao Y (2016) DREADD in parvalbumin interneurons of the dentate gyrus modulates anxiety, social interaction and memory extinction. Curr Mol Med 16:91-102.